UNIVERSITÀ DI PISA

Scuola di Dottorato in Ingegneria "Leonardo da Vinci"

Corso di Dottorato di Ricerca in
Ingegneria dell'Informazione
SSD ING/INF-03

Tesi di Dottorato di Ricerca

The interplay between mapping/demapping and non-binary LDPC coding in MIMO wireless communication systems

Autore:

Ottavio Maria Picchi

Tutori:
Prof. Marco Luise
Prof. Filippo Giannetti

Anno 2012

Manuscript submitted on February 28th, 2012

Accepted March 28th, 2012

Sommario

Il mondo delle telecomunicazioni è alla continua ricerca di innovazioni tecnologiche che permettano nuovi servizi, da implementare nei nuovi standard di comunicazione wireless. Questi nuovi servizi possono richiedere requisiti piuttosto stringenti in termini di throughput, cosicché una possibile soluzione per soddisfare questi requisiti, aumentando l'efficienza spettrale, è rappresentata dall'impiego di più antenne sia in trasmissione sia in ricezione. Al tempo stesso aumentando il throughput, aumenta inevitabilmente la banda di trasmissione, cosicché effetti di canale come fading e shadowing introducono effetti potenzialmente distruttivi sull'informazione trasmessa. Per questo motivo nasce la ricerca di nuovi codici a protezione di errore, che cercano di combattere gli effetti del canale di propagazione.

In questo contesto si inserisce questo lavoro, che si prefigge come obiettivo principale la combinazione di tecniche MIMO con i codici a protezione di errore LDPC non binari, basati cioè sull'aritmetica dei campi di Galois. Questo tipo di combinazione richiede la risoluzione di problematiche legate alla natura non binaria di questi codici, in particolare il calcolo delle informazioni soft (demapping) da fornire al decoder, che può risultare assai più complesso rispetto al tipico demapping binario.

In letteratura i principali lavori inerenti i codici LDPC non binari si concentrano su implementazioni low complexity del decoder, mentre il demapping viene spesso trascurato. Tuttavia la complessità del demapping non binario può avere un impatto rilevante sulla complessità totale di un ricevitore non binario. Invece questo lavoro si dedica interamente all'analisi del mapping e demapping dell'informazione non binaria. In particolare viene presentata una strategia per garantire un mapping efficiente al trasmettitore, così come algoritmi a bassa complessità per il demapping lato ricevitore. La soluzione proposta da questo lavoro si propone di ottenere il miglior compromesso tra prestazioni e complessità del ricevitore per ogni combinazione di ordine di campo di Galois, modulazione e codice spazio-tempo.

Abstract

Recently, the need for innovative services available for the end users has led to an increasing demand of higher throughputs of wireless systems. On the other hand higher throughput means wider bandwidth, so that channel selectivity and fading might be a severe challenge to combat in order to ensure high level of Quality of Service (QoS). In this scenario one of the possible approach to increase the system throughput is the use of multiple antennas, both at the transmitter and the receiver side. Instead the typical manner to combat channel effects is to employ powerful channel coding schemes, which target the mitigation of these propagation effects.

This work follows this approach combining the MIMO techniques jointly with the powerful channel coding scheme of non-binary LDPC. The expression "non-binary" refers to the fact that these codes are defined over high order Galois Field. These codes have been researched in the literature to achieve higher error protection than conventional binary codes for transmission over different noisy channels.

The main novelty of this work is related to the mapping and demapping of the non-binary information. Typically the main contributions in the literature focus on the low complexity decoders, whilst the demapping complexity is neglected. However, the demapping complexity might become a real bottleneck in the global receiver complexity, so that we decide to investigate this topic. A strategy is devised to guarantee an efficient mapping at the transmitter, together with an algorithm for low complexity soft demapping at the receiver. The proposed solutions target the best trade-off between performance and complexity, for any combination of the Galois field order, QAM constellation order, and MIMO scheme.

Acknowledgments

First of all I desire to express my sincere gratitude to my advisor Prof. Marco Luise for having offered me the PhD opportunity, for his technical guidance and supervision. His knowledge and support have played a crucial role in the achievements of my activity.

Then I would like to thank Dr. Alain Mourad for having offered me the opportunity of my internship at Samsung Electronics Research Institute, for his technical guidance and for his hard questions and high expectations on my work, which enhanced the quality of my activity. It has been an honor for me to work with him.

I would like to thank Dr. Giacomo Bacci, who is always available to help and support with his problem-solving approach and positive thinking. Working with him has been a real pleasure and allowed me to learn a lot. From personal perspective I also thank Giacomo for having become a trustworthy point of reference.

I desire to thank also Dr. Ismael Gutierrez, who helped me a lot during my period in Samsung Electronics. His technical advice and support permitted me to achieve important results and for this I really thank him.

I owe my deepest gratitude to my DSPCoLa labmates Andrea, Vincenzo e Mario. Our technical discussions and exchange of ideas have allowed me a professional growth. I also thank them for the great friendship we have created during these years.

I would like to thank the Standard and Industry Affairs department of Samsung Electronics Research Institute and the rest of the guys, who I met during my internship, for having shared a great atmosphere. Specifically, I would like to thank Angelo, German, Exequiel and Nicholas.

Then I would like to thank my parents for having supported me throughout my life. I have never reached the current achievements without their help and love. For this I will never thank them enough.

Finally, I desire to thank my beloved Silvia, who has always been next to me in any

difficulty I had to face during the last years. Moreover, I thank her for having shared with me the wonderful experience in Staines, placing our relationship ahead of her studies. For all these reasons I deeply thank my love.

Pisa, April 2012 Ottavio Maria Picchi

Contents

List of Figures

List of Tables

List of Acronyms

APP	A Posteriori Probability
AWGN	Additive White Gaussian Noise
BER	Bit Error Rate
BICM	Bit Interleaved Coded Modulation
CM	Coded Modulation
DBTC	Duo Binary Turbo Codes
DCM	Dispersion Character Matrix
DCMC	Discrete-input Continuous-output Memoryless Channel
DGFS	Diversity per GF Symbol
EXIT	EXtrinsic Information Transfer
FER	Frame Error Rate
FFT	Fast Fourier Transform
GC	Golden Code
GF	Galois Field
GSM	Global System for Mobile communications
LAN	Local Area Network
LDC	Linear Dispersion Code
LE	Linear Equalization
LLR	Log Likelihood Ratio
LTE	Long Term Evolution
MAP	Maximum A Posteriori
MIMO	Multiple Input Multiple Output
MIMO CW	MIMO Codeword

MISO	Multiple Input Single Output
ML	Maximum Likelihood
MMSE	Minimum Mean Square Error
MRC	Maximal Ratio combining
NB LDPC	Non-Binary Low Density Parity Check
QAM	Quadrature Amplitude Modulation
QPSK	Quadrature Phase Shift Keying
RS LDC	Random Search-based LDC
SD	Sphere Decoder
SIC	Soft Information Computation
SINR	Signal-to-Interference+Noise Ratio
SISO	Single Input Single Output
SIMO	Single Input Multiple Output
SM	Spatial Multiplexing
SNR	Signal-to-Noise Ratio
STBC	Space-Time-Block-Code
STC	Space-Time Codes
UMTS	Universal Mobile Telecommunications System
WER	Word Error Rate
WiMAX	Worldwide Interoperability for Microwave Access
ZF	Zero Forcing

List of Symbols and Operators

Number of Transmit antennas	N_T
Number of Receive antennas	N_R
Galois Field order	q
Most significant LLR values to the NB LDPC decoder	q_m
Modulation order	M
FEC codeword length (in GF(q) symbols)	N
FEC input-word length (in GF(q) symbols)	K
Check node degree	d_c
Variable node degree	d_v
Channel code rate	R_c
k-th APP value of the i-th received GF(q) symbol	$L_{i,k}$
Non-binary parity check matrix	$\mathbf{W}$
Time-depth of a STC	T
Spatial Rate	R_{sp}
Number of QAM symbols in a MIMO CW	Q
Equivalent MIMO channel matrix	$\mathcal{H}$
Number of GF(64) symbols in an integer number of MIMO CWs	m_1
Number of QAM symbols in m_1 GF(64) symbols	m_2
Number of MIMO CWs carrying m_1 GF(64) symbols	m_3

Galois Field	Ω
Effective SINR	η
Length (in bits) of a GF(64) symbol	γ
Received SNR at each receive antenna	ρ
mapping function	$\mu(\cdot)$
the golden number	θ
absolute value	$\|\cdot\|$
vector norm	$\|\|\cdot\|\|$
conjugate transposition	$(\cdot)^H$
transposition	$(\cdot)^T$
picks the elements on a matrix diagonal	$diag(\cdot)$
trace of the matrix (.)	Tr(.)

Introduction

Motivations

Non-binary Low Density Parity Check (NB LDPC) codes have been researched in the literature to achieve higher error protection than conventional binary codes for transmission over different noisy channels [1], [2], [3]. More recently, the European FP7 DAVINCI project [4] has explored the design of novel outperforming non-binary LDPC codes with tailored link level technologies over wireless fading channels, whilst aiming at small added complexity to conventional binary receivers. Specifically, most of recent works in literature have focused on low complexity decoding algorithms for high Galois Field (GF) order [5]. Meanwhile the use of multiple antennas in wireless links with appropriate Space-Time Codes (STC) has become the new frontier of wireless communications. Traditionally, multiple-antennas have been employed to combat the channel fading. Each pair of transmit antennas provides a signal path from the transmitter to the receiver. By sending signals with the same information through different paths, multiple independently faded replicas of data symbols can be obtained at the receiver side; hence, more reliable reception can be achieved. A different approach suggests that if the path gain between individual pairs fade independently, we can transmit independent information, in order to increase the data rate. In literature there is also a great amount of works based on the combination of NB LDPC codes jointly with MIMO techniques, but most of them stick to decoder implementations, without focusing on mapping and demapping topics. There are some very recent works partially discussing this topic [6], [7], however they stick to very specific cases, assuming that one Galois Field symbol is transmitted exactly in one MIMO codeword. This might lead in same cases to non-practical assumption, such as MIMO 3x3 or MIMO 4x4. Instead all along this work we will stick to practical MIMO systems, i.e. MIMO 2x2, focusing on mapping and demapping. We strong believe that

the complexity of the soft demapper at the receiver might represent a real bottleneck, especially when one GF symbol spreads across multiple QAM constellation symbols and MIMO codewords. This motivates us to analyze mapping and demapping issues in case of non-binary transmissions, with the aim of achieving the best trade-off between performance and complexity. A strategy is devised to guarantee an efficient mapping at the transmitter, together with an algorithm for low complexity soft demapping at the receiver.

Main Contributions

The main contribution of this thesis are listed and detailed below:

a. First of all we investigate different methods for computing the soft information for non-binary transmissions, deriving a novel approach which is based on a soft version of the Maximum Likelihood (ML). Specifically, we obtain a generalize method, which can be used for any combination of Galois Field order, modulation order and MIMO scheme. Previous works instead focused only on the soft information computation under very particular hyphotesis, i.e. one Galois Field symbol is transmitted over exactly one MIMO codeword. We generalize this also for those cases, where one Galois Field symbol is transmitted over different MIMO codewords.

b. We investigate also the performance of different Space-Time Codes in combination with NB LDPC codes, and we compare these results at different spectral efficiencies. This enables us to understand which Space-Time Code is best suitable with NB LDPC codes.

c. We figure out three heuristic rules, which enable the design of mapping patterns of non-binary information over the MIMO codewords. These rules are derived aiming at maximizing the diversity of the information of each Galois Field symbol, with the constraint of the demapping complexity at the receiver side. For this reason mapping patterns, obtained following these rules, are not optimum from performance perspectives but they maximize the trade-off between performance and demapping complexity.

d. We also derive a low complexity demapping algorithm for the MIMO case, which can be perfectly matched with the mapping pattern definition stated above. This low complexity algorithm implements a soft version of the Soft ML, but it exploits the *already available soft information* to reduce demapping complexity. This algorithm works perfectly in all the cases where one Galois Field symbol is transmitted in more than one MIMO codewords.

Outline

This thesis is structured as follows:

a. **Chapter1** presents the non-binary LDPC codes, detailing their coding and decoding. We deeply focus on the DAVINCI NB LDPC codes and their low complexity implementation. We also present the demapping in case of SISO transmission, before analyzing the performance of a SISO transmission system, employing NB LDPC codes. Then we compare their performance with the one of a very powerful binary FEC scheme, i.e. Duo Binary Turbo Codes (DBTCs).

b. **Chapter2** summarizes the main achievements on the multiple antennas topic, presenting the main parameter to quantify a Space-Time Code, before introducing the main Space-Time Codes we analyze all along this thesis. Then we present the universal framework of the Linear Dispersion Codes, before moving to the Performance analysis. Specifically, we analyze the performance of the selected Space-Time Codes in case of Maximum Likelihood Receiver and Linear Equalizers.

c. **Chapter3** presents the main issues to be faced when combining NB LDPC codes with MIMO techniques, especially if it is required to stick to a MIMO 2x2 system (as in our case). We analytically detail two different methods for computing the soft information in case of MIMO transmission. Later we present the performance analysis as well as the complexity considerations.

d. **Chapter4** first presents the channel capacity considerations and shows how to derive an adhoc Space-Time Code, which maximizes *equivalent channel capacity*. Then we state three heuristic rules, which enable the design of mapping patterns that maximize the trade-off between information diversity and demapping

complexity. Finally, it presents the low complexity demapping algorithm, before showing the performance analysis with and without the proposed algorithm.

e. **Conclusions** concludes this work, highlighting the most relevant achievements of this thesis.

Chapter 1

Non-binary LDPC coding

In this first chapter we will present the motivation behind the use of non-binary (NB) Low Density Parity Check (LDPC) codes, focusing on the weak points of the alternative (to NB LDPC codes) channel coding schemes, i.e. Turbo codes and binary LDPC codes. Then we will briefly analyze the most significant details of the NB LDPC codec, before focusing on the performance analysis in the context of SISO systems. Furthermore, a comparison with a powerful binary channel coding scheme, i.e. Duo Binary Turbo Codes (DBTC), will be performed for a matter of completeness.

1.1 Motivation behind the use of non-binary LDPC

This section presents the state-of-the-art and the motivation behind the necessity of further studying the NB LDPC codes. Specifically, with the term "non-binary" we mean that each non-zero element in the mapping and demapping matrices is defined over a Galois Field of order q (GF(q)) with $q > 2$. The first study of NB LDPC codes was conducted by Davey and MacKay in 1998 [1]. In this paper, they generalized the Sum Product Algorithm (SPA) for decoding binary LDPC codes to decode the q-ary LDPC codes. Later, in 2000, MacKay and Davey introduced a *Fast-Fourier-Transform* (FFT)-based method to reduce the decoding computational complexity [8]. This decoding algorith is referred to as FFT-QSPA. This work was further improved by Barnault and Declercq in 2003 [9] and by Declercq and Fossorier in 2007 [3]. Significant works on the design, construction and analysis of NB LDPC codes did not appear until the middle of 2000. Results in these works are very promising. They show that NB LDPC codes have a great potential to replace current channel codes in communication and storage systems. More recently, the European

FP7 DAVINCI project [4] has explored the design of novel outperforming NB LDPC codes, aiming at small added complexity compared to conventional binary receivers. Furthermore, the increasing demand for high-speed wireless communications calls for efficient technologies in terms of energy expenditure and bandwidth occupation. In the area of forward error correction (FEC) coding, NB LDPC codes were shown to bear a potential compared to other techniques [1]. To mention a few, NB LDPC codes show a lower error floor with respect to their binary counterpart (LDPC codes), while providing a steep waterfall region in terms of word error rate (WER) compared to convolutional turbo codes [10]. Although this feature comes at the expense of an increased complexity at the receiver, NB LDPC coding can be considered as a viable technology for beyond-4G communication systems [10].

1.2 Introduction of Non-binary LDPC codec

In this section we present a simple transmission system, employing the NB LDPC codes. This allows us to illustrate the features, the benefits and the complexities of this kind of system, when NB LDPC are used. According to [10], let us consider the parity check matrix $\mathbf{W}$ associated with a regular NB LDPC code with the parameters (d_v, d_c, N) representing the number of non-zero entries of $\mathbf{W}$ for the columns, for the rows and the code length respectively. All the non-zero elements of $\mathbf{W}$ are elements defined over the Galois field GF(q) and belong to the set $\Omega = \{\alpha_1, \alpha_2, .., \alpha_q\}$, where α_k (with $k = 1, .., q$) are the primitive element of the Galois Field. The Galois field (GF(q)), described usually using a polynomial (or vector) representation, can be also represented using matrices, as shown in [11]. If $p(x) = a_0 + a_1 \cdot x + \cdots + x^p$ is a polynomial of degree p having its coefficients in (GF(2)). The companion matrix of $p(x)$ is the $p \times p$ matrix

$$\mathbf{A}_c = \begin{bmatrix} 0 & 1 & 0 & \cdots & 0 \\ 0 & 0 & 1 & \cdots & 0 \\ 0 & 0 & 0 & \cdots & 1 \\ \alpha_1 & \alpha_2 & \alpha_3 & \cdots & \alpha_q \end{bmatrix} \tag{1.1}$$

The characteristic polynomial of this matrix is given by

$$det(\mathbf{A}_c\mathbf{x} \cdot \mathbf{I}) = p(x) \tag{1.2}$$

where $\mathbf{I}$ is the identity matrix. If p(x) is a primitive polynomial, it can be shown [11] that the matrix $\mathbf{A}_c$ is the primitive element of the Galois field (2^p) under a matrix representation and thus the powers of $\mathbf{A}_c$ are the non-zero elements of this field, defining the set $\mathcal{M} = \{0, A_k : k = 1, \cdots, q\}$. Additions and multiplications in the field correspond to additions and multiplications modulo 2 of these matrices. Based on the matrix representation of each nonzero entry, we give thereafter the equivalent vector representation of the parity check equations associated with the rows of $\mathbf{W}$. Let $\mathbf{x} = [x_0, \cdots, x_{N-1}]$ be a codeword. For the i-th parity equation of $\mathbf{W}$, we have

$$\sum_{j:h_{i,j}\neq 0} w_{i,j} \cdot x_j = 0 \tag{1.3}$$

Translating (1.4) into the vector domain, we can write

$$\sum_{j:h_{i,j}\neq 0} \mathbf{W}_{i,j} \cdot \mathbf{x}_j^t = 0^t \tag{1.4}$$

where $\mathbf{W}_{i,j}$ is the transpose of the matrix representation of the Galois field element $w_{i,j}$, $\mathbf{x}_j$ is the vector representation (binary mapping) of the symbol element x_j and t holds for transpose. The vector 0 is the all zero component vector. Considering the i-th parity check equation of $\mathbf{W}$, we indicate the equivalent binary parity check matrix as $\mathbf{W}_i = [\mathbf{W}_{i,j_0}, \cdots \mathbf{W}_{i,j_m}, \cdots \mathbf{W}_{i,j_{d_c-1}}]$, with $\{j_m : m = 0, \cdots d_c - 1\}$ the indexes of the non-zero elements of the i-th row. Now let us define $\mathbf{X}_i = [\mathbf{x}_{j,0}, \cdots, \mathbf{x}_{j,d_c-1}]$ as the binary representation of the symbols of the codeword $\mathbf{x}$ involved in the i-th parity check equation. When using the binary representation, the i-th parity check equation of $\mathbf{W}$, can be written as

$$\mathbf{W}_i \cdot \mathbf{X}_i^t = 0^t \tag{1.5}$$

We define $d_{min}(i)$ as the minimum distance of the binary code associated with $\mathbf{W}_i$. *Example:* Let $p(x) = x^3 + x + 1$ be the primitive polynomial used to generate the elements of $(\mathrm{GF}(2^3))$. The primitive element for the matrix representation is given by

$$\mathbf{A}_c = \begin{bmatrix} 0 & 1 & 0 \\ 0 & 0 & 1 \\ 1 & 1 & 0 \end{bmatrix} \tag{1.6}$$

Thus, $\{\mathbf{A}_k : k = 0, \cdots, 6\}$ are the non-zero elements of $(\mathrm{GF}(2^3))$ under this matrix representation and it is readily checked for our example that $\{A_k \cdot \alpha_1^t = \alpha_{k+l}^t\}$.

1.2.1 The DAVINCI NB LDPC codec

In this section we report the main features of the NB LDPC codec, developed and employed in the context of the DAVINCI project. We focus on the DAVINCI implementation of the NB LDPC codec because we have used this implementation all along this study. The DAVINCI project [4], funded by the European Community in the context of the FP7 programme, aimed at setting up foundations of pioneering Non-Binary Digital Wireless Transmission targeting the high spectral efficiency requirements of next generation wireless communications. The major achievements towards the above five main objectives can be summarized as follows: Development of new structures of non-binary LDPC codes outperforming the binary codes but also enjoying highly desirable features such as flexibility in trading-off the performance and complexity, rate-compatibility, reliability in fading scenarios, and compliance with hardware parallel implementation. The DAVINCI matrices have been designed over a Galois field of order $q = 64$, so that $\Omega = \{\alpha_1, \alpha_2, .., \alpha_{64}\}$. Each GF(64) symbol is represented by $\gamma = log_2(64) = 6$ bits. These codes have been designed with a very sparse parity check matrix. The variable node degree is fixed to $d_v = 2$ (optimal when $q \rightarrow \infty$ and codeword length $N \rightarrow \infty$), whereas the check node degree d_c is variable and adapted to the coding rate (i.e. $d_c = \{4, 6, 8, 12\}$ for channel code rate $R_c = \{1/2, 2/3, 3/4, 5/6\}$, respectively). The DAVINCI codes are obtained as regular LDPC codes over the Galois Field Ω following the optimization process described in [10]. The binary images of the (GF(64)) are obtained from the primitive polynomial below used in the DAVINCI project to optimize the DAVINCI codes [4]:

$$p(x) = x^6 + x + 1 \tag{1.7}$$

At the encoder side, blocks of K GF(64) symbols are then passed to the non-binary LDPC encoder, which generates the non-binary codeword of length N GF(64) symbols. The resulting *channel code rate* is $R_c = \frac{K}{N}$. At the receiver side, we use a reduced complexity non-binary decoder based on the Extended Min-Sum algorithm proposed in [5] for practical hardware implementation of the DAVINCI codes. This low complexity decoder takes only the q_m ($q_m < q$) highest APP values out of the q values available at the output of the soft demapper. This truncation of the APP values at the input of the decoder reduces significantly the decoder complexity at the cost of slight performance degradation. From now on in this thesis with the expression "NB LDPC encoder/decoder" we refer to the DAVINCI implementation [5].

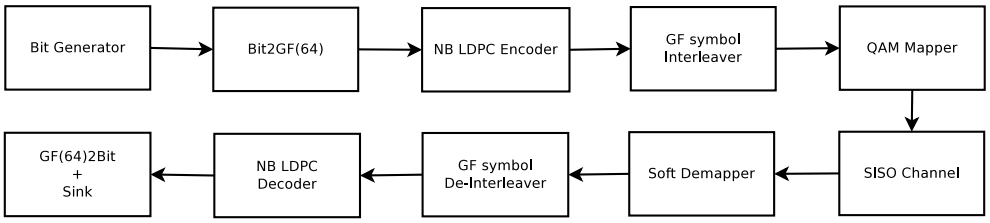

Figure 1.1: *SISO system architecture using NB LDPC codec*

1.3 Architecture of Non-binary systems

In this section we will analyze the architecture of a typical transmission system, employing NB LDPC codes as *Forward-Error-Correction* (FEC) scheme, addressing the issues arising from the non-binary nature of these powerful codes. Figure 1.1 shows this architecture. The first block generates information bits, which are then grouped by the *Bit2GF(64)* block. Each stream of K GF(64) symbols is encoded by the NB LDPC encoder, presented in the previous section. Specifically, the message $\mathbf{u} \in \Omega^K$ is encoded into a codeword $\mathbf{b} = [b_0, b_1, \cdots, b_{N-1}] \in \Omega^N$, which is interleaved at GF(64) symbol level. It is known that many communication channels are not memoryless; this implies that errors typically occur in burst and not independently. The GF(q) symbol interleaver aims to avoid such kind of burst errors. The output stream of N interleaved GF(q) symbols is mapped onto modulation symbols by the *QAM Mapper* block. As reported in [12] the mapping function $\mu(\cdot)$ is responsible for assigning symbols out of a QAM constellation $\mathcal{A}_x$ to the interleaved code GF(q) symbols which are taken out of a Galois field of order q. Since the cardinality of both sets is generally not identical, we have to gather m_1 coded GF(q) symbols and map them onto m_2 QAM symbols. Specifically, m_1 is the minimum number of GF(64) symbols necessary to have an integer number of modulation symbols, whilst m_2 is the number of modulation symbols necessary to map m_1 GF(64) symbols.

$$\mu : {\Omega^m}_1 \rightarrow {\mathcal{A}_x^m}_2 \tag{1.8}$$

In order to have a bijective mapping, the number of elements on both sides must be equal, i.e. m_1 coded GF(64) symbols out of Ω are mapped onto m_2 QAM symbols,

such that

$$q^m{}_1 = M^m{}_2 \tag{1.9}$$

where M is the cardinality of the QAM modulation. Values of m_1 and m_2 for different QAM modulations are reported in Table 1.1.

Table 1.1: *Mapping GF(64) symbols over QAM symbols*

Modulation	**QPSK**	**16-QAM**	**64-QAM**
$(\mathbf{m_1}, \mathbf{m_2})$	(1,3)	(2,3)	(1,1)

The mapping function hence gathers m_1 code symbols to $\mathbf{b} = [b_0, b_1, \cdots, b_{m_1-1}]$ and maps them onto m_2 QAM symbols:

$$\mathbf{x} = [x_0, x_1, \cdots, x_{m_2-1}] = \mu(\mathbf{b}) = [\mu_0(\mathbf{b}), \mu_1(\mathbf{b}), \cdots, \mu_{m_2-1}(\mathbf{b})] \tag{1.10}$$

Let us note that $\mathbf{x}$ in (1.10) is different from $\mathbf{x}$ presented in Section (1.2). Specifically, from now on with the vector $\mathbf{x}$ we will refer to the modulation symbols vector. The resulting stream of modulation symbols is then transmitted over the Single-Input-Single-Output (SISO) channel, which is first assumed to be Additive-White-Gassian-Noise (AWGN) and later a temporally uncorrelated fading channel. At the receiver, the output of the SISO channel, in case of AWGN, is given by:

$$y_i = x_i + v_i, x_i = \mu_i(\mathbf{b}) \tag{1.11}$$

where $i = 0, \cdots, m_2$, x_i is the transmitted signal (i.e. the modulation symbol) and v_i is the thermal noise, so that each I,Q component of v_i is $\mathcal{N}(0, \sigma_v^2)$. For the temporally uncorrelated fading channel, the output becomes:

$$y_i = h_i \cdot x_i + v_i \tag{1.12}$$

where h_i simulates the effects of a frequency-flat, time independent Rayleigh fading channel, i.e. $h_i \in \mathcal{CN}(0, 1)$. The received signal, represented by (1.11) and (1.12), is passed to the *Soft Demapper*, which is responsible of computing the A Posteriori Probability (APP) information, as it will be detailed in the next section. The APP information, computed by the Soft Demapper, is passed to the *GF(64) symbol de-interleaver*, which performs the de-interleaving operation, counterpart of the one at

the transmitter side. The de-interleaved APP information is then conveyed to the NB LDPC decoder, which produces the output stream of GF(64) decided symbols. Finally, the decided stream of GF(64) symbols is converted into its binary image by the *GF2Bit* block, before being collected by the *Sink*.

1.4 Soft demapping for NB LDPC codes

The Soft Demapper for SISO systems has been investigated in [12]. Its main role is computing the APP information for each received GF(64) symbols, which, in the context of non-binary transmissions, is the Logarithmic Likelihood Ratio (LLR) vector. According to [12], for each (GF(q)) symbol $b_i \in \Omega$, a vector of q APP values has to be computed, and each value is defined as:

$$L_{i,k} = \ln\left(\frac{P[b_i = \alpha_k|\mathbf{y}]}{P[b_i = \alpha_0|\mathbf{y}]}\right) \tag{1.13}$$

where $i \in 1, \cdots, m_1$, $k \in 1, \cdots, q-1$, $\mathbf{y}$ is the received signal, where we omitted the temporal dependancy. Instead α_k are the elements of the Galois Field Ω. Since generally more than one coded GF(64) symbol is involved in the mapping, in order to calculate the LLR vector we require a marginalization,

$$L_{i,k} = \ln\frac{\sum\limits_{\mathbf{b}\in B_i^k} P[\mathbf{b}|\mathbf{y}]}{\sum\limits_{\mathbf{b}\in B_i^0} P[\mathbf{b}|\mathbf{y}]} = \ln\frac{\sum\limits_{\mathbf{b}\in B_i^k} p[\mathbf{y}|\mathbf{b}]\cdot P[\mathbf{b}]}{\sum\limits_{\mathbf{b}\in B_i^0} p[\mathbf{y}|\mathbf{b}]\cdot P[\mathbf{b}]} \tag{1.14}$$

Assuming all the coded symbol vector (with length m_1 GF(64) symbols) to be equiprobable, i.e. $P[b] = q^{-m_1}$ and the channel memoryless, we can rewrite the (1.14) as:

$$L_{i,k} = \ln\left(\frac{\sum\limits_{\mathbf{b}\in B_i^k}\prod\limits_{j=0}^{m_2-1} p(y_j|\mathbf{b})}{\sum\limits_{\mathbf{b}\in B_i^0}\prod\limits_{j=0}^{m_2-1} p(y_j|\mathbf{b})}\right) \tag{1.15}$$

where $\mathbf{b} = [b_0, \cdots, b_{m_1-1}]$ is the coded GF(64) symbol vector, $B_i^k = \{\mathbf{b} : b_i = \alpha_k\}$ is the set of all coded GF(64) symbol vectors where the i-th component equal to α_k.

The pdf of the receiver input can be expressed by:

$$p(y_j|s_j) = \frac{1}{\pi \cdot N_0} \cdot \exp\left[-\frac{1}{N_0}\left|y_j - h_j \cdot x_j\right|^2\right] \tag{1.16}$$

where perfect channel state information is assumed at the receiver side, but not at the transmitter. In case of AWGN channel, the channel coefficient assumes the value $h_j = 1$. Let us note that $N_0 = 2\sigma_v^2$. Now substituting (1.16) in (1.15) we obtain:

$$L_{i,k} = \ln \frac{\sum\limits_{\mathbf{b}\in B_i^k} \exp\left(-\sum\limits_{j=0}^{m_2-1} \frac{\left|y_j - h_j \cdot x_j\right|^2}{N_0}\right)}{\sum\limits_{\mathbf{b}\in B_i^0} \exp\left(-\sum\limits_{j=0}^{m_2-1} \frac{\left|y_j - h_j \cdot x_j\right|^2}{N_0}\right)} \tag{1.17}$$

Since the denominator does not depend on k, we can compute only the first term and then normalize such that $L_{i,0} = 1$.

$$L_{i,k} = \ln\left(\sum_{\mathbf{b}\in B_i^k} \exp\left(-\sum_{j=0}^{m_2-1} \frac{\left|y_j - h_j \cdot x_j\right|^2}{N_0}\right)\right) \tag{1.18}$$

1.4.1 Comparison with binary soft demapping

In this paragraph we briefly present a simple binary SISO system, which will be compared with the NB LDPC-based one just depicted. This approach allows us to further emphasize the challenges arising from the exploitation of a non-binary FEC scheme, as the NB LDPC codes. Specifically, in this paragraph we focus on demonstrating that non-binary systems are intrinsically more complex than a binary one. This can be simply explained observing that non-binary encoders introduce a correlation between information bits (i.e. GF(64) symbols), and these GF(64) symbols might be transmitted over different modulation symbols. It is clear that this separation of a GF(64) symbol onto different modulation symbols, jointly with the correlation introduced among information bits are the causes of a complexity increase at the non-binary receiver side. This complexity increase is mainly related to the Soft demapper, so that we quickly have an insight at the binary soft demapping in order to appreciate the differences between binary and non-binary demapping. In this binary system we employ the DBTCs. The binary system model used for the sake of

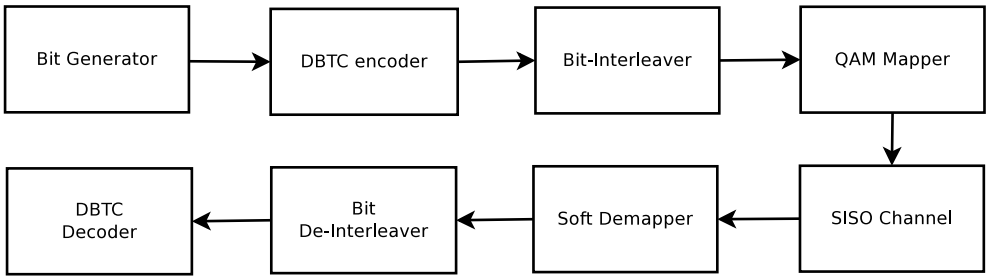

Figure 1.2: *SISO system architecture using DBTC codec*

comparison with the non-binary system, described in the previous section is depicted in Figure 1.2. The *Bit Info Generator* passes K' information bits to the DBTC Encoder, which produces a stream of N' coded bits. Then, the *Modulation Mapper* maps the coded bits into the modulation symbols (QPSK, 16QAM and 64QAM), which are transmitted over the SISO channel (AWGN and uncorrelated Rayleigh). At the receiver side, the Soft Demapper extracts the *bit LLR* from the receive signal, as explained below. It is obvious that no correlation among the modulation symbols is introduced here, so that the bit LLR computation turns out to be simpler than the non-binary case.

Thanks to the general description of the Soft Demapper introduced in [12] and followed in the previous section, the Soft Demapper for binary FECs can be easily derived from (1.15) considering the binary case as a particular case of Galois field with $q = 2$, so that we obtain

$$L_i = \ln \frac{\sum\limits_{\mathbf{d} \in B_i^1} p(y|\mathbf{d})}{\sum\limits_{\mathbf{d} \in B_i^0} p(y|\mathbf{d})} \tag{1.19}$$

where $\mathbf{d}$ are the bits mapped in a modulation symbol B_i^1, B_i^0 are the sets having the i-th bit equal to 1 and 0, respectively. Now substituting the pdf of the received signal

in 1.19, we obtain

$$L_i = \ln \frac{\sum_{\mathbf{d} \in B_i^1} \exp\left[-\frac{\left| y - h \cdot s^{(k)} \right|^2}{N_0} \right]}{\sum_{\mathbf{d} \in B_i^0} \exp\left[-\frac{\left| y - h \cdot s^{(k)} \right|^2}{N_0} \right]} \tag{1.20}$$

where $k = 0, \cdots, M-1$. Using the max-Log-MAP approximation for the binary case, the (1.21) becomes

$$L_i = \max_{\mathbf{d} \in B_i^1} \left[-\frac{\left| y - h \cdot s^{(k)} \right|^2}{N_0} \right] - \max_{\mathbf{d} \in B_i^0} \left[-\frac{\left| y - h \cdot s^{(k)} \right|^2}{N_0} \right] \tag{1.21}$$

The bit LLR computed by the binary soft Demapper are then sent to the DBTC decoder, which extracts the decided information bits.

1.5 Performance Analysis

In this section we present the numerical results, obtained simulating the behaviour of the systems presented in the previous sections. As already mentioned, in the context of the NB system we use the DAVINCI matrices and the decoder implementation introduced in [5]. Instead in the binary system we exploit the open-source implementation of the Coded Modulation Libraries [13]. Table 1.2 and Table 1.3 gives the list of the parameters used to evaluate the performance of the NB LDPC and DBTC FEC schemes, respectively, in the SISO context.

Figure 1.3 depicts the performance (in terms of CoWord Error Rate, CWER) of NB LDPC and DBTCs for a codeword length of $N_{bin} = 576$ bits (i.e. equivalent to $N = 96$ GF(64) symbols for the NB LDPC), assuming the channel to be AWGN. We can observe that NB LDPC outperforms DBTC for any analyzed modulation. Specifically, we can appreciate that the gain of NB LDPC is about 0.1 dB, 0.3 dB and 0.8 dB for QPSK, 16QAM and 64QAM, respectively. We notice that there is an increase of the gain whether the modulation order increases. Figure 1.4 compares the performance in the case of uncorrelated Rayleigh channel. Similarly to the AWGN case, we can clearly appreciate here that NB LDPC outperforms DBTC for all constellations in the simulated Rayleigh fading scenario. Specifically, we notice that

Table 1.2: *NB LDPC coding and decoder parameters*

Parameter	Value
Code Rate	$\frac{1}{2}$
Galois Field order, q	64
Codeword length, N GF(64) symbols	96
Decoder Type	EMS with L-bubble check
Number of decoding iterations	30
LLR vector size per received GF symbol, q_m	16
Number of sorting operations	18
Decoder Offset	1.0
Demapping method	Max-Log-Map (16-QAM) Log-Map (QPSK, 64-QAM)

Table 1.3: *DBTC coding and decoder parameters*

Parameter	Value
Code Rate	$\frac{1}{2}$
Codeword length (bit), N'	576
Number of decoding iterations	8
Number of sorting operations	18
Decoder Offset	0.7
Demapping method	Max-Log-Map

NB LDPC outperforms DBTC about 0.1 dB, 0.2 dB and 0.5 dB for QPSK, 16QAM and 64QAM, respectively. A deeper analysis on the performance comparison between NB LDPC and DBTC in SISO system could be found in [14].

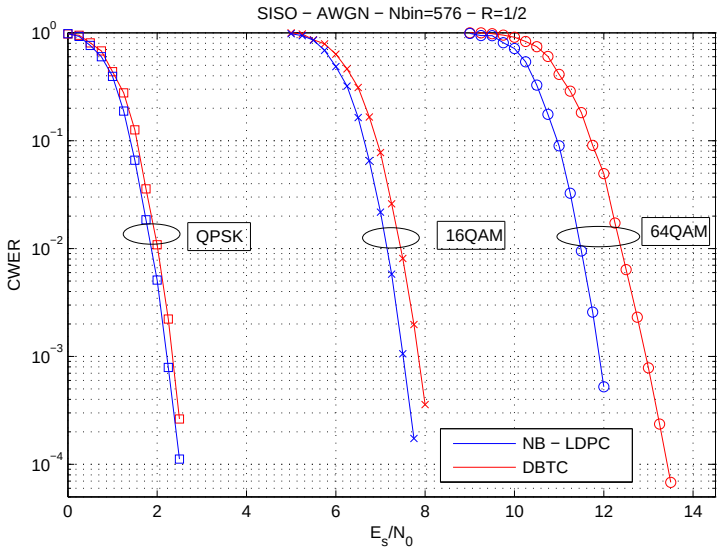

Figure 1.3: *Performance for SISO systems over AWGN channel*

1.6 Conclusions

In this chapter, we have presented the NB LDPC channel coding scheme, highlighting the codec features, but also deriving the demapping operations for the SISO scenario. We have also compared them with a binary channel coding scheme, such as DBTCs. Later we have also carried out a CWER performance analysis by which we can conclude that for single antenna transmission, NB LDPC codes outperform advanced binary FEC scheme (DBTC) for all the scenarios. The gain is found to increase with the constellation order, from 0.1 dB in QPSK to 0.8 dB in 64QAM. The average gain between NB LDPC and DBTC is found around 0.25 dB, in line with the results obtained in the DAVINCI project [14]. However, it must be said that in case of NB LDPC the receiver is more complex than the binary receiver and this complexity increase can be quantified around 10 times. Considering this complexity increase, we have decided to further analyze the NB LDPC in a multi-antenna scenario, aiming to evaluate the evolution of the gain in favor of NB LDPC. Before focusing on the application of NB LDPC in multiple antenna systems, in the following chapter we will

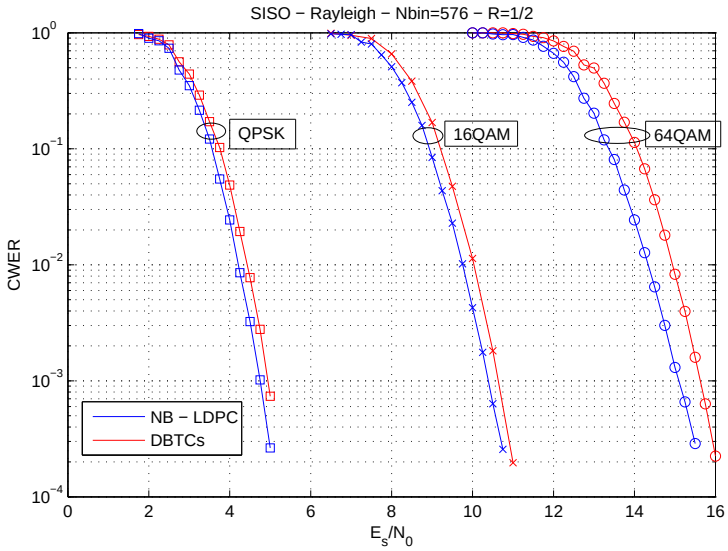

Figure 1.4: *Performance for SISO systems over Rayleigh channel*

briefly analyze the Multiple-Input-Multiple-Output (MIMO) system model without FEC schemes. Specifically, we will introduce the main parameters enabling to evaluate the Space-Time codes, the analythical description of the multi-antennas model, before presenting the selected Space-Time codes.

Chapter 2

MIMO and Space-Time codes in uncoded systems

In this we first present the motivation behind our choise of employing multi-antennas techniques. Later we will introduce the multiple-antenna concepts in uncoded systems and the main parameters necessary to analyze a Space-Time Code (STC), before presenting the STCs under analysis in this thesis. A STC is a method employed to improve the reliability or throughput of data transmission in wireless communication systems using multiple transmit antennas. A general framework based on the Linear Dispersion codes (LDC) is then presented allowing for universal study of all kinds of STCs. Later we will show results for the reference STCs and MIMO configurations considered in our study, before drawing the chapter conclusions.

2.1 Motivation behind the use of MIMO systems

The use of multiple antennas in wireless links with appropiate STC is rapidly becoming the new frontier of wireless communications. Recent years have seen the field mature substantially, both in theory and practice. Recent advances in theory include the solid understanding of capacity and other performance limits of wireless links, propagation and channel models. A growing awareness of the huge performance gains possible with STC techniques has spurred efforts to integrate this technology into practical systems. Traditionally, multiple-antennas have been employed to combat the channel fading. Each pair of transmit antennas provides a signal path from the transmitter to the receiver. By sending signals with the same information through different paths,

multiple independently faded replicas of data symbols can be obtained at the receiver side; hence, more reliable reception can be achieved. One example of the previous mentioned integration is the transmit diversity technique currently incorporated into different 2.5G and 3G standards. A different approach suggests that if the path gain between individual pairs fade independently, we can transmit independent information, in order to increase the data rate. This approach is commonly known as *Spatial Multiplexing* (SM). Recent effort have focused on introducing SM concepts into the UMTS standard for mobile wireless, the IEEE 802.16 standard for fixed and nomadic wireless and the IEEE 802.11 standard for wireless LANs. Thus, whilst the first approach, i.e. Diversity technique, aims at improving the performance in terms of error-protection, the second (SM) rather targets an increase of the data rate. All the STC existing in the literature attempt to achieve the best trade-off between these commonly opposing objectives as explained in [15].

2.2 MIMO channel model

In this section we aim to model the MIMO channel we have considered all along this study. Specifically, let us consider a wireless link with N_T transmit antennas and N_R receive antennas. Denoting the channel path coefficient between the j-th ($j = 1, \cdots, N_T$) transmit antenna and the i-th ($i = 1, \cdots, N_R$) receive antenna by $h_{i,j}(t)$, the MIMO channel is given by the $N_R \times N_T$ $\mathbf{H}(t)$ with

$$\mathbf{H}(t) = \begin{bmatrix} h_{1,1}(t) & h_{1,2}(t) & \cdots & h_{1,N_T}(t) \\ h_{2,1}(t) & h_{2,2}(t) & \cdots & h_{2,N_T}(t) \\ \vdots & \vdots & \ddots & \vdots \\ h_{N_R,1}(t) & h_{N_R,2}(t) & \cdots & h_{N_R,N_T}(t) \end{bmatrix} \tag{2.1}$$

Specifically, each channel path coefficient models the fading effects caused by the superposition of a large number of independent scattered components, then the in-phase and quadrature components of each channel path coefficient can be assumed to be independent zero mean Gaussian processes. The envelope of the channel path coefficient has a Rayleigh density function given by

$$f(h) = \frac{2h}{\sigma^2} \cdot e^{-\frac{h^2}{\sigma^2}}, h > 0 \tag{2.2}$$

where σ^2 is the average power of each channel coeffiecient. Furthermore, we assume the channel path coeffiecients to be temporally independent, i.e. they vary inpendently from a realization to the following one. Moreover, for the rest of this thesis we will omit the temporal index in the channel path coefficients.

2.3 Definition of the multiple-antenna model

According to [16] in a narrow band flat fading multi-antenna communication system with N_T transmit and N_R receive antennas, the received signal can be expressed by:

$$\mathbf{y} = \sqrt{\frac{\rho}{N_T}} \cdot \mathbf{H} \cdot \mathbf{s} + \mathbf{v} \tag{2.3}$$

where $\mathbf{y} \in \mathbb{C}^{N_R}$ denotes the vector of complex received signal for each channel use, $\mathbf{s} \in \mathbb{C}^{N_T}$ is the vector of complex transmitted signals, $\mathbf{H} \in \mathbb{C}^{N_R \times N_T}$ denotes the channel matrix, and $\mathbf{v} \in \mathbb{C}^{N_R}$ is the $\mathcal{CN}(0,1)$ (zero-mean, unit variance, complex-Gaussian) distributed, that is spatially and temporally white. The normalization $\sqrt{\frac{\rho}{N_T}}$ ensures that ρ is the SNR at each receive antenna, independently of N_T. As mentioned in the previous section, we assume $\mathbf{H}$ to denote the uncorrelated Rayleigh MIMO channel, i.e. all the entries of the $\mathbf{H}$ matrix are $\mathcal{CN}(0,1)$ distributed, spatially and temporally independent. Furthermore, we assume perfect channel knowledge at the receiver side, but not at the transmitter side. If the channel is constant for T channel uses, we can write:

$$\mathbf{y}_\tau = \sqrt{\frac{\rho}{N_T}} \cdot \mathbf{H} \cdot \mathbf{s}_\tau + \mathbf{v}_\tau, \quad \tau = 1, ..., T \tag{2.4}$$

Now defining $\mathbf{Y} = [\mathbf{y}_1, \mathbf{y}_2, ..., \mathbf{y}_T]^t$, $\mathbf{S} = [\mathbf{s}_1, \mathbf{s}_2, ..., \mathbf{s}_T]^t$ and $\mathbf{V} = [\mathbf{v}_1, \mathbf{v}_2, ..., \mathbf{v}_T]^t$, we obtain

$$\mathbf{Y}^t = \sqrt{\frac{\rho}{N_T}} \cdot \mathbf{H} \cdot \mathbf{S}^t + \mathbf{V}^t \tag{2.5}$$

It is more convenient to rewrite the previous equation in its transposed form, i.e.

$$\mathbf{Y} = \sqrt{\frac{\rho}{N_T}} \cdot \mathbf{S} \cdot \mathbf{H} + \mathbf{V} \tag{2.6}$$

where the transpose notation of $\mathbf{H}$ is omitted by simply redefining this matrix to have dimension $N_T \times N_R$. The matrix $\mathbf{Y} \in \mathbb{C}^{T \times N_R}$ is the received signal, $\mathbf{S} \in \mathbb{C}^{T \times N_T}$ is the transmitted signal and $\mathbf{V} \in \mathbb{C}^{T \times N_R}$ is the additive noise. The way, the information is organized within a MIMO codeword, i.e. $\mathbf{S}$, is specific to the given MIMO technique.

2.3.1 Space-Time Codes parameters definition

In this section we present the main features to analyze any STC . These include the spatial rate, diversity order, and orthogonality.

a. *Time-depth*

The Time-depth T of a STC is defined as the number of channel uses over which a MIMO codeword is transmitted. Normally the channel is assumed to be constant over T time interval. This is a reasonable assumption, because T is tipically ≤ 2.

b. *Parameter Q*

The Q parameter sets the number of modulation symbols transmitted in a MIMO codeword. This value is normally an even number, tipically 2 or 4.

c. *Spatial Rate*

The spatial rate is defined as

$$R_{sp} = \frac{Q}{T \cdot \min\left(N_T, N_R\right)} \tag{2.7}$$

If $R_{sp} = 1$ the STC is said to be *Full-Rate*. This parameter is important as it reflects how much redundancy lies in the MIMO codeword.

d. *Diversity order*

The diversity order is given by the number of independent fading experienced by one transmitted data symbol. The best performance (in terms of error-protection) is obtained when each symbol experiences independent fading on all the paths it is transmitted across. The maximum achievable diversity for different MIMO configurations is given in the Table 2.1.

The employment of a STC with higher Diversity order leads to a *Diversity gain* in the error-rate performance. Let us briefly focus on the effects of a diversity gain. As described in [17], assuming ML detection at the receiver, the corresponding probability of symbol error is given by

$$P_e = \overline{N_e} \cdot Q\left(\sqrt{\frac{\eta \cdot d_{min}^2}{2}}\right) \tag{2.8}$$

Table 2.1: *Maximum achievable diversity*

Configuration	Max Diversity
SISO	1
MISO	N_T
SIMO	N_R
MIMO	$N_T \times N_R$

where $\overline{N_e}$ and d_{min} are the number of nearest neighbors and the minimum distance of separation of the underlaying scalar constellation, respectively. The coefficient η is the Effective Signal-to-Interference-plus-Noise-Ratio (ESINR) for that wireless path. For high SNR regime ($\rho >> 1$), Eq. (2.8) may be semplified as

$$P_e \leq \overline{N_e} \left(\frac{\rho \cdot d_{min}^2}{4N_T} \right)^{-N_T} \tag{2.9}$$

Diversity hence affects the slope of the error-rate performance, as it will be shown in the numerical results section fo this chapter. Specifically, the magnitude of the slope equals the diversity order.

e. *Orthogonality and decoding complexity*

A STC is said to be orthogonal if the columns of its encoding matrix, i.e. **S** in (2.6), are orthogonal. This means that, for orthogonal schemes, transmitted symbols can be easily decoupled through a linear operation, i.e. a multiplication by a matrix. This has an impact on the decoding complexity. In general the decoding process for a maximum likelihood receiver involves the joint decoding of Q complex symbols. For example, assuming $Q = 4$ and 16QAM modulation, there are 2^{16} possible combinations to explore by the ML search, which reflects a huge complexity. Having orthogonal encoding matrix can drastically reduce the complexity thanks to the possibility of performing simple linear operations at the same performance than the non-linear ML operation.

2.3.2 Analyzed Space-Time Codes

In this study we consider the following STCs: Alamouti, Spatial Multiplexing and the Golden Code. Note that all these schemes are considered in *WiMAX IEEE 802.16m* standard, as specified in [18].

a. *Alamouti Code*

This well-known STC was presented in [19] and it has been originally designed for MISO systems. According to this techniques, two different modulation symbols s_1 and s_2 are transmitted simultaneously from antennas 1 and 2 respectively during the first channel use, followed by signals $-s_2^*$ and s_1^* from antennas 1 and 2 respectively during the second channel use. The resulting MIMO codeword for Alamouti code can be composed as

$$\mathbf{S} = \begin{bmatrix} s_1 & s_2 \\ -s_2^* & s_1^* \end{bmatrix} \tag{2.10}$$

Eq. (2.10) shows that, for the Alamouti code, the time-depth is $T = 2$ and $Q = 2$. Despite Alamouti code has been designed for MISO transmissions, we will employ it in MIMO systems, i.e. $N_R = 2$. This scheme is *half-rate*, i.e. from (2.7) $R_{sp} = \frac{1}{2}$. However, it has *full-diversity* and it is also *orthogonal*. This means that for Alamouti the optimal ML decoding performance can be achieved with linear receivers benefitting of significantly reduced complexity.

b. *Spatial Multiplexing*

Spatial Multiplexing (SM) offers a linear (in the number of transmit-receive antenna pairs) increase in the transmission rate (or capacity) for the same bandwidth and with no additional power expediture. SM is possible only in MIMO systems. The bit stream to be transmitted is demultiplexed into two half-rate sub-streams, modulated and transmitted simultaneously from each transmit antenna. Under favorable channel conditions, we can assume the received signals (one for each receive antenna) to be independent. The receiver, having knowledge of the channel, can differentiate between the two co-channel signals and extract both ones, after which demodulation yields the original sub-streams that can now be combined to yield the original bit stream. Thus SM increases transmission rate proportionally with the number of transmit-receive

antenna pairs. This scheme is designed for $T = 1$, $N_T = 2$ and $Q = 2$. The resulting MIMO codeword for SM can be composed as

$$\mathbf{S} = [\ s_1 \quad s_2\ ] \tag{2.11}$$

Spatial Multiplexing (SM) is *full-rate* but *half-diversity*. Specifically, SM has a diversity order equal to 2, with a potential maximum diversity order of 4 (see Table 2.1). This explains the expression *half-diversity*. However, this code is not orthogonal; this means that non-linear ML decoding must be used in order to achieve the optimum performance for this STC.

c. *Golden Code*

The Golden Code (GC) has been first introduced in [20] and it is designed for MIMO 2×2 systems. It is a *full-rate* STC with *diversity order* equal to 4 based on the Golden number, i.e. $\theta = \frac{1+\sqrt{5}}{2}$. This scheme is designed assuming $T = 2$, $N_T = 2$, $Q = 4$. The GC is not orthogonal, and this might lead to complexity issues considering that each MIMO CW based on GC encapsulates 4 modulation symbols, i.e. $Q = 4$, so that the ML decoding requires $o(M^4)$ operations. The resulting MIMO CW for GC can be composed as

$$\mathbf{S} = \frac{1}{\sqrt{5}} \cdot \begin{bmatrix} \alpha(s_1 + s_2 \cdot \theta) & j\sigma(\alpha) \cdot (s_3 + s_4 \cdot \sigma(\theta)) \\ \alpha(s_3 + s_4 \cdot \theta) & \sigma(\alpha) \cdot (s_1 + s_2 \cdot \sigma(\theta)) \end{bmatrix} \tag{2.12}$$

where $\sigma(\alpha) = 1 + j \cdot \theta$, $\sigma(\theta) = 1 - \theta$ and $\alpha = 1 + j \cdot \sigma(\theta)$.

Table 2.2 summarizes the main parameters presented for each analyzed STCs.

Table 2.2: *Summary of the selected STCs*

	Q	T	R_{sp}	Diversity Order	Orthogonality
Alamouti	2	2	$\frac{1}{2}$	4	Yes
SM	2	1	1	2	No
GC	4	2	1	4	No

2.4 Universal framework of Linear Dispersion Codes

Linear Dispersion Codes (LDCs) were introduced in [16], and represent an interesting framework to handle different STCs in a unique manner. Specifically, in this paragraph first we will detail the analytical model of the LDC and then re-analyze the selected STCs through the universal framework of the LDC.

2.4.1 Analytical description of Linear Dispersion Codes

Let each space-time transmission matrix $\mathbf{S}$ introduced in the previous sections represents the linear combination of Q modulation symbols, such as PSK or QAM symbols, which are dispersed over both space and time with the motivation of exploiting both the spatial and temporal diversity. We simply refer to this structure as Linear Dispersion Code (LDC). According to [16], a linear-dispersion codeword can be written as follows:

$$\mathbf{S} = \sum_{l=1}^{Q} (\alpha_l \cdot \mathbf{A}_l + j \cdot \beta_l \cdot \mathbf{B}_l) \tag{2.13}$$

where $s_l = \alpha_l + j \cdot \beta_l$ are the modulation symbols, whereas $\mathbf{A}_l$ and $\mathbf{B}_l$ are fixed $T \times N_T$ matrices that characterize each STC. Now the received signal expressed in (2.6) can be modified as follows:

$$\mathbf{Y} = \sqrt{\frac{\rho}{N_T}} \cdot \sum_{l=1}^{Q} (\alpha_l \cdot \mathbf{A}_l + j \cdot \beta_l \cdot \mathbf{B}_l) \cdot \mathbf{H} + \mathbf{V} \tag{2.14}$$

The real and imaginary components of each matrix can then be written as:

$$\begin{aligned} \mathbf{Y}_R + j \cdot \mathbf{Y}_I = & \sqrt{\frac{\rho}{N_T}} \cdot \sum_{l=1}^{Q} [\alpha_l \cdot (\mathbf{A}_{R,l} + j \cdot \mathbf{A}_{I,l}) + j \cdot \beta_l \cdot (\mathbf{B}_{R,l} + j \cdot \mathbf{B}_{I,l})] \cdot \\ & (\mathbf{H}_R + j \cdot \mathbf{H}_I) + (\mathbf{V}_R + j \cdot \mathbf{V}_I) \end{aligned} \tag{2.15}$$

Moreover, we denote the columns of $\mathbf{Y}_R$, $\mathbf{Y}_I$, $\mathbf{H}_R$, $\mathbf{H}_I$, $\mathbf{V}_R$, $\mathbf{V}_I$ as $y_{R,n}$, $y_{I,n}$, $h_{R,n}$, $h_{I,n}$, $v_{R,n}$, $v_{I,n}$ and define

$$\mathcal{A}_l = \begin{bmatrix} \mathbf{A}_{R,l} & -\mathbf{A}_{I,l} \\ \mathbf{A}_{I,l} & \mathbf{A}_{R,l} \end{bmatrix}, \quad \mathcal{B}_l = \begin{bmatrix} -\mathbf{B}_{R,l} & -\mathbf{B}_{I,l} \\ \mathbf{B}_{I,l} & -\mathbf{B}_{R,l} \end{bmatrix}, \quad \mathbf{h}_l = \begin{bmatrix} h_{R,l} \\ h_{I,l} \end{bmatrix} \tag{2.16}$$

where n ranges within $1, ..., N_R$ (number of receive antennas). Finally, we rewrite (2.6) into its equivalent real-valued vector form as follows:

$$\mathbf{y} = \begin{bmatrix} y_{R,1} \\ y_{I,1} \\ \cdots \\ y_{R,N_R} \\ y_{I,N_R} \end{bmatrix} = \sqrt{\frac{\rho}{N_T}} \cdot \mathcal{H} \cdot \begin{bmatrix} \alpha_1 \\ \beta_1 \\ \cdots \\ \alpha_Q \\ \beta_Q \end{bmatrix} + \begin{bmatrix} v_{R,1} \\ v_{I,1} \\ \cdots \\ v_{R,N_R} \\ v_{I,N_R} \end{bmatrix} = \sqrt{\frac{\rho}{N_T}} \cdot \mathcal{H} \cdot \mathbf{s} + \mathbf{v} \tag{2.17}$$

where $\mathbf{y}$ has dimensions equal to $2 \cdot N_R \cdot T \times 1$. $\mathcal{H}$ is the equivalent $2 \cdot N_R \cdot T \times 2 \cdot Q$ real-valued channel matrix and it is given by 2.18.

$$\mathcal{H} = \begin{bmatrix} \mathcal{A}_1 \cdot \mathbf{h}_1 & \mathcal{B}_1 \cdot \mathbf{h}_1 & \cdots & \mathcal{A}_Q \cdot \mathbf{h}_1 & \mathcal{B}_Q \cdot \mathbf{h}_1 \\ \cdots & \cdots & \cdots & \cdots & \cdots \\ \mathcal{A}_1 \cdot \mathbf{h}_{N_R} & \mathcal{B}_1 \cdot \mathbf{h}_{N_R} & \cdots & \mathcal{A}_Q \cdot \mathbf{h}_{N_R} & \mathcal{B}_Q \cdot \mathbf{h}_{N_R} \end{bmatrix} \tag{2.18}$$

$\mathcal{H}$ incorporates the effects of the channel matrix $\mathbf{H}$ and the dispersion matrices $\{\mathbf{A}_l, \mathbf{B}_l\}$, which are all known to the receiver. Hence the receiver uses (2.18) to find the equivalent channel matrix $\mathcal{H}$. The system of equations between transmitter and receiver is not underdetermined as long as

$$Q \leq N_R \cdot T \tag{2.19}$$

2.4.2 Reference STCs under the LDC framework

In this paragraph we will reanalyze the selected STCs (presented in the previous section) with the perspective of the LDC framework. Specifically, we aim to isolate the linear dispersion matrices for any analyzed STC.

a. *Alamouti*

The $T \times N_T$ linear dispersion matrices for Alamouti are reported in (2.20).

$$\begin{cases} \mathbf{A}_1 = \begin{bmatrix} 1 & 0 \\ 0 & 1 \end{bmatrix}, \mathbf{B}_1 = \begin{bmatrix} 1 & 0 \\ 0 & -1 \end{bmatrix} \\ \mathbf{A}_2 = \begin{bmatrix} 0 & -1 \\ -1 & 0 \end{bmatrix}, \mathbf{B}_2 = \begin{bmatrix} 0 & 1 \\ 1 & 0 \end{bmatrix} \end{cases} \tag{2.20}$$

b. *Spatial Multiplexing*

The $T \times N_T$ linear dispersion matrices for SM are reported in (2.21).

$$\mathbf{A}_1 = \mathbf{B}_1 = [\ 1 \quad 0\ ], \quad \mathbf{A}_2 = \mathbf{B}_2 = [\ 1 \quad 0\ ] \tag{2.21}$$

c. *Golden Code*

The $T \times N_T$ linear dispersion matrices for GC are reported in (2.22).

$$\begin{cases} \mathbf{A}_1 = \mathbf{B}_1 = \frac{1}{\sqrt{5}} \cdot \begin{bmatrix} 1+j-j\cdot\theta & 0 \\ 0 & 1+j-j\cdot\overline{\theta} \end{bmatrix} \\ \mathbf{A}_2 = \mathbf{B}_2 = \frac{1}{\sqrt{5}} \cdot \begin{bmatrix} \theta(1+j-j\cdot\theta) & 0 \\ 0 & \overline{\theta}(1+j-j\cdot\overline{\theta}) \end{bmatrix} \\ \mathbf{A}_3 = \mathbf{B}_3 = \frac{1}{\sqrt{5}} \cdot \begin{bmatrix} 0 & 1+j-j\cdot\theta \\ j(1+j-j\cdot\overline{\theta}) & 0 \end{bmatrix} \\ \mathbf{A}_4 = \mathbf{B}_4 = \frac{1}{\sqrt{5}} \cdot \begin{bmatrix} 0 & \theta(1+j-j\cdot\theta) \\ j\overline{\theta}(1+j-j\cdot\overline{\theta}) & 0 \end{bmatrix} \end{cases} \tag{2.22}$$

2.5 Simulated Scenarios and Performance Analysis

Figure 2.1 depicts the system model used to simulate the transmission chain and obtain the numerical results. In the baseline MIMO system depicted above, we can observe that Bit Information is first mapped onto a stream of modulation symbols and then organized in MIMO codewords by the MIMO Encoder. Specifically, the MIMO Encoder uses the Linear Dispersion Matrices, presented in the previous section in order to construct the MIMO codewords. The MIMO codewords are transmitted over the MIMO Channel specified in Section 2.2. Then, the output of the MIMO channel is received and processed by the MIMO Receiver in order to recover the transmitted information. In the analysis of uncoded MIMO systems, we consider two different receivers, i.e. the cascade Linear Equalizer - Hard Detector and the traditional Maximum Likelihood (ML). In the following, we briefly specify the operations carried out by each receiver. The first receiver, i.e. the cascade Linear Equalizer and Hard Detector, first performs a multiplication between the received signal by the

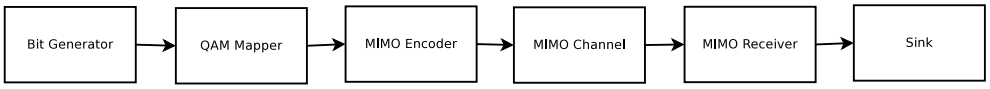

Figure 2.1: *Architecture of the simulated uncoded MIMO system*

equalization matrix, as shown in (2.23).

$$\hat{\mathbf{x}} = \mathbf{G} \cdot \mathbf{y} = \mathbf{M} \cdot \mathbf{s} + \mathbf{G} \cdot \mathbf{v} \tag{2.23}$$

where $\mathbf{y}$ is specified in (2.17), $\mathbf{M}$ is a $2Q \times 2Q$ real-values matrix, which links equalized signal with transmitted signal. Matrix $\mathbf{G}$ is the equalization matrix, which could be defined as $\mathbf{G}_{MMSE}$ or $\mathbf{G}_{ZF}$, whether the Minimum Mean Square Error (MMSE) or Zero-Forcing (ZF) technique is selected.

$$\begin{cases} \mathbf{G}_{MMSE} = \sqrt{\frac{\rho}{N_T}} \cdot \left(\frac{\rho}{N_T} \cdot \mathcal{H}^T \cdot \mathcal{H} + \mathbf{I}_{2Q} \right)^{-1} \cdot \mathcal{H}^T \\ \\ \mathbf{G}_{ZF} = \sqrt{\frac{N_T}{\rho}} \cdot \left(\mathcal{H}^T \cdot \mathcal{H} \right)^{-1} \cdot \mathcal{H}^T \end{cases} \tag{2.24}$$

Then, the equalized signal is passed to a Hard Detector, which produces the stream of decided bits. Instead, if the Maximum Likelihood is employed, the receiver selects the symbols which minimizes the following:

$$\mathbf{s}_{hd} = \underset{\overline{\mathbf{s}} \in \Xi}{\operatorname{argmin}} \| \mathbf{y} - \frac{\rho}{N_T} \cdot \mathcal{H} \cdot \overline{\mathbf{s}} \|^2 \tag{2.25}$$

(equal to 4) where $\mathbf{s}_{hd}$ is the hard detected MIMO codeword, i.e. the combination of Q modulation symbols, that minimizes the euclidean distance from the received signal $\mathbf{y}$. The term $\overline{\mathbf{s}}$ indicates a possible combination of Q modulation belonging to the set Ξ. Figure 2.2 shows the performance for a 4 Bits-per-channel-use (Bpcu) in case of ML receiver. Specifically, we report the SNR vs Bit-Error-Rate (BER) performance, where $SNR = \rho$. In this way we perform a fair comparison between the different STCs analyzed in terms of net spectral efficiency as well as power efficiency. In fact the BER performance of the analyzed STCs are functions of the SNR, i.e. the global transmit power normalized by the thermal noise of each receive antenna, so that it is fair comparing modulation of different orders. We can notice that GC (black line) performs better than SM (red line) and Alamouti (blue line). In fact GC is a full

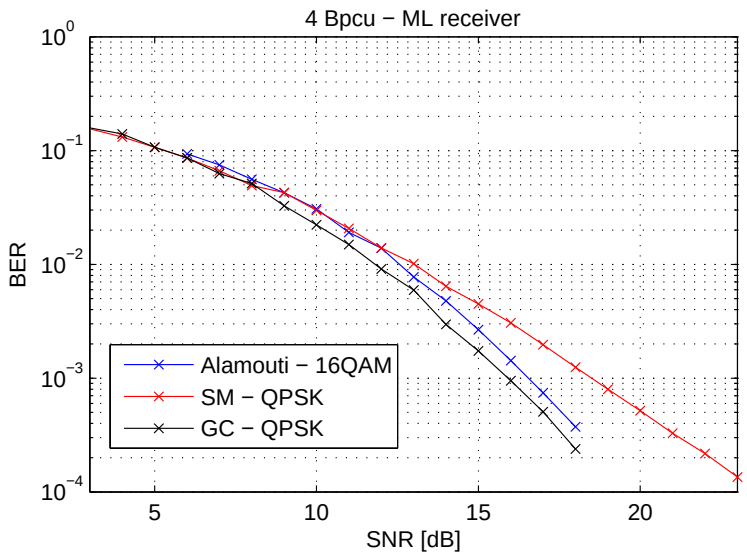

Figure 2.2: *Performance of different STCs detected with ML receiver*

spatial rate $R_{sp} = 1$ and full-diversity (equal to 4) STC, so that it performs better than SM because GC has a higher diversity order than SM. Alamouti code instead has full diversity order, but it is an half rate STC and for this reason we need to increase the modulation order to be fairly compared with SM and GC. Hence the coding gain between Alamouti and GC at low BER is due to the difference in the spatial rate. We can also appreciate that the slope of the GC curve is the same as Alamouti, since both STCs have diversity order equal to 4. The SM instead has a diversity order equal to 2 which is reflected by lower BER slope compared to Alamouti and GC.

Figure 2.3 shows the performance when the linear receiver is employed. Here we can observe that only Alamouti achieves the optimum performance in terms of BER. This is clearly thanks to the orthogonal structure of Alamouti. The other schemes not orthogonal, suffer from cross-channels interference, which cannot be mitigated through linear equalization. This explains the strong degradation for SM and GC. Moreover, the performance gap due to the difference in diversity order between GC and SM is much reduced due to the dominant interference.

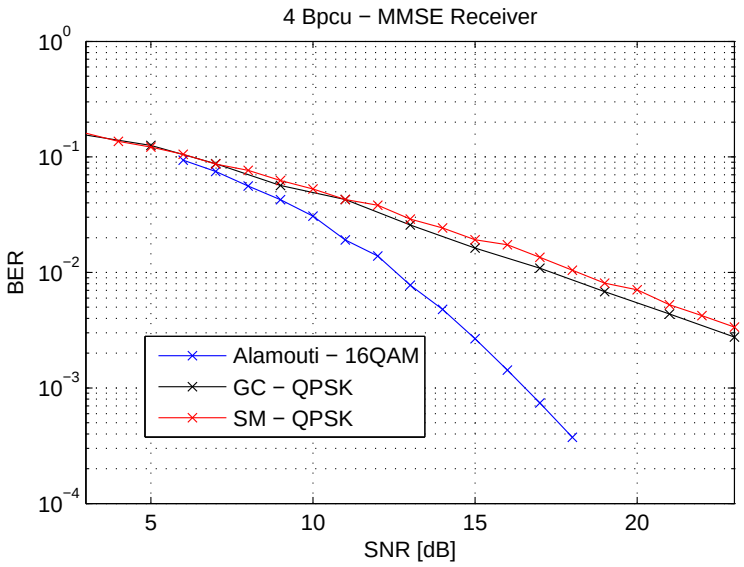

Figure 2.3: *Performance of different STCs detected with MMSE-based receiver*

2.6 Conclusions

In this chapter we have introduced the MIMO concepts in uncoded systems, i.e. without channel coding. Specifically, we have first detailed the MIMO channel model, which will be used all along this work. Later we have analyzed the multiple-antenna system model and presented the STCs under analysis. We have also introduced the universal framework of the LDC, and characterized the selected STCs through the linear dispersion matrices. From the simulation results we can end up that Alamouti has been shown to always outperform SM and Golden codes in terms of error protection at constant spectral efficiency of 4 Bpcu. Linear receivers are verified to achieve the optimal performance for orthogonal codes. Next, we will show that using a very powerful channel coding (in combination with these STCs), linear receivers could still be used to decode non orthogonal codes.

Chapter 3

Exploiting non-binary LDPC in MIMO systems

In this chapter we analyze the application of the powerful channel coding scheme of NB LDPC codes in system employing multiple antennas. Specifically, first we describe a typical system model using NB LDPC codes jointly with MIMO concepts. Second we state the issues to face when a non-binary channel code is combined with multiple antennas techniques. Later we present the demapping techniques we have adopted in order to compute the soft information, which must be passed to NB LDPC decoder in order to obtain the decided GF(64) stream. Furthermore, we highlight the necessary changes to apply to this non-binary system whether exploiting a conventional binary FEC, such as DBTC. Performance analysis and comparison is presented not only from the error protection perspective but also from complexity point of view.

3.1 System model description

Figure 3.1 shows the system model under analysis in this chapter. A stream of K information GF(64) symbols is passed to the NB LDPC encoder, which produces a stream of N coded GF(64) symbols. The coded stream is interleaved by the interleaver and then mapped onto modulation symbols. The stream of modulation symbols is later organized in MIMO codewords and transmitted over the channel.

It is worth mentioning that we stick to practical MIMO systems, i.e. 2 transmit antennas and 2 receive antennas. At the receiver side, the received signal is first passed in the Soft Information Computation (SIC) block, which extracts the LLR.

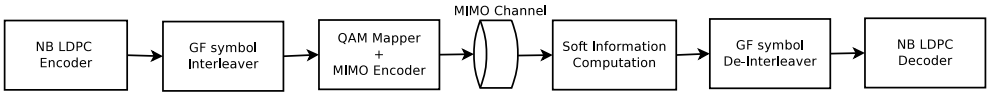

Figure 3.1: *Architecture of the transmission system*

The soft information is then passed to the de-interleaver, which performs the inverse operation done at the transmitter side. Finally, the output of the de-interleaver block is passed to the NB LDPC decoder, which produces the decided stream of GF(64) symbols. Now let us focus on the system blocks, which we have not detailed in the previous chapters yet. Specifically, hereafter we will present the interleaver/de-interleaver, the QAM mapper and the MIMO encoder. Algorithms designed for the LLR computation (implemented by the SIC block) will be deeply analyzed in the following of this chapter.

a. *Interleaver/De-Interlaver*

The interleaver applies an interleaving operation on the stream of N GF(64) symbols. This interleaving is performed at GF(64) symbol-level. This means that we are assuming our system to be a Coded Modulation (CM) one . At the receiver side the de-interleaver performs the inverse of the interleaving operation.

b. *QAM mapper*

In order to map the stream of coded GF(64) symbols onto the QAM constellation symbols, each GF(64) symbols in the FEC codeword is first converted back to its binary image of $log_2(q)$ bits, so that each group of $log_2(M)$ is mapped onto a modulation symbol, using Gray-mapping. Let us note that some modulation symbols may carry parts of different GF(64) symbols from the non-binary codeword.

c. *MIMO Encoder*

The stream of QAM symbols undergoes spatial coding, which means that QAM symbols are arranged in groups of Q symbols. Each group is encoded by the MIMO encoder into a MIMO codeword $\mathbf{S}$ of $T \times N_T$ complex symbols, with N_T being the number of transmitter antennas and T the STC length. In our

analysis the MIMO encoder can select different STBCs: in the first part of this chapter we focus only on two of those STBCs, i.e. Alamouti and SM (both with $Q = 2$). It is worth noting that Alamouti maximizes the Space-Time robustness of the information, whereas SM maximizes the throughput. Later in the following chapter we will include also two additional STBCs, i.e. Golden Code and an iterative STC (both with $Q = 4$), presented in [21].

At the receiver side each received MIMO codeword can be expressed by:

$$\mathbf{Y} = \sqrt{\frac{\rho}{N_T}} \cdot \mathbf{S} \cdot \mathbf{H} + \mathbf{V} \tag{3.1}$$

where $\mathbf{H} \in \mathbb{C}^{N_T \times N_R}$ denotes the Rayleigh fading channel matrix, N_R is the number of receive antennas, $\mathbf{V} \in \mathbb{C}^{T \times N_R}$ has zero-mean, unit-variance, and spatially and temporally white distributed entries. Furthermore, the normalization $\sqrt{\frac{\rho}{N_T}}$ ensures that ρ is the SNR at each receive antenna. In the sequel, we assume perfect knowledge of the channel state information only at the receiver side, but not at the transmitter.

3.2 Problem statement

As suggested in [6], in order to ensure a bijective mapping between GF(64), QAM symbols and MIMO codewords we have to map first a vector $\mathbf{d}$ of m_1 GF(64) symbols onto a vector $\mathbf{x} = [x_1, \cdots, x_{m2}]$ of m_2 QAM symbols; then, the vector $\mathbf{x}$ must be mapped onto m_3 MIMO codewords, such that the three vectors have the same length expressed in (coded) bits:

$$m_1 \times log_2(q) = m_2 \times log_2(M) = m_3 \times Q \times log_2(M) \tag{3.2}$$

Figure 3.2 shows the different layers of encapsulation of the information as also shown in (3.2). Specifically, we can observe that the stream of K information GF(64) symbols is first encoded onto N coded GF(64) symbols. Then the binary image of each coded GF(64) symbol must be explicited in order to be mapped onto QAM symbols. Finally, the stream $\mathbf{x}$ of QAM symbols is organized in MIMO codewords by the MIMO encoder. In [6], one of the configurations analyzed is based on GF(64), mapped onto QPSK symbols, and transmitted through Spatial Multiplexing (SM) with a 3×3 MIMO configuration. In this particular case, the above parameters in

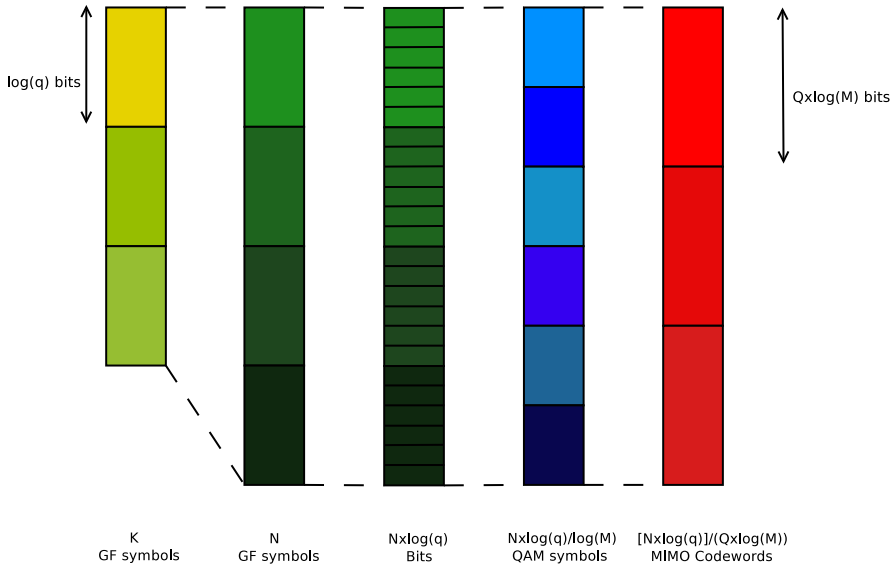

Figure 3.2: *Different layers of information encapsulation*

(3.2) take the following values: $m_1 = 1, m_2 = 3, m_3 = 1$. A second case studied in [6] is based on GF(256), mapped onto QPSK symbols, and transmitted through SM with a 4×4 MIMO configuration. In this second case the parameters in (3.2) take the values: $m_1 = 1, m_2 = 4, m_3 = 1$. It is worth noting that in both cases the setting of Galois Field order, constellation size, and MIMO configuration, is particularly chosen to yield m_1 and m_3 both equal to 1, so that the problem of soft information computation complexity at the receiver is avoided. For those specific cases, where one GF(q) symbol is transmitted over exactly on MIMO CW, the demapping complexity is extremely simplified as long as the complexity could have the same order of magnitude of the SISO case, with equivalent spectral efficiency. However, along this work we consider those cases as very particular corner cases and we will not focus on them. In this work, one of the main target is to remove any constraint on such settings and focus on a more practical MIMO configuration (2×2), with different QAM constellation sizes (QPSK, 16-QAM, 64-QAM) and different STCs. Assuming $q = 64$, Table 1 gives the values of m_1, m_2 and m_3 for each constellation assuming to use STBCs with $Q = 2$ (Alamouti or SM). Assuming a Galois Field order $q = 64$ with 2×2 MIMO

Table 3.1: *Values of m_1, m_2 and m_3*

Modulation	**QPSK**	**16-QAM**	**64-QAM**
$(\mathbf{m_1}, \mathbf{m_2}, \mathbf{m_3})$	(2,6,3)	(4,6,3)	(2,2,1)

configuration and allowing any constellation size, we clearly fall in the general case where one GF(64) symbol is transmitted over more than one MIMO codewords (e.g. QPSK and 16QAM in Table 3.1 where $m_1 \neq 1$). This is when the complexity of the soft information computation becomes challenging as detailed and mitigated by the solutions proposed in the next chapter.

3.3 Soft Information Computation

This section details the Soft Information Computation (SIC) for NB LDPC codes in multi-antennas systems. Specifically, two solutions are presented: a straightforward solution based on linear equalizers and a second solution based on a soft version of maximum likelihood demapper. As known from chapter 1, the NB LDPC decoder requires, for each received GF(64) symbol, a vector of 64 Logarithmic Likelihood Ratio (LLR) values. Note that in the binary case only one LLR value is required as commonly known.

3.3.1 Linear Equalizer-based demapper

In this section we present the first receiver employed in our study. This receiver is essentially based on a cascade of a MIMO Linear Equalizer and a Soft Demapper. We divide the analysis of this receiver in two subsections, where the first depicts the concepts of the MIMO Linear Equalization (coherently with what was presented in Chapter 2), and the second focuses on the soft demapper, where the analysis performed for the SISO transmission in Chapter 1 will be generalized considering multiple antennas. For this receiver, we have considered the LDC model more convenient to handle, so we consider (2.17) as the received signal.

3.3.1.1 MIMO linear equalization

As explained in chapter 2, MIMO linear decoders represent interesting solutions for their simplicity. Specifically, the MIMO Linear Equalizer performs simply a multiplication by a matrix, which allows to extract modulation symbols from the received MIMO CW. In fact one additional benefit deriving from the use of the MIMO Linear Equalizer is that its output is a single stream, as if it has passed through an equivalent SISO channel. Therefore, soft demappers, previously defined for SISO, can be used with minor changes. So the received MIMO CW is first equalized, obtaining the signal in (2.23) and then passed to the soft demapper. Two possible equalizations matrices, presented in (2.24), have been considered in our study, i.e. ZF and MMSE.

3.3.1.2 MIMO soft demapper

In this paragraph we will generalize the analytical details of the soft demapping, presented for SISO systems, for the MIMO system using linear equalizers. Assuming of having received (2.23), eq. (1.13) for SISO can be modified as shown in (3.3).

$$L_{i,k} = \ln\left(\frac{P[b_i = \alpha_k|\hat{\mathbf{x}}]}{P[b_i = \alpha_0|\hat{\mathbf{x}}]}\right) \tag{3.3}$$

where $i \in 1, \cdots, m_1$, $k \in 1, \cdots, q-1$. Like the SISO case, generally more than one coded GF(64) symbol is involved in the mapping, so that, in order to calculate the LLR vector, we require a marginalization,

$$L_{i,k} = \ln \frac{\sum\limits_{\mathbf{b}\in B_i^k} P[\mathbf{b}|\hat{\mathbf{x}}]}{\sum\limits_{\mathbf{b}\in B_i^0} P[\mathbf{b}|\hat{\mathbf{x}}]} = \ln \frac{\sum\limits_{\mathbf{b}\in B_i^k} p[\hat{\mathbf{x}}|\mathbf{b}] \cdot P[\mathbf{b}]}{\sum\limits_{\mathbf{b}\in B_i^0} p[\hat{\mathbf{x}}|\mathbf{b}] \cdot P[\mathbf{b}]} \tag{3.4}$$

where $\mathbf{b} = [b_0, \cdots, b_{m_1-1}]$ is the coded GF(64) symbol vector, $B_i^k = \{\mathbf{b} : b_i = \alpha_k\}$ is the set of all coded GF(64) symbol vectors where the i-th component equal to α_k. Assuming again all the coded symbol vector (with length m_1 GF(64) symbols) to be equiprobable and the channel memoryless, we can rewrite the (3.4) as:

$$L_{i,k} = \ln\left(\frac{\sum\limits_{\mathbf{b}\in B_i^k} \prod\limits_{j=0}^{m_2-1} p(\hat{x}_j|\mathbf{b})}{\sum\limits_{\mathbf{b}\in B_i^0} \prod\limits_{j=0}^{m_2-1} p(\hat{x}_j|\mathbf{b})}\right) \tag{3.5}$$

where $\hat{x}_j$ is the j-th component of the equalized vector $\hat{\mathbf{x}} = [\hat{x}_1, \cdots, \hat{x}_{m2}]$. However, for a matter of implementation complexity, it is more convenient to rewrite (3.5) without considering the vector $\mathbf{b}$, but each b_i element (with $i = \{1, \cdots, m_1\}$). In fact each b_i element is exactly mapped onto n_2 modulation symbols. Specifically, n_2 ($\leq m_2$) is the number of modulation symbols over which the i-th GF(q) symbol is mapped. Hence Eq. (3.5) can be rewritten as

$$L_{i,k} = \ln \left(\frac{\prod_{j=0}^{n_2-1} p(\hat{x}_j | b_i = \alpha_k)}{\prod_{j=0}^{n_2-1} p(\hat{x}_j | b_i = \alpha_0)} \right) \tag{3.6}$$

Let us note that (3.5) can be rewritten as (3.6) thanks to the linear equalization, which allows to decouple modulation symbols from each MIMO codeword, so that the stream of equalized modulation symbols can be reorganized in order to obtain each *equalized GF(q) symbol*. Furthermore, the pdf of the equalized signal can be expressed by:

$$p(\hat{x}_j | x_j^{(k)}) = \frac{\rho}{\pi} \cdot \exp \left[-\rho \frac{|\hat{x}_j - \beta_j \cdot x_j^{(k)}|^2}{\lambda_j} \right] \tag{3.7}$$

where $x_j^{(k)} = \mu_j(\alpha_k)$, being $\mu(\cdot)$ the mapping function. The parameter λ takes into account the effects of the matrix $\mathbf{G}$ on the noise realization received on each antenna. Specifically, the coefficient λ is defined as

$$\lambda_j = \frac{\eta_j}{\rho} \tag{3.8}$$

where η is the Effective-Signal-to-Interference-plus-Noise-Ratio and is defined as [22]

$$\eta_j = \frac{diag[\mathbf{D} \cdot \mathbf{D}^T]_j}{diag[\frac{1}{\rho}\mathbf{G} \cdot \mathbf{G}^T + \mathbf{I}_{self} \cdot \mathbf{I}_{self}^T]_j} \tag{3.9}$$

where $\mathbf{D} = diag[\mathbf{G} \cdot \mathcal{H}]$ and $\mathbf{I}_{self} = \mathbf{G} \cdot \mathcal{H} - \mathbf{D}$. The operator $diag[.]$ takes the elements on the diagonal and creates another matrix having those elements on the diagonal and null elements elsewhere. According to [23], assuming the exploitation of the ZF equalization, Eq. (3.9) becomes

$$\eta_j^{(ZF)} = \frac{\rho}{[\mathcal{H} \cdot \mathcal{H}^T]_{j,j}^{-1}} \tag{3.10}$$

Instead eq. (3.9) becomes (3.11) whether the MMSE equalization is used, according to [23].

$$\eta_j^{(MMSE)} = \frac{\rho}{[\mathcal{H} \cdot \mathcal{H}^T + \frac{N_T}{\rho} \cdot \mathbf{I}_{2Q}]^{-1}_{j,j}} - 1 \tag{3.11}$$

The coefficients β reflect the amplification effect introduced by the equalization matrix G on the transmitted information signal at each receive antenna. These coefficients are obtained as:

$$\beta_j = \mathbf{M}_{j,j} \tag{3.12}$$

where $\mathbf{M}$ has been introduced in (2.23). The coefficients λ and β might be considered constant for T intervals if the channel is *static* during T channel uses. Now substituting (3.7) in (3.6) we obtain:

$$L_{i,k} = \ln \left(\frac{\exp\left(-\rho \sum_{j=0}^{n_2-1} \frac{\left| \hat{x}_j - \beta_j \cdot x_j^{(k)} \right|^2}{\lambda_j} \right)}{\exp\left(-\rho \sum_{j=0}^{n_2-1} \frac{\left| \hat{x}_j - \beta_j \cdot x_j^{(0)} \right|^2}{\lambda_j} \right)} \right) \tag{3.13}$$

Similarly to the SISO case, since the denominator does not depend on k, we can compute only the first term and then normalize such that $L_{i,0} = 1$.

$$L_{i,k} = \ln \left(\exp\left(-\rho \sum_{j=0}^{n_2-1} \frac{\left| \hat{x}_j - \beta_j \cdot x_j^{(k)} \right|^2}{\lambda_j} \right) \right) \tag{3.14}$$

Specifically, the general Eq. (3.14) can be specified for any considered modulation, reminding that the Galois Field order q has been set to 64.

a. *QPSK*

In this case a GF(64) symbol is mapped exactly onto 3 QPSK symbols, so that three equalized QPSK symbols need to be considered in the computation of the LLRs for the given GF(64) symbol. The LLRs for each received GF(64) symbols can be computed as devised in (3.15).

$$L_{i,k} = \ln \left(\exp\left(-\rho \sum_{j=0}^{2} \frac{\left| \hat{x}_j - \beta_j \cdot x_j^{(k)} \right|^2}{\lambda_j} \right) \right) \tag{3.15}$$

where all the parameters were presented above. Let us note that all the quantities in (3.15) are complex values.

b. *16-QAM*

Here the computation of the LLRs seems to be slightly more complex because one GF(64) symbol does not match into an integer number of 16-QAM symbols. However, if we assume to use the Gray mapping, i.e. real and imaginary parts of the same symbol are uncorrelated, we can assume that each GF(64) symbol is mapped exactly onto one 16-QAM plus one real or imaginary part. The LLRs for each received GF(64) symbols can be computed as devised in (3.16).

$$L_{i,k} = \ln\left(\exp\left(-\rho\sum_{j=0}^{2}\frac{\left(\hat{x}_j - \beta_j \cdot x_j^{(k)}\right)^2}{\lambda_j}\right)\right) \tag{3.16}$$

Unlike the QPSK case the quantities in (3.16) are real values.

c. *64-QAM*

Here the computation of the LLRs is simple thanks to the perfect matching between one GF(64) symbol and a 64-QAM symbol. So the LLRs for each received signal can be computed according to (3.17).

$$L_{i,k} = \ln\left(\exp\left(-\rho\frac{\left|\hat{x}_j - \beta_j \cdot x_j^{(k)}\right|^2}{\lambda_j}\right)\right) \tag{3.17}$$

Similarly to the QPSK case all the quantities in (3.17) are complex values.

3.3.2 Soft Maximum Likelihood demapper

In this section we present the second solution for non-binary demapping, which is based on the ML approach. For uncoded systems (without channel coding) the ML receiver achieves the best performance for orthogonal and non-orthogonal codes. However, this ML receiver performs hard decisions and is not suited for the case of soft-decoders. On the other hand, we observe that the distances in the ML expression perfectly match what is required for the LLRs computation. This second solution aims at obtaining the LLR vector directly from the received MIMO codewords without any operation of equalization, thus avoiding potential information losses in any

intermediate step and hence guaranteeing closer-to-the-optimal performance. This solution is referred as Soft Maximum Likelihood (SoftML) [24].

3.3.2.1 LLR computation using SoftML

Unlike the previous solution, for this SoftML method we stick to matrix-based multi-antenna signal model, i.e. we consider (2.6) as received signal. In this paragraph we will detail the soft demapping, presented for SISO systems for the MIMO system using softML method. Assuming of having received (2.6), eq. (3.4) for MIMO using linear equalizers can be modified as shown in (3.18).

$$L_{i,k} = \ln \frac{\sum\limits_{\mathbf{b} \in B_i^k} P[\mathbf{b}|\overline{\mathbf{Y}}]}{\sum\limits_{\mathbf{b} \in B_i^0} P[\mathbf{b}|\overline{\mathbf{Y}}]} = \ln \frac{\sum\limits_{\mathbf{b} \in B_i^k} p[\overline{\mathbf{Y}}|\mathbf{b}] \cdot P[\mathbf{b}]}{\sum\limits_{\mathbf{b} \in B_i^0} p[\overline{\mathbf{Y}}|\mathbf{b}] \cdot P[\mathbf{b}]} \tag{3.18}$$

where once again $k = 1, \cdots, q$, $\mathbf{b} = [b_0, \cdots, b_{m_1-1}]$ is the coded GF(64) symbol vector and $\overline{\mathbf{Y}}$ is a vector of m_3 matrices, i.e. one for each MIMO codeword. Specifically, each group $\mathbf{b}$ of m_1 GF(64) symbols is mapped over a group of m_3 MIMO codeword, denoted $\overline{\mathbf{Y}}$, where $\overline{\mathbf{Y}} = [\mathbf{Y}_1, \cdots, \mathbf{Y}_{m_3}]$. Assuming again all the coded symbol vector (with length m_1 GF(64) symbols) to be equiprobable and the channel memoryless, we can rewrite the (3.18) as:

$$L_{i,k} = \ln \left(\frac{\sum\limits_{\mathbf{b} \in B_i^k} \prod\limits_{j=0}^{m_3-1} p(\mathbf{Y}_j|\mathbf{b})}{\sum\limits_{\mathbf{b} \in B_i^0} \prod\limits_{j=0}^{m_3-1} p(\mathbf{Y}_j|\mathbf{b})} \right) \tag{3.19}$$

where $\mathbf{Y}_j$ is the j-th received MIMO CW in the vector $\overline{\mathbf{Y}}$. However, for a matter of complexity, it is more convenient to rewrite (3.19) without considering the vector $\mathbf{b}$, but each b_i element (with $i = \{1, \cdots, m_1\}$). In fact each b_i element is mapped onto n_3 MIMO codewords. Specifically, n_3 ($\leq m_3$) is the number of MIMO codewords over which the i-th GF(q) symbol is transmitted. It is fundamental to specify that n_3 *MIMO codewords do not carry exactly one GF(q) symbol, but they transport a piece*

of information greater or equal to a GF(q) symbol. Eq. (3.19) can be rewritten as

$$L_{i,k} = \ln \left(\frac{\prod_{j=0}^{n_3-1} p(\mathbf{Y}_j | b_i = \alpha_k)}{\prod_{j=0}^{n_3-1} p(\mathbf{Y}_j | b_i = \alpha_0)} \right) \tag{3.20}$$

Let us note that, in this second demapping method, modulations symbols are not decoupled from the MIMO codewords, so there might be no matching between one GF(q) symbol and an integer number of MIMO codewords. For this reason we have specified that n_3 MIMO CWs do not necessarely match to one GF(q) symbol, so that this fact might affect the demapping complexity.In the context of this second method, the pdf of the received signal (i.e. the received MIMO CW) can be expressed by:

$$p(\mathbf{Y}_j | \mathbf{S}_j^{(k)}) = \frac{\rho}{\pi} \cdot \exp \left[-\rho \left\| \mathbf{Y}_j - \sqrt{\frac{\rho}{N_T}} \cdot \mathbf{H}_j \cdot \mathbf{S}_j^{(k)} \right\|_F^2 \right] \tag{3.21}$$

where $\mathbf{S}_j^{(k)} = \phi_j(\mu(\alpha_k))$, being $\phi(.)$ and $\mu(\cdot)$ the MIMO coding function and the mapping function, respectively. Instead the Frobenius norm has been indicated by $\|(.)\|_F$. Now substituting (3.21) in (3.20) we obtain:

$$L_{i,k} = \ln \left(\frac{\exp \left(-\rho \sum_{j=0}^{n_3-1} \left\| \mathbf{Y}_j - \sqrt{\frac{\rho}{N_T}} \cdot \mathbf{H}_j \cdot \mathbf{S}_j^{(k)} \right\|_F^2 \right)}{\exp \left(-\rho \sum_{j=0}^{n_3-1} \left\| \mathbf{Y}_j - \sqrt{\frac{\rho}{N_T}} \cdot \mathbf{H}_j \cdot \mathbf{S}_j^{(0)} \right\|_F^2 \right)} \right) \tag{3.22}$$

Since the denominator does not depend on k, we can compute only the first term and then normalize such that $L_{i,0} = 1$.

$$L_{i,k} = \ln \left(\exp \left(-\rho \sum_{j=0}^{n_3-1} \left\| \mathbf{Y}_j - \sqrt{\frac{\rho}{N_T}} \cdot \mathbf{H}_j \cdot \mathbf{S}_j^{(k)} \right\|_F^2 \right) \right) \tag{3.23}$$

However, hereafter we present another manner of formulating the LLR extraction [24], more implementation-oriented. According to [24], the LLR computation using this method can be splitted into two major steps: i) *Euclidean distances computation*, and ii) *Marginalization across all possible combinations*. In the first step, we compute the

distances between each received MIMO CW and any possible combination having the same bit length. In the second step the LLR vector of any received GF(64) symbol is computed. This approach limits the number of distances computed to its lower bound (binary case). Denoting by $\gamma = log_2(q)$ and $\delta = log_2(M) \times Q$, let us introduce the two parameters as shown in (3.24).

$$l_i^{\min} = \left\lfloor \frac{i \cdot \gamma}{\delta} \right\rfloor, l_i^{\max} = \left\lfloor \frac{(i+1) \cdot \gamma}{\delta} - 1 \right\rfloor \tag{3.24}$$

Specifically, parameters $l_i^{\min}$ and $l_i^{\max}$ allow to select the proper MIMO codewords for any received GF(64) symbol, so that the marginatization for each received GF(64) symbol is performed only among the n_3 MIMO codewords encapsulating it. In (3.24) the index i ranges from 0 to $m_1 - 1$. For a memoryless MIMO channel, we can write the k-th ($k = 0, \cdots, q-1$) LLR value for the i-th ($i = 0, \cdots, m_1 - 1$) GF(64) coded symbol as

$$L_{i,k} = \ln \frac{\sum_{\mathbf{b} \in \Delta_i^k} \exp \sum_{l=l_i^{\min}}^{l_i^{\max}} \left\| \mathbf{Y}_l - \sqrt{\frac{\rho}{N_T}} \cdot \mathbf{H}_l \cdot \phi_l \left(\mu(\mathbf{d}) \right) \right\|_F^2}{\sum_{\mathbf{b} \in \Delta_i^0} \exp \sum_{l=l_i^{\min}}^{l_i^{\max}} \left\| \mathbf{Y}_l - \sqrt{\frac{\rho}{N_T}} \cdot \mathbf{H}_l \cdot \phi_l \left(\mu(\mathbf{d}) \right) \right\|_F^2} \tag{3.25}$$

where $\phi_l \left(\mu(\mathbf{d}) \right)$ denotes the l-th MIMO codeword obtained mapping and MIMO encoding vector $\mathbf{d}$. Instead the set Δ_i^k can be computed following the hereafter detailed steps:

a. Allocate a vector of $m_3 \times \log_2(M) \times Q$ bits

b. Insert the binary image of the GF symbol α_k in the positions $[i \cdot \gamma \div (i+1) \cdot \gamma - 1]$, and complete with any possible binary configuration in the remaining positions.

c. Select the $[l_i^{\min} \cdot \delta \div (l_i^{\max} + 1) \cdot \delta - 1]$ bits and discard the others.

The vector $\mathbf{d}$ is one combination within the set Δ_i^k. Since the denominator in (3.25) does not depend on k, we can compute only the first term and then normalize such that $L_{i,0} = 1$.

$$L_{i,k} = \ln \sum_{\mathbf{b} \in \Delta_i^k} \exp \sum_{l=l_i^{\min}}^{l_i^{\max}} \left\| \mathbf{Y}_l - \sqrt{\frac{\rho}{N_T}} \cdot \mathbf{H}_l \cdot \phi_l \left(\mu(\mathbf{d}) \right) \right\|_F^2 \tag{3.26}$$

3.4 Performance Analysis

In this section we present the performance (in terms of Frame-Error-Rate) analysis for different scenarios. The main goal of this section is to achieve a better understanding of: i) which demapping strategy produces better results, when combined with non-binary LDPC codes, ii) which STC is best suited to be integrated in systems employing non-binary LDPC, iii) how the gain between NB LDPC codes and DBTCs evolves from SISO scenarios to the MIMO ones. The complete list of analyzed scenarios is reported in Table (3.2). Specifically, in Table (3.2) we refer to the number of Coded-Bits-per-Channel-use and to the FEC Codeword Length as *CBpcu* and *Cw Length*, respectively.

Table 3.2: *List of simulated scenarios*

Scenario	CBpcu	Code Rate	Cw Length
Scenario 1	4	1/2	96 GF(64) symbols
Scenario 2	4	1/2	384 GF(64) symbols
Scenario 3	4	2/3	96 GF(64) symbols
Scenario 4	4	3/4	96 GF(64) symbols
Scenario 5	4	5/6	96 GF(64) symbols
Scenario 6	4	5/6	384 GF(64) symbols
Scenario 7	12	1/2	96 GF(64) symbols
Scenario 8	12	1/2	384 GF(64) symbols
Scenario 9	4	1/2	48 GF(64) symbols

All the simulations have been performed assuming to exploit the max-Log-MAP approximation of the demapping expression, so that the sum in (3.26) becomes a comparison. This enables to reduce the receiver complexity without introducing appreciable degradation.

3.4.1 Scenarios with spectral efficiency of 2 Bits/s/Hz

The first scenario targets a net spectral efficiency of 2 bits/s/Hz, achieved using STCs providing 4 CBpcu and having a FEC coding rate equal to $\frac{1}{2}$. The codeword length is equal to 576 bits (equivalent to 96 GF(64) symbols). We assume a frequency-flat and time and space independent Rayleigh fading channel. In this first scenario, three different MIMO configurations are evaluated:

a. First configuration (diamond markers) is based on QPSK with SM, detected by the cascade of Linear Equalizers (MMSE) and the Soft Demapper;

b. Second configuration (square markers) is based on QPSK with SM detected by a Soft ML receiver;

c. Third configuration (circular markers) is based on 16-QAM and Alamouti, detected by the cascade of Linear Equalizer (ZF) and the Soft Demapper.

For each configuration, we include the performance of NB LDPC (continuous lines) and its binary counterpart (dashed lines), i.e. DBTCs. We also show the SISO curves (lower triangular markers) at the same spectral efficiency (i.e. 16QAM is used) in order to quantify the evolution of the performance gap between NB LDPC and DBTC when moving from SISO to MIMO configurations. The performance for scenario 1 is depicted in Figure 3.3.

First, let us focus on the non-binary performance and compare the first (a) and the second (b) configurations. The SoftML demapper is shown to outperform the MMSE-based one with a gain of around 1.8 dB at $FER \sim 10^{-3}$. This coding gain can be explained mainly by the fact that the SoftML manages to eliminate cross-channel interference, whilst the MMSE-based demapper does not. This highlight the main drawback with Linear Equalizers used to demap non-orthogonal STCs. Instead Alamouti can be detected using linear equalizers (ZF), without any performance loss (with respect to the SoftML). Let us then compare the second (b) and the third (c) configurations. We can observe that SM (demapped with SoftML) outperforms Alamouti with 0.9 dB SNR gain: this could be explained reminding that Alamouti is a *half-rate* STC, unlike the SM, which is *full-rate*. For this reason in order to perform a fair comparison (at the same spectral efficiency) between Alamouti and SM, we needed to increase the order of the modulation symbols, transmitted in the Alamouti MIMO

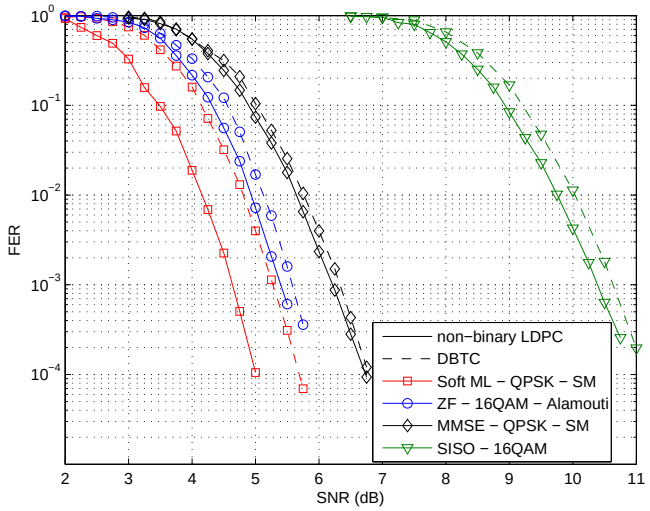

Figure 3.3: *Performance for Scenario 1*

CW. However, Alamouti is a good solution, because it can be demapped with linear equalizers, without any performance detritment, being Alamouti code orthogonal. At the same time we have proved that that SM jointly with NB LDPC has very interesting performance. Now with comparison to DBTC, NB LDPC is shown to provide more gain for the second configuration, i.e. where the SoftML is able to better exploit the channel diversity. For this second configuration, the gain provided by NB LDPC with respect to DBTC is around 0.7 dB. In order to better explain the reasons why the gain between NB LDPC codes and DBTCs is particulary high for the (b) configuration let us introduce the definition of Diversity-per-GF-symbol.

Definition 1 *The* Diversity-per-GF-symbol *(DGFS) is the number of independent paths over which a GF(q) symbol is transmitted.*

Let us note that this definition is different from the traditional definition of *Diversity* in [25]. Specifically, the conventional *Diversity* definition states that the same signal is transmitted over different independent paths, equal to the Diversity order. The DGFS is not the same since one GF(q) symbol might be transmitted in more than one signal

(i.e. MIMO CW). Even though these two definitions are different, using the term Diversity (in the acronym DGFS) we want to emphasize that a GF(q) symbol might be transmitted over different channels, which fade independently. In this way the robustness of the GF(q) symbol turns out to increase, whether the DGFS increases. After having introduced the DGFS definition, we can continue with the explaination of the simulation results for the Scenario 1. Let us observe that for the configuration (b) each GF(64) symbol is mapped onto three modulation symbols and transmitted over two MIMO CWs (note that two MIMO CWs carry more than one GF(64) symbol). So the DGFS is equal to 6 for any transmitted GF(64) symbol. Configuration (a) has the same DGFS, but the cross-channel interferences introduce here a distructive effect. Instead for configuration (c) each GF(64) symbol has a DGFS equal to 4, considering that each MIMO codewords is transmitted over 2 channel uses and also that the Alamouti code (thanks to its orthogonality) eliminates cross-channel signals. For the SISO case the DGFS is instead equal to 2. In summary there is more *diversity* to be recover for the configuration (b), so that this explains why NB LDPC codes provide more gain (wrt DBTCs) in this case. Finally, we can also observe that the gain of NB LDPC increases from SISO to MIMO, when most DGFS is available to be recovered by the NB LDPC codes, i.e. for the configuration (b).

Let us focus now on the second scenario (Figure 3.4). The second scenario targets a net spectral efficiency of 2 bits/s/Hz, achieved using STCs providing 4 CBpcu and having a FEC coding rate equal to $\frac{1}{2}$, but this time the codeword length has been set to 2304 bits (equivalent to 384 GF(64) symbols). The simulated configurations are the same of the previous scenario. The main difference from this scenario and scenario 1 is that the slopes of any simulated configurations are now steeper than their counterpart of scenario 1. This can be easily explained having increased the FEC codeword length from 96 GF(64) symbols to 384 GF(64) symbols, so that longer FEC codewords allow to achieve lower FER performance at lower SNR values. The remaining conclusions that can be drawn from this scenario are the same drawn from Scenario 1: configuration (b) in combination with NB LDPC outperforms any other configurations; NB LDPC are shown to outperform DBTCs with greater gap where more DGFS is available, i.e. configuration (b). Once again NB LDPC codes are shown to produce a greater gain (wrt DBTCs) when moving from SISO to MIMO (when configuration (b) is selected).

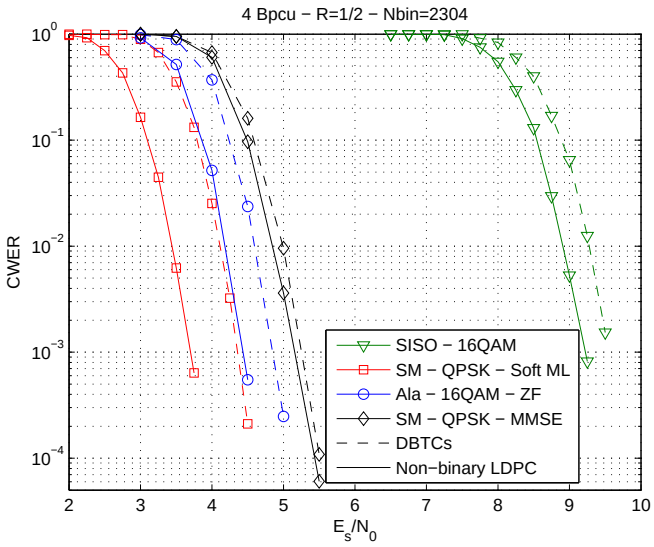

Figure 3.4: *Performance for Scenario 2*

3.4.2 Scenario with spectral efficiency of 2.66 Bits/s/Hz

In this subsection we present the FER performance of the analyzed configurations at a net spectral efficiency of 2.66 Bits/s/Hz, achieved using STCs providing 4 CBpcu and having a FEC coding rate equal to $\frac{2}{3}$. For this scenario the FEC codeword length is equal to 576 bits (equivalent to 96 GF(64) symbols). Once again we assume a frequency-flat and time and space independent Rayleigh fading channel. The analyzed configurations are the same presented in the previous subsection. The performance for this scenario is depicted in Figure 3.5. First let us observe configuration (a) with NB LDPC and compare it with configuration (b): we can appreciate that the gain in favor of configuration (b) now increases up to 2.5 dB at $FER \sim 10^{-3}$. This increase of the SNR gap compared to the two previous scenarios can be explained by the fact that using a channel coding rate of $\frac{2}{3}$, the information is less protected than in the first scenario. So, the cross-channel interference introduces here a more destructive effect than in the first scenario. Similar to our conclusion in the previous scenarios, we find that configuration (b) is the optimal solution and that NB LDPC codes perform

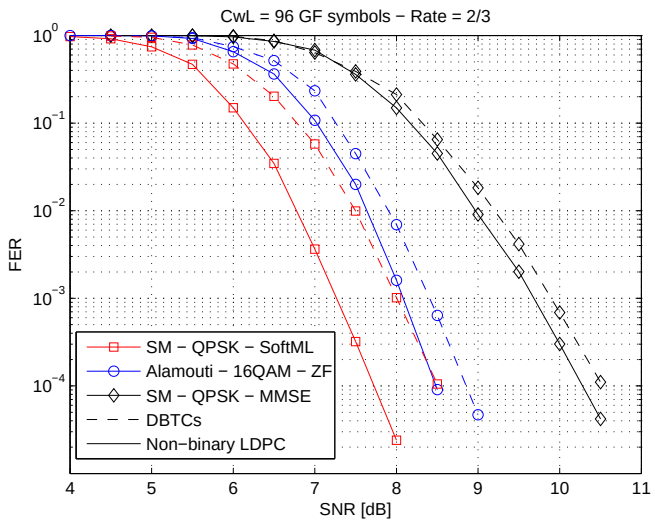

Figure 3.5: *Performance for Scenario 3*

better than DBTCs for any configuration. Specifically, for any configurations we can also notice that the gap between NB LDPC codes and DBTCs is slighly increased (about 0.1 dB) wrt the scenarios with spectral efficiency equal to 2 Bits/s/Hz: this proves that NB LDPC codes perform better than DBTCs for higher code rates.

We can also observe that the slope of the curve representing configuration (c) with NB LDPC codes is now steeper than the one for configuration (b) (still with NB LDPC codes): this is due to the fact that Alamouti code has a diversity order of 4, whereas SM only of 2. This fact does not have any appreciable effect in the previous scenarios, since the information was well protected by the FEC scheme. Now the FEC scheme, being the rate higher, protects transmitted information in a less robust manner, so that the higher diversity of Alamouti permits a steeper slope (than the one for SM) in the waterfall region of the FER performance. Finally, we can observe that the gain in favor of NB LDPC increases from SISO to MIMO whether configuration (b) is employed. This gain for configuration (b) is about 0.9 dB and it can be explained considering that configuration (b) has more DGFS to be recovered than any other analyzed configuration.

3.4.3 Scenario with spectral efficiency of 3 Bits/s/Hz

In this subsection we present the FER performance of the analyzed configurations at a net spectral efficiency of 3 Bits/s/Hz, achieved using STCs providing 4 CBpcu and having a FEC coding rate equal to $\frac{3}{4}$. For the fourth scenario the FEC codeword length is equal to 576 bits (equivalent to 96 GF(64) symbols). Once again we assume a frequency-flat and time and space independent Rayleigh fading channel. The analyzed configurations are the same analyzed in the previous scenarios, i.e.

a. First configuration (diamond markers) is based on QPSK with SM, detected by the cascade of Linear Equalizers (MMSE) and the Soft Demapper;

b. Second configuration (square markers) is based on QPSK with SM detected by a Soft ML receiver;

c. Third configuration (circular markers) is based on 16-QAM and Alamouti, detected by the cascade of Linear Equalizer (ZF) and the Soft Demapper.

The performance for this scenario is depicted in Figure 3.6. Let us observe configuration (a) combined with NB LDPC and compare it with configuration (b) (still in combination with NB LDPC): we can appreciate that the gain in favor of configuration (b) now increases up to 3 dB at $FER \sim 10^{-3}$. This increase of the SNR gap can be explained, coherently with what has been said for the Scenario 3, by the fact that using a channel coding rate of $\frac{3}{4}$, the information is less protected than in the previous three scenarios.

Similar to our conclusion in the previous scenarios, we find that configuration (b) is the optimal solution and that NB LDPC codes perform better than DBTCs for any configuration. For this scenario we can appreciate that each configuration combined with NB LDPC codes has an higher slope in the waterfall region of the FER performance wrt its counterpart employing DBTCs. This clearly confirms that NB LDPC codes performs better than DBTCs in higher spetral efficiencies regimes. Coherently with scenario 3, we can observe that the slope of the curve representing configuration (c) with NB LDPC codes is even more steeper than the one for configuration (b) due to the fact that Alamouti code has higher diversity order than SM. Finally, we can observe that the gain in favor of NB LDPC increases from SISO to MIMO whether configuration (b) is employed. This gain for configuration (b) is about 0.9 dB and it

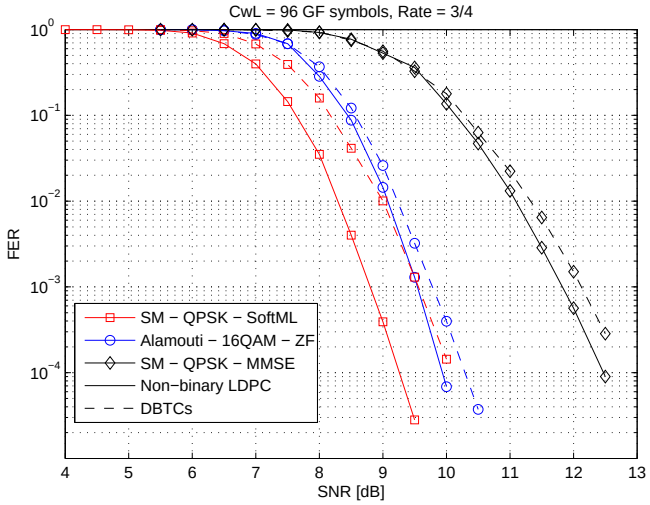

Figure 3.6: *Performance for Scenario 4*

can be explained considering that configuration (b) has more DGFS to be recovered than any other analyzed configuration.

3.4.4 Scenario with spectral efficiency of 3.33 Bits/s/Hz

In this subsection we present the FER performance of the analyzed configurations at a net spectral efficiency of 3.33 Bits/s/Hz, achieved using STCs providing 4 CBpcu and having a FEC coding rate equal to $\frac{5}{6}$. For the fifth scenario the FEC codeword length is equal to 576 bits (equivalent to 96 GF(64) symbols). Once again the analyzed configurations are the same, but we included also the SISO curve at the same spectral efficiency in order to appreciate the evolution of the gap between NB LDPC codes and DBTCs when moving from SISO to MIMO. The performance for this scenario is depicted in Figure 3.7. Let us observe configuration (a) combined with NB LDPC and compare it with configuration (b) (still in combination with NB LDPC): we can appreciate that the gain in favor of configuration (b) now increases up to 4 dB at $FER \sim 10^{-3}$. Once again we observe that configuration (b) is the optimal solution and that NB LDPC codes perform better than DBTCs for any

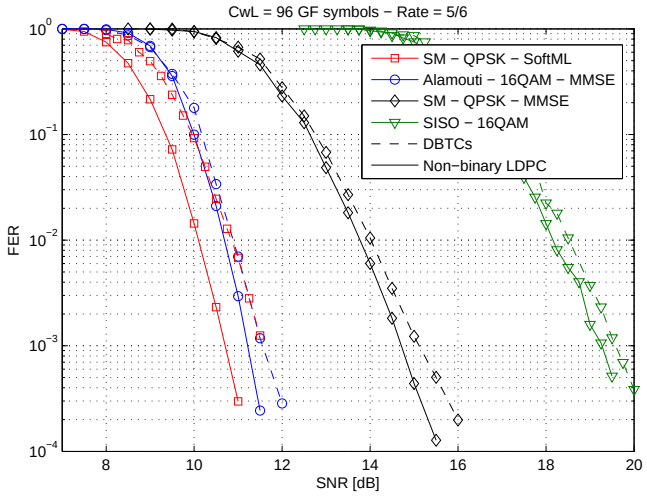

Figure 3.7: *Performance for Scenario 5*

configuration. Coherently with scenario 3, we can observe that the slope of the curve representing configuration (c) with NB LDPC codes is even more steeper than the one for configuration (b) due to the fact that Alamouti code has higher diversity order than SM. Finally, we can observe that the gain in favor of NB LDPC increases from SISO to MIMO whether configuration (b) is employed. This gain for configuration (b) is about 0.9 dB and it can be explained considering that configuration (b) has more DGFS to be recovered than any other analyzed configuration (including SISO).

Figure 3.8 instead reports the performance for Scenario 6, which is based on a spectral efficiency of 3.33 Bits/s/Hz but the FEC codeword length has been set to 2304 bits (equivalent to 384 GF(64) symbols). The only one significant difference from this scenario and scenario 5 is that the slopes of any simulated configurations are now steeper than their counterpart of scenario 5. This can be easily explained having increased the FEC codeword length from 96 GF(64) symbols to 384 GF(64) symbols, so that longer FEC codewords allow to achieve lower FER performance at lower SNR values.

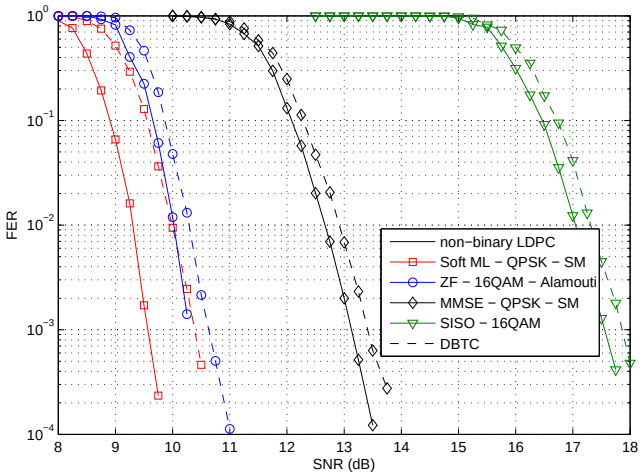

Figure 3.8: *Performance for Scenario 6*

3.4.5 Scenarios with spectral efficiency of 6 Bits/s/Hz

In this subsection we present the FER performance of the analyzed configurations at a net spectral efficiency of 6 Bits/s/Hz, achieved using STCs providing 12 CBpcu and having a FEC coding rate equal to $\frac{1}{2}$. For the seventh scenario the FEC codeword length is equal to 576 bits (equivalent to 96 GF(64) symbols). Once again we assume a frequency-flat and time and space independent Rayleigh fading channel. The analyzed configurations are:

a. First configuration (diamond markers) is based on 64QAM with SM, detected by the cascade of Linear Equalizers (MMSE) and the Soft Demapper;

b. Second configuration (square markers) is based on 64QAM with SM detected by a Soft ML receiver;

The performance for this scenario is reported in Figure 3.9. Once again continuos lines are the performance for configurations with NB LDPC codes, whilst dashed lines are for DBTCs. First of all we can observe that the gain between Soft ML and MMSE is now reduced wrt the previous scenarios. This can be explained considering

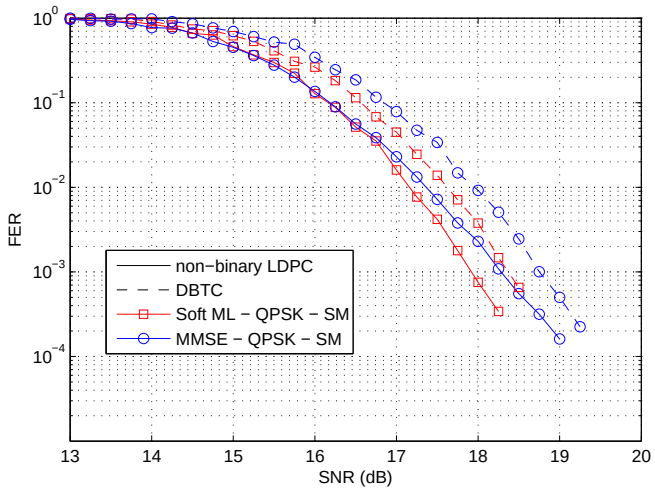

Figure 3.9: *Performance for Scenario 7*

that the DGFS for both configurations is now only 2. This means that there is less *diversity* to be recovered by the Soft ML receiver. However, Soft ML is shown to provide the optimum solution also for cases requiring very high spectral efficiency. In fact the slope of the curve for the configuration (b) is higher than the one for the configuration (a) in the waterfall region. Let us notice that NB LDPC codes perform better than DBTCs also for this scenario.

For the eighth scenario (see Figure 3.10) the FEC codeword length is equal to 2304 bits (equivalent to 384 GF(64) symbols). For this scenario we can draw similar conclusions, with the difference that all the curves are now steeper than in the scenario 6. This is because of the longer channel coding codeword.

3.4.6 Scenario with very short codeword length

In this subsection we present the FER performance of the analyzed configurations at a net spectral efficiency of 2 Bits/s/Hz, achieved using STCs providing 4 CBpcu and having a FEC coding rate equal to $\frac{1}{2}$. For the seventh scenario the FEC codeword length is equal to 288 bits (equivalent to 48 GF(64) symbols). Once again we assume a

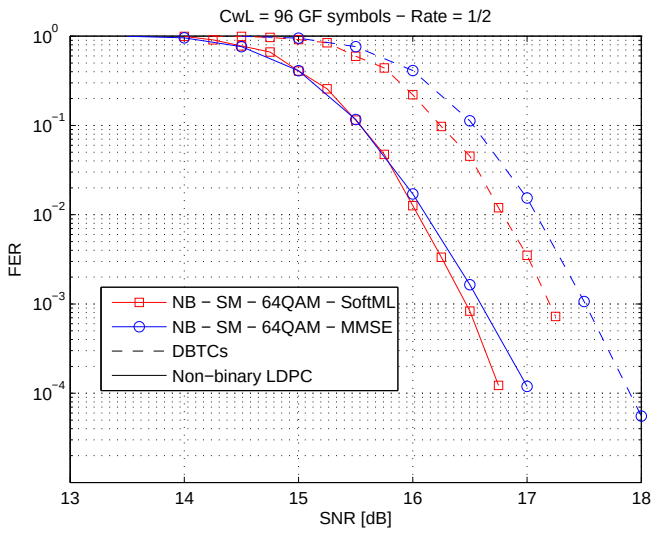

Figure 3.10: *Performance for Scenario 8*

frequency-flat and time and space independent Rayleigh fading channel. The analyzed configurations are:

a. First configuration (diamond markers) is based on QPSK with SM, detected by the cascade of Linear Equalizers (MMSE) and the Soft Demapper;

b. Second configuration (square markers) is based on QPSK with SM detected by a Soft ML receiver;

c. Third configuration (circular markers) is based on 16-QAM and Alamouti, detected by the cascade of Linear Equalizer (ZF) and the Soft Demapper.

First let us observe configuration (a) with NB LDPC and compare it with configuration (b): we can appreciate that the gain in favor of configuration (b) is equal to 1.8 dB at $FER \sim 10^{-3}$. This shows that this gain between configuration (a) and (b) is independent of the FEC codeword length, as can be observed from Figures 3.3, 3.4 and 3.11. Even for scenarios involving very short FEC codeword lengths, we notice that configuration (b) is the optimal solution and that NB LDPC codes

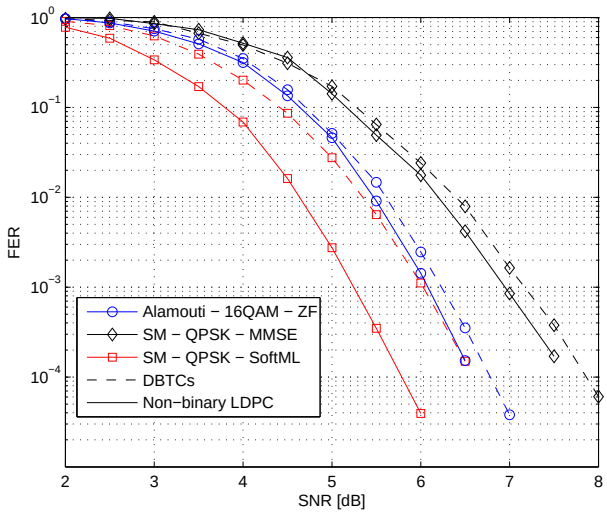

Figure 3.11: *Performance for Scenario 9*

perform better than DBTCs for any configuration. For this scenario the slopes of any curves is now lower than in all the previous scenarios, because of the short codeword length. Now let us observe the three configurations combined with NB LDPC codes: we notice that Alamouti is now steeper than the other curves. This reflects that the short codeword length does not allow to achieve the maximum diversity as instead happened for scenario 1 and 2 (remind that Scenario 1 and 2 have the same spectral efficiency but longer codeword lengths), where no difference in the slopes (between the three MIMO configuration) could be appreciated.

3.5 Complexity of the demapping algorithms

In this section we perform a comparison of the analyzed STCs from the receiver complexity standpoint. First of all we emphasize the causes, which increase the demapping complexity when passing from a linear equalizers-based approach to the Soft ML one. Then we quantify the complexity for the both studied methods in case of different modulation orders. As mentioned in Section 3.3.1 the linear equalizer-based

demapping allows to decouple modulation symbols from the MIMO codewords, so that only the modulation symbols carrying the information associated to the GF(64) symbol under analysis are considered. Hence the complexity of the LLR extraction using linear equalizers depends on the matching between modulation symbols and GF(64) symbols. Specifically, one GF(64) symbol perfectly matches with three QPSK symbols, or one 16QAM plus one real or imaginary part of another 16QAM symbol (assuming to use Gray mapping), or one 64QAM symbol. For this reason the complexity of this method does not necessarily increase if the modulation order (M) increases. We can approximate the complexity of the linear equalizer-based (Γ_{LEd}) demapping with expression (3.27).

$$\Gamma_{LEd} \sim \Gamma_{Eq} + W\left(\frac{\gamma}{ld(M)}\right) \cdot q \tag{3.27}$$

where Γ_{Eq} is the complexity of the linear equalization, and it is independent of the modulation order. The function $W(.)$ takes into account the number of real operation for each element of the LLR vector and depends only on the matching between GF(64) symbol and modulation symbols. Instead the Soft ML demapping does not decouple modulation symbols from MIMO codewords, so that for the computation of the LLR of each GF(64) symbol it might be necessary to consider also part of the MIMO codeword carrying part of another GF(64) symbol. The situation can be better explained through the following Figure 3.12. The stream above represents the m_3 MIMO codewords, which encapsulate the m_1 GF(64) symbols (represented below the MIMO CWs stream). Specifically, this figure is specific for 16-QAM with a STC with $Q = 2$, i.e. Alamouti or SM, where $m_1 = 4$ GF(64) symbols are mapped onto $m_2 = 6$ modulation symbols and transmitted over $m_3 = 3$ MIMO CWs. We can clearly appreciate that GF(64) symbols on the edges (we will refer to them as GF(64) symbol a and d) are transmitted over one MIMO CW, so that, being $n_3 = 1$, the marginalization will be worked out over configurations of δ bits. Instead GF(64) symbols in the middle (we will refer to them as GF(64) symbol b and c) are transmitted over two MIMO CWs, i.e. $n_3 = 2$, so that these marginalizations are more complex. In fact they will be worked out over configurations of $2 \cdot \delta$ bits. The complexity (in terms of performed operations) of the LLR computation using Soft ML can be determined analyzing the computational weight of (3.26). For each received

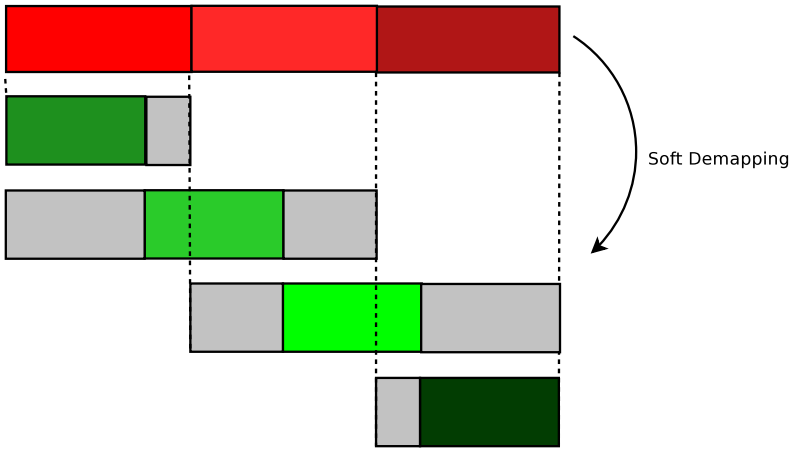

Figure 3.12: *Mismatch between GF(64) symbols and MIMO codewords*

GF(64) symbol, the complexity (Γ_{ML}) of the LLR computationis as follows:

$$\Gamma_{LEd} \leq K\left(N_R, T, Q\right) \cdot 2M^Q + 2^{2\delta-\gamma} \tag{3.28}$$

Table (3.3) reports the complexities for the analyzed demapping methods, in case of different modulations. Specifically, the complexities of the soft demapping are expressed in terms of number of real operations per transmitted coded bit (so that complexities are independent of the FEC rate).

Table 3.3: *Complexities for demapping computation*

	QPSK	**16QAM**	**64QAM**
Alamouti	250	110	65
SM-Soft ML	240	9.6×10^3	1.4×10^6
SM-MMSE	300	150	100

Table (3.3) shows that the Alamouti code can be used with any modulations thanks to the use of (low-complexity) linear equalizers, despite not being the optimum solution in the simulated scenarios. The same conclusion can be drawn for SM

detected with MMSE, but this configuration has been proved not to be particularly interesting from FER perspective. Table (3.3) also shows that SM with Soft ML can be employed with QPSK without complexity issues. The employment of SM with Soft ML in combination with 16QAM and 64QAM might turn out to be too complex, depending on the target hardware and/or application. However, considering that Soft ML (used to demap SM) produces the best FER performance (as proved all along Section 3.4) we would like to be able to apply this demapping method for any modulation orders, without incurring in a complexity bottleneck. For this reason we decided to investigate low complexity algorithms for reducing the intrinsic complexity of the Soft ML demapping. This study will be detailed in the following chapter.

3.6 Conclusions

In this chapter we have investigated two different demapping approaches for non-binary systems, i.e. the linear equalizer-based one and a second technique, which implements a soft version of the Maximum Likelihood demapper (Soft ML). First we have detailed these approaches through analythical descriptions. Then we have compared these methods with their binary counterparts, emphasizing similarities and differences. Later we have moved to the FER performance analysis, which aims to better understand which demapping technique is best suited for non-binary transmission. Specifically, different scenarios have been investigated in order to better understand the general behaviour of the presented methods for different STCs. In some of the analyzed MIMO scenarios we have included the SISO performance at the same spectral efficiency in order to perform a more complete analysis. Through the observation of the simulations results we can draw the following conclusions:

a. The configuration SM with Soft ML has been shown to produce the best results in terms of FER performance. Specifically, the benefits of this configuration are more evident whether combined with a low channel code rate ($\frac{1}{2}$). If the channel code rate increases this configuration keeps on having a coding gain wrt any other configurations, but the slope in the FER curve is not the steeper one. In fact Alamouti (independently of the demapping technique, thanks to the orthogonality) in combination with high channel code rate has been shown to achieve the highest slope.

b. Focusing on SM, the coding gain between Soft ML and linear equalizer-based demapper increases if the channel code rate increases.

c. NB LDPC codes have been shown to outperform DBTCs for any configurations in any simulated scenarios.

d. The gain between NB LDPC codes and DBTCs increases when moving from SISO to MIMO whether the configuration SM with Soft ML is adopted.

Later we have also carry out a complexity analysis for both methods, when different combinations of modulations and STCs are selected. From the complexity analysis we can end up that:

a. The Alamouti code can be used with any modulations thanks to the use of (low-complexity) linear equalizers, despite not being the optimum solution.

b. The same conclusion can be drawn for SM detected with MMSE, but this configuration has been proved not to be particularly interesting from FER perspective.

c. SM with Soft ML can be employed with QPSK without complexity issues. The employment of SM with Soft ML in combination with 16QAM and 64QAM might turn out to be too complex, depending on the target hardware and/or application.

For all these reasons we have decided to deeper analyze the Soft ML algorithm, trying to derive sub-optimal versions, which allow to reduce the demapping complexity. This study will be presented in the following chapter.

Chapter 4

Advances in Mapping and Demapping non-binary LDPC

In the previous chapter we have analyzed the performance of two STCs, combined with NB LDPC codes, using two different soft demapping techniques. In this chapter we will extend our analysis including new STCs, in order to understand which STC is best suitable for MIMO 2×2 systems, employing NB LDPC codes. Then we will derive a low complexity algorithm for soft demapping, jointly with a set of heuristic rules, which state how to design efficient patterns for mapping non-binary information over modulation symbols and/or MIMO codewords.

4.1 Motivation

In chapter 3 we have investigated two different demapping approaches for non-binary systems, i.e. the linear equalizer-based one and a second technique, which implements a soft version of the Maximum Likelihood demapper (Soft ML). Specifically, we have detailed these approaches through analythical and numerical analysis. Different scenarios have been investigated in order to draw preliminary conclusions on the combination between NB LDPC codes and MIMO. Basing on these results, we have realized that different aspects still need to be tackled, i.e.

a. We have observed the performance of two STCs with opposite features, i.e. one aiming at maximizing the system throughput (SM), whilst the other enabling the highest system diversity (Alamouti code). We have ended up that SM is more suitable to be combined in a MIMO 2×2 system from performance

perspective. This is valid only whether SM is demapped using a Soft ML demapping. However, with the current knowledge we cannot conclude that SM is the most suitable STC to be combined with NB LDPC codes. For this reason we still need to analyze the performance of other STCs, which are full rate, but with an higher diversity order as well, e.g. the Golden Code. It will be interesting to evaluate the behaviour of other STCs, which do not maximize throughput or diversity separately, but rather they aim at maximizing the trade-off between throughput and diversity. It might be also interesting to design an ad-hoc STC, and use it as a reference in order to evaluate the goodness of the other STCs.

b. At the end of chapter 3 we have underlined a potential complexity issue, related to the use of the outperforming Soft ML demapping technique. This complexity issue occurs with high order modulation. For this reason we will derived a novel low complexity algorithm, based on the Soft ML.

c. We have also observed that no rules have been devised right now in order to optimize the mapping of the non-binary information over modulation symbols and/or MIMO codewords.

4.2 New STBCs combined with NB LDPC codes

In this section we present the STCs, which we investigate in order to have a deeper understanding of the combination of STCs with NB LDPC codes. The first STC that we analyze, is the Golden Code, introduced in Chapter 2. We strong believe that GC will show interesting results, considering that it has the same diversity order of Alamouti code (i.e. equal to 4), being at the same time *full-rate* like SM. Furthermore, we design an ad-hoc STC, which aims at maximizing the equivalent channel capacity, through an iterative procedure. The choise of designing a STC, which maximize the channel capacity, has been made because, as known from literature [26], [27], the performance of a system using LDPC (binary and NB) or turbo codes depends on the channel capacity. For this reason, before describing the iterative procedure, which enables to derive the ad-hoc space-time matrix, we briefly discuss about the MIMO channel capacity.

4.2.1 Capacity of the MIMO channel

Assuming to have received (3.1), the MIMO channel capacity is defined as [28], [29]

$$C = \max_{p(\mathbf{S})} I(\mathbf{S};\mathbf{Y}) \tag{4.1}$$

where $p(\mathbf{S})$ is the probability distribution of the matrix $\mathbf{S}$, whereas $I(\mathbf{S};\mathbf{Y})$ is the mutual information between matrices $\mathbf{S}$ and $\mathbf{Y}$. Let us remind that

$$I(\mathbf{S};\mathbf{Y}) = H(\mathbf{Y}) - H(\mathbf{Y}|\mathbf{S}) \tag{4.2}$$

where $H(\mathbf{Y})$ is differential entropy of matrix $\mathbf{Y}$, whilst $H(\mathbf{Y}|\mathbf{S})$ is the conditional differential entropy of the vector of matrix $\mathbf{Y}$, given knowledge of matrix $\mathbf{S}$. Since the matrices $\mathbf{S}$ and $\mathbf{V}$ are independent $H(\mathbf{Y}|\mathbf{S}) = H(\mathbf{V})$, Eq. (4.2) becomes

$$I(\mathbf{S};\mathbf{Y}) = H(\mathbf{Y}) - H(\mathbf{V}) \tag{4.3}$$

Maximizing the mutual information $I(\mathbf{S};\mathbf{Y})$ is equivalent to maximizing $H(\mathbf{Y})$. Thus, we can write

$$\mathbf{R_{YY}} = \frac{\rho}{N_T}\mathbf{H}\cdot\mathbf{R_{SS}}\cdot\mathbf{H}^H + \mathbf{I}_{N_R} \tag{4.4}$$

where $\mathbf{R_{SS}} = E\{\mathbf{S}\mathbf{S}^H\}$ is the covariance matrix of $\mathbf{S}$. From literature is well known that the differential entropy $H(\mathbf{Y})$ is maximized when $\mathbf{Y}$ is Zero-Mean Circulant Symmetric Complex Gaussian (ZMCSCG), so that it implies that $\mathbf{S}$ must be ZMCSCG. In this case the differential entropies of matrices $\mathbf{Y}$ and $\mathbf{V}$ are given by:

$$\begin{cases} H(\mathbf{Y}) = \log_2(det(\pi\cdot e\cdot\mathbf{R_{YY}})) \\ H(\mathbf{V}) = \log_2(det(\pi\cdot e\cdot\mathbf{I}_{N_R})) \end{cases} \tag{4.5}$$

Hence the capacity of the MIMO channel can be written as

$$C = \max_{Tr(\mathbf{R_{SS}})=N_T} \log_2\det\left(\mathbf{I}_{N_R} + \frac{\rho}{N_T}\mathbf{H}\cdot\mathbf{R_{SS}}\cdot\mathbf{H}^H\right) \tag{4.6}$$

For a fading channel, the channel matrix $\mathbf{H}$ is random, and so also the associated capacity defined in (4.6) is a random variable. For this reason we define the *Ergodic channel capacity* as the average of (4.6) over the distribution of $\mathbf{H}$:

$$C_E = \max_{Tr(\mathbf{R_{SS}})=N_T} E_{\mathbf{H}}\{\log_2\det\left(\mathbf{I}_{N_R} + \frac{\rho}{N_T}\mathbf{H}\cdot\mathbf{R_{SS}}\cdot\mathbf{H}^H\right)\} \tag{4.7}$$

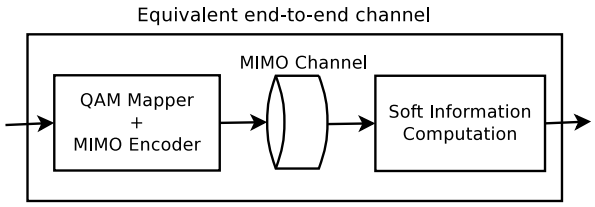

Figure 4.1: *Equivalent end-to-end MIMO channel*

In case of perfect Channel State Information (CSI) at the receiver side, it has been demonstrated that the optimal signal covariance matrix is the identity matrix, i.e. $\mathbf{R_{YY}} = \mathbf{I}_{N_R}$. This means that the antennas should transmit uncorrelated streams with the same average power, so that we can write the Ergodic capacity for systems with perfect CSI at the receiver side, but not at the transmitter:

$$C_E = \max_{Tr(\mathbf{R_{SS}})=N_T} E_{\mathbf{H}}\{\log_2 \det\left(\mathbf{I}_{N_R} + \frac{\rho}{N_T}\mathbf{H}\cdot\mathbf{H}^H\right)\} \tag{4.8}$$

Assuming to analyze a Coded Modulation (CM) system, we need to compute the capacity of the equivalent end-to-end MIMO channel, composed by the blocks of *QAM Mapper+MIMO Encoder*, the *MIMO Channel* and the *Soft Information Computation* (as shown in Figure 4.1). Considering the CM system, the end-to-end capacity can be written as [6],

$$C_{CM} = R_0 - E_{\mathbf{H},\mathbf{S},\mathbf{Y}}\{\log_2\left(\frac{\sum_{\mathbf{S}'\in\Xi} p(\mathbf{Y}|\mathbf{S}',\mathbf{H})}{p(\mathbf{Y}|\mathbf{S},\mathbf{H})}\right)\} \tag{4.9}$$

where $R_0 = \log_2(M)\times N_T$ is the total number of transmitted bits per channel use, Ξ is the set of all the possible MIMO codewords, whereas $p(\mathbf{Y}|\mathbf{S}',\mathbf{H})$ is probability density function of $\mathbf{Y}$ given the matrix channel $\mathbf{H}$ and the transmitted MIMO codeword $\mathbf{S}'$. An efficient method, which is specific for the non-binary case, for computing the end-to-end MIMO channel capacity, instead of working out (4.1), has been proposed in [30]. This method is substantially based on information averaging. According to [30], after some analytical manipulations, we can rewrite (4.1) as,

$$C_{CM} = \log_2(q) + \frac{1}{\zeta\cdot\ln(2)} E\{\sum_{k=0}^{q-1} e^{L_k}\cdot(L_k-\zeta)\} \tag{4.10}$$

where

$$\zeta = \sum_{k=0}^{q-1} e^{L_k} \tag{4.11}$$

where L_k is the LLR vector with q components. Thanks to this method a great complexity reduction in the capacity computation is achieved.

4.2.2 Maximizing the Discrete-input Continuous-output Memoryless Channel capacity

After having introduced the channel capacity, in this section we present the method, which aims to maximize the Discrete-input Continuous-output Memoryless Channel capacity. Before detailing this method, we need to slightly modify the LDC model introduced in 2.4.1. This new LDC model has appeared first on [31]. Following [31] the transmitted space-time matrix $\mathbf{S}$ may be defined as:

$$\mathbf{S} = \sum_{l=1}^{Q} (\alpha_l \cdot \mathbf{A}_l) \tag{4.12}$$

More explicitly, each symbol α_l is dispersed to the N_T spatial and T temporal dimensions using a specific dispersion matrix $\mathbf{A}_l$ and the transmission space-time codeword $\mathbf{S}$ is attained by the linear combination of all the weighted dispersion matrices. Therefore, the codeword is uniquely determined by the set of dispersion matrices $\mathbf{A}_l$ that are known to both the transmitter and the receiver, which are arranged to be linked by $N_T \times N_R$ number of independent paths. Note that in contrast to Eq. (2.13), this model modulates the real and imaginary parts of the symbols using the same dispersion matrix $\mathbf{A}_l$, rather than using another dispersion matrix $\mathbf{B}_l$. The transmitted codewords should satisfy the power constraint given by

$$\mathrm{Tr}\left(\sum_{l=1}^{Q} \mathbf{A}_l^H \cdot \mathbf{A}_l\right) = T \tag{4.13}$$

At the receiver side we can write the received signal in a vector-based notation as:

$$\mathbf{y} = \mathcal{H} \cdot \chi \cdot \mathbf{s} + \mathbf{v} \tag{4.14}$$

where all the matrices and vectors are complex valued, $\mathbf{y} \in \mathcal{C}^{N_R \cdot T \times 1}$, $\mathcal{H} \in \mathcal{C}^{N_R \cdot T \times N_T \cdot T}$, $\chi \in \mathcal{C}^{N_T \cdot T \times Q}$, $\mathbf{s} \in \mathcal{C}^{Q \times 1}$ and $\mathbf{v} \in \mathcal{C}^{N_T \cdot T \times 1}$. Tipically χ is called Dispersion Character

Matrix (DCM) and is defined as:

$$\chi = [vec(A_1), vec(A_2), \cdots, vec(A_Q)] \tag{4.15}$$

where we have defined vec(.) operation as the vertical stacking of the columns of the target matrix. Instead $\mathcal{H}$ is obtained as

$$\mathcal{H} = \mathbf{I} \otimes \mathbf{H} \tag{4.16}$$

where $\otimes$ denotes the Kronecker product and $\mathbf{I}$ is the identity matrix having a size of $T \times T$. The ML estimation of the transmitted signal vector $\mathbf{s}$ is formulated as:

$$\hat{\mathbf{s}} = \underset{\overline{\mathbf{s}} \in \Xi}{\operatorname{argmin}} \|\mathbf{y} - \mathcal{H} \cdot \chi \cdot \overline{\mathbf{s}}\|^2 \tag{4.17}$$

where $\overline{\mathbf{s}}$ is an entry belonging to the set Ξ of all the possible MIMO codewords.

Let us now introduce the definition of DCMC capacity, following the notation of [21]. The DCMC capacity of the ML-detected MIMO system using QAM or PSK signalling is given by:

$$C_{LDC}^{DCMC} = \frac{1}{T}\left(\log_2[F] - \frac{1}{F}\sum_{f=1}^{F} E\{\log_2[\sum_{g=1}^{F} \Upsilon_{f,g}|\mathbf{s}_f]\}\right) \tag{4.18}$$

where F is number of MIMO codeword transmitted over the channel, $f = 1, \cdots, F$ and

$$\Upsilon_{f,g} = -\|\mathcal{H} \cdot \chi(\mathbf{s}_f - \mathbf{s}_g) + \mathbf{v}\|^2 + \|\mathbf{v}\|^2 \tag{4.19}$$

After having defined the new LDC model, we can present the random search algorithm (RSA), which targets the maximization of DCMC capacity. This algorithm was introduced in [31]. The RSA randomly generates a matrix χ from some specific distribution, for example the Gaussian one. This fact explains the reason why Heath and Paulraj needed to remodel the LDC: thanks to their new model just one matrix needs to be randomly searched, whilst with the original LDC model, the RSA would have required two iterative processes, i.e. one for LD matrix multiplying the real part of the transmitted symbols and another multiplying the imaginary part. Then, the corresponding diversity order and the coding gain is maximized by checking the rank and determinant criteria [32]. The RSA has the advantage of providing a wide variety of legitimate LDCs. However, since the search is random based, the algorithm

does not guarantee to find the optimum matrix, i.e. the matrix, which maximizes the DCMC capacity. Finally, we can state the steps of the RSA:

a. Randomly generate the complex-valued matrix $\overline{\chi} \in \mathcal{C}^{N_T \cdot T \times N_T \cdot T}$ using the Gaussian distribution.

b. If we arrange the system to satisfy $Q \geq N_T \cdot T$, the candidate DCM χ has to be a unitary matrix. It has been shown in [33] that a complex-valued matrix can be factored into the product of a unitary matrix and an upper triangular matrix using the QR decomposition [33]. Thus, a random dispersion character matrix can be obtained by $\chi = \frac{1}{\sqrt{N_T}} \cdot QR(\overline{\chi})$, which satisfies $\chi\chi^H = \frac{1}{N_T} \cdot \mathbf{I}$.

c. By contrast, if we confine the LDC schemes to $Q < N_T \cdot T$, the DCM χ has to satisfy $\chi\chi^H = \frac{T}{Q} \cdot \mathbf{I}$ and it can be generated by retaining the first Q columns of the unitary matrix obtained using the QR decomposition of $\sqrt{\frac{T}{Q}} \cdot QR(\overline{\chi})$.

d. Having searched through the entire set of legitimate dispersion character matrices, we choose that particular one, which maximizes the DCMC capacity.

Following the procedure just described we manage to obtain a linear dispersion code, which maximizes the DCMC capacity. From now on we will refer to this numerically derived STC as Random Search-based STC (RS LDC). Figure 4.2 reports the channel capacities for different STCs, i.e. SM, GC and RS LDC. These curves have been obtained through numerical simulations of Eq. (4.10). Ergodic curve has been included as reference. We can clearly appreciate that RS LDC outperforms the other analyzed STCs in terms of capacity, as expected from the theory described above. This gain in favor of RS LDC might reach the value of 1 dB in the SNR regime around 6-10 dB.

Now we concern on the evaluation of the FER performance of the new STCs, in order to evaluate if a gain in the capacity curve necessarily traduces into a gain in the FER performance. Results jointly with related conclusions are reported in the following subsection.

4.2.3 Performance analysis of the new STCs

In this section we evaluate the numerical results of the Soft ML demapping used to demap the new STCs, i.e. the Golden Code and the RS LDC. For every configuration,

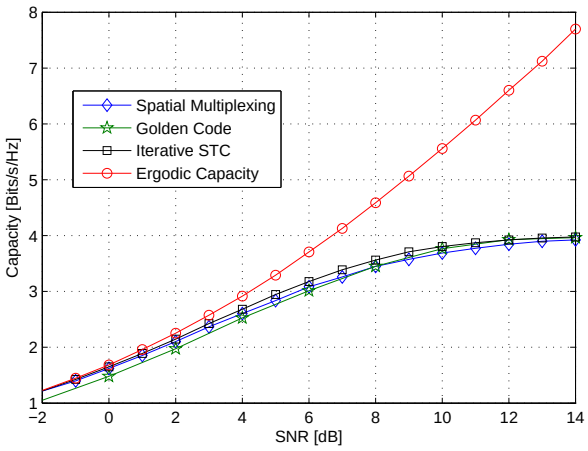

Figure 4.2: *Capacity of different STCs*

the NB LDPC block length is $N_{bin} = 576$ bits, i.e., 96 coded GF(64) symbols. The first and the second scenarios present a spectral efficiency of 2 bits/s/Hz and 2.66 bits/s/Hz, obtained with STCs providing up to 4 bits-per-channel-use and adopting a NB LDPC matrix with code rate equal to $\frac{1}{2}$ and $\frac{2}{3}$, respectively. For all the STCs, apart from Alamouti, we compute the LLRs with the Soft ML technique specified in the previous section. Performance for the different scenarios is reported in Fig. 4.3 and 4.4, respectively. In Fig. 4.3 we can observe that Spatial Multiplexing (square markers) has a coding gain of 0.5 dB at $FER \sim 10^{-4}$ with respect to the couple GC (lower triangular markers) and RS LDC (diamond markers). This coding gain is even more relevant with respect to the Alamouti code (circular markers). Let us now observe Fig. 4.4: we can appreciate that the coding gain between SM and the couple GC and RS LDC is now reduced up to 0.1 dB at $FER \sim 10^{-4}$. We can also observe that the curve for the Alamouti code has the higher slope in this scenario.

Fig. 4.5 and 4.6 show the performance of the 3 bits/s/Hz and 3.33 bits/s/Hz scenarios, respectively. These figures have been obtained with STCs providing 4 Bits-per-channel-use and employing a NB LDPC matrix with code rate equal to $\frac{3}{4}$ or $\frac{5}{6}$. In these scenarios GC and RS LDC outperform SM. Specifically, the gain in favor of GC/RS LDC (wrt SM) is negligible at $FER \sim 10^{-4}$ for code rate =

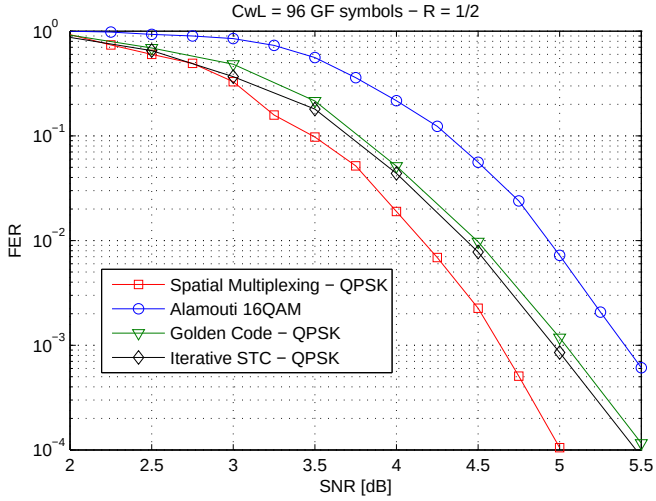

Figure 4.3: *Performance at 2 bits/s/Hz*

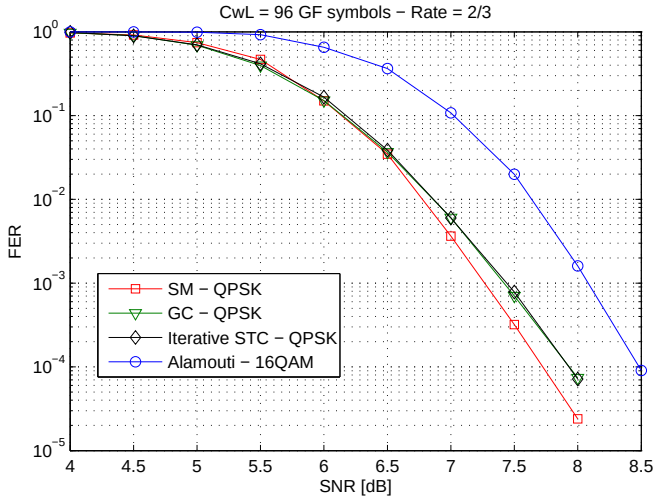

Figure 4.4: *Performance at 2.66 bits/s/Hz*

$\frac{3}{4}$ and 0.3 dB at $FER \sim 10^{-3}$ for code rate $=\frac{5}{6}$. Our results can be explained considering that SM has diversity order equal to 2, whereas GC and RS LDC have a diversity of 4. This difference in diversity order has no impact for those cases where information is well protected with a low code rate, as shown in Fig. 4.3 and 4.4. When on the contrary information is less protected by the FEC, the intrinsic higher robustness of STC with diversity order equal to 4 (GC and RS LDC) outperforms SM. We also notice that the performance of GC and SM is very similar to that of RS LDC, in spite of the latter having been explicitly designed to maximize the end-to-end DCMC capacity: this proves that both GC and SM have excellent performance. Alamouti code has a diversity order equal to 4, but it is a half rate STC, so it needs a 16QAM modulation in order to be compared with the other STCs at the same spectral efficiency in terms of bits/MIMO channel use. This increase in the constellation order affects the performance, so that 16QAM with Alamouti code is outperformed by the other STCs.

Finally, we compare the analyzed STCs from the receiver complexity standpoint. The complexity (in terms of performed operations) of the LLR computation for the STCs, using soft ML and the ZF can be computed as stated by (3.28) and (3.27), respectively. Table 1 reports the complexities of the soft demapping, in terms of number of real operations per transmitted coded bit (so that complexities are independent of the FEC rate). Table 1 shows that GC and RS LDC used in combination with 16QAM and 64QAM are unpractical solutions owing to their huge demapping complexity; the Alamouti code can be used with any modulations thanks to the use of (low-complexity) linear equalizers, despite being outperformed by the other STCs in the simulated scenarios. SM can be employed with QPSK and 16QAM without complexity issues.

Table 4.1: *Complexities for demapping computation, including new STCs*

	QPSK	**16QAM**	**64QAM**
Alamouti	250	110	65
SM-Soft ML	240	9.6×10^3	1.4×10^6
GC-Soft ML	2.6×10^4	5.4×10^8	2.4×10^{13}
RS LDC-Soft ML	2.6×10^4	5.4×10^8	2.4×10^{13}

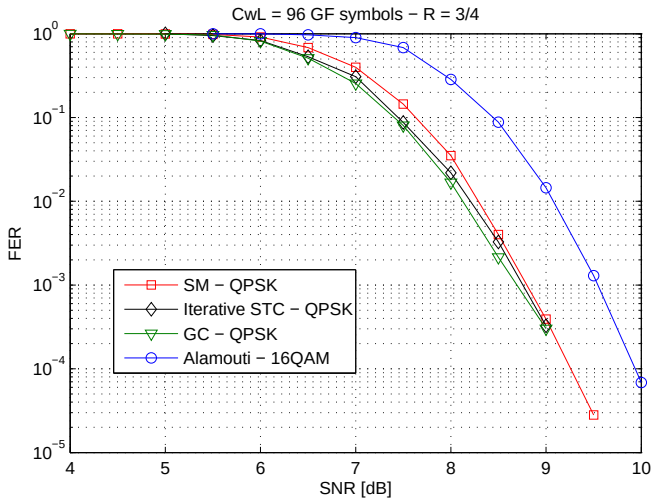

Figure 4.5: *Performance at 3 bits/s/Hz*

In this section we have investigated the combination of NB LDPC codes with MIMO techniques from the FER performance perspectives, including new STCs. Specifically, we have derived the performance of the link with different STCs and in scenarios with spectral efficiencies ≤ 3.33 Bits-per-channel-use. For low channel code rates ($\leq \frac{2}{3}$) SM outperforms any other STCs by up to 0.5 dB in the waterfall region; for scenarios with higher channel code rate, GC and RS LDC are shown to have better performance than SM by about 0.3 dB. Unfortunately complexity analysis of demapping in terms of the required number of real operations per coded bit shows that SoftML becomes unaffordable in the case of GC or RS LDC with high order modulations (16QAM and 64QAM). Hence the only concrete possibility for very high spectral efficiencies (up to 10 Bits-per-channel-use), detected with SoftML, is represented by SM, which is not particularly affected by complexity issues. Alamouti coding is admittedly the least complex solution, but it is outperformed by the other STCs.

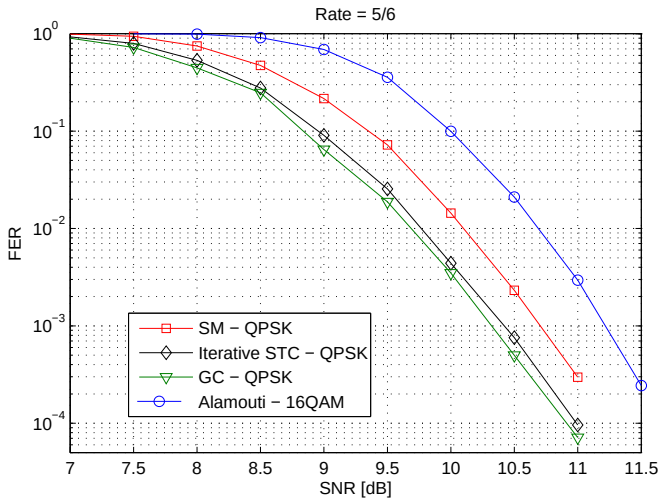

Figure 4.6: *Performance at 3.33 bits/s/Hz*

4.3 Design of advanced mapping patterns

In this section we introduce one of the main contribution of this work, i.e. the definition of a set of rules, which states how to map non-binary information over the modulation symbols (for the SISO case) and over the MIMO codewords (obviously in the MIMO case). From now on in this chapter we focus on those cases, where one GF(q) coded symbol spreads across multiple QAM symbols and MIMO codewords, i.e. where the complexity of the non-binary soft demapping might be more severe. For this reason in the mapping patterns definition we do not target the diversity maximization, rather the optimization of the trade-off between diversity and demapping complexity. A block diagram, reflecting the changes applied to the non-binary transmitter in order to implement the "optimized" patterns, is depicted in Figure 4.7.

In order then to map the non-binary FEC codeword onto the QAM constellation symbols, each of the GF(q) symbols in the interleaved FEC codeword is first converted back to its binary image of γ bits (using the same primitive polynomial in (1.7)). The resulting binary stream is then passed to the *Intra-block Permutation*, which permutes/rearranges the bits (per block of m_1 GF(q) symbols) in the binary

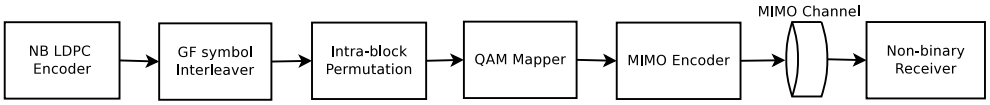

Figure 4.7: *System model including the* Intra-block Permutation

stream in accordance with three design rules devised hereafter to achieve the trade-off between performance and complexity. Next to the intra-block permutation, each group of $log_2(M)$ adjacent bits of the permuted output stream is mapped onto one QAM constellation symbol. A conventional gray-mapping is used to produce the stream of complex-valued QAM symbols. The QAM symbols are then directly sent for transmission over the wireless multi-path fading channel in case of a single antenna transmission. In the context of multiple multi-antennas transmissionat the transmitter, the stream of QAM symbols undergoes a further step of spatial encoding represented by the MIMO encoder depicted in Figure 4.7. The QAM symbols are arranged in groups of Q symbols, and each group is encoded by the MIMO encoder resulting into a MIMO codeword, which is then transmitted across the multiple antennas through the multi-path fading channel.

Let us now detail the *Intra-block Permutation*, which implements the novel mapping strategy targeting the maximization of the trade-off between information diversity and demapping complexity. This mapping strategy has been first introduced in [34]. Once again let us recall that our solution is particularly efficient for those case, where one GF(q) symbol spreads across different QAM symbols and MIMO codewords (i.e. $m_1 > 1$). Specifically, the proposed mapping strategy consists of a set rules, which stem from an in-depth understanding of the APP computation required for non-binary LDPC coupled with ML detection for MIMO receivers. We can observe that these rules are designed for MIMO scenarios, but they can be applied even in the SISO case. Let us now specify that we refer to the in-phase and quadrature components of a modulation symbol as the **I** and **C** component. We use the letter **C** for the quadrature component in order to avoid misunderstanding with the term Q, i.e. the number of modulation symbols in a MIMO codeword.

- **First Rule: The I and C component of an QAM symbol should carry (in part or in full) the binary image of only one GF(q) symbol.**

This rule naturally applies to the particular case of $m_1 = 1$, and can always be met whenever the number of bits per GF(q) symbol γ is an integer multiple of the number of bits per I or C component $log_2(M)/2$. Otherwise, the rule requires mapping as many I and C components as possible to binary sub-parts issued from the binary image of only one single GF(q) symbol. This ensures better performance compared to all other schemes not obeying to this rule, as will be proven shown in Section 4.5.

Assuming SISO 16QAM with $m_1 = 2$ and $m_2 = 3$, Table 4.2 gives four possible patterns to map the two GF(64) symbols **a** and **b** with binary images respectively, $a_0a_1a_2a_3a_4a_5$ and $b_0b_1b_2b_3b_4b_5$, onto the three 16QAM symbols with **I** and **C** components, $\mathbf{I_0C_0}$, $\mathbf{I_1C_1}$, and $\mathbf{I_2C_2}$. Amongst the four patterns shown in Table 4.2, only **P1** and **P3** obey the first rule.

Table 4.2: *Four mapping patterns for SISO case, specific for $q = 64$ with 16QAM*

Pattern	$\boldsymbol{I_0}$	$\boldsymbol{C_0}$	$\boldsymbol{I_1}$	$\boldsymbol{C_1}$	$\boldsymbol{I_2}$	$\boldsymbol{C_2}$
P1	a_0a_1	a_2a_3	a_4a_5	b_0b_1	b_2b_3	b_4b_5
P2	a_0b_0	a_1b_1	a_2b_2	a_3b_3	a_4b_4	a_5b_5
P3	a_0a_1	b_0b_1	a_2a_3	b_2b_3	a_4a_5	b_4b_5
P4	a_0b_0	b_1a_1	a_2b_2	b_3a_3	a_4b_4	b_5a_5

- **Second Rule: Map as many I/C components as possible issued from the same GF(q) symbol onto the same MIMO codeword.**

  This will ensure a minimum number ($n_3 \leq m_3$) of MIMO codewords to be considered by the soft demapper for the computation of the APP values of each GF(q) symbol, and so will contribute to the reduction of the complexity of Soft ML demapping as proposed in Section 4.4, but to the detriment of limiting the maximum DGFS that can be achieved within one GF(q) symbol. This is because ideally by letting each I or C component issued from one GF(q) symbol map onto different MIMO codewords, we create higher chance for these parts of the same GF(q) symbol to experience uncorrelated channel fading. This rule clearly restricts the freedom to let the GF(q) symbol benefit higher channel selectivity,

but fortunately has the advantage of reducing drastically the complexity of the soft ML demapper. This is where the complexity of the soft ML demapper is traded off with the error protection performance of the GF(q) symbols.

- **Third Rule: Under the constraint of the second rule, map the I/C components issued from one GF(q) symbol onto the transmission units ideally of independent channel fading within the MIMO codeword carrying this GF(q) symbol.**

  This rule obviously targets the maximum achievable DGFS for each GF(q) symbol under the constraint of the second rule. As introduced in Chapter 3, the DGFS is number of independent paths over which a GF(q) symbol is transmitted. The higher the DGFS, the better error protection performance is expected to be. The margin for this rule to achieve higher DGFS is clearly bound by the second rule.

For example, in the case of MIMO spatial multiplexing ($Q = 2$) and 16QAM where $m_1 = 4$, $m_2 = 6$, and $m_3 = 3$, we give three possible patterns (Table 4.3 for mapping the four GF(64) symbols, **a**, **b**, **c**, and **d**, of binary images respectively, $a_0a_1a_2a_3a_4a_5$, $b_0b_1b_2b_3b_4b_5$, $c_0c_1c_2c_3c_4c_5$, $d_0d_1d_2d_3d_4d_5$, onto the six 16QAM symbols representing three MIMO codewordSTBC codewords. Each MIMO codeword carries $Q = 2$ 16QAM symbols concurrently transmitted over 2 antennas (**A1** and **A2**).

Table 4.3: *Different mapping patterns for MIMO case with 16QAM*

Pattern	Antenna	I_0	C_0	I_1	C_1	I_2	C_2
P1	**A1**	a_0a_1	a_4a_5	b_2b_3	b_4b_5	c_4c_5	d_0d_1
	A2	a_2a_3	b_0b_1	c_0c_1	c_2c_3	d_2d_3	d_4d_5
P2	**A1**	a_0a_1	b_0b_1	a_2a_3	b_2b_3	a_4a_5	b_4b_5
	A2	c_0c_1	d_0d_1	c_2c_3	d_2d_3	c_4c_5	d_4d_5
P3	**A1**	a_0a_1	a_4a_5	b_2b_3	c_0c_1	c_4c_5	d_0d_1
	A2	a_2a_3	b_0b_1	b_4b_5	c_2c_3	d_2d_3	d_4d_5

All three patterns follow the first rule by not mixing bits from different GF(64) symbols into the same I or C component. Patterns **P1** and **P3** further obey the second

rule by mapping as many I/Q components from the same GF(64) symbol as possible into the same MIMO codeword, whilst pattern **P2** does not. For patterns **P1** and **P3**, GF(64) symbols a and d are carried within one single MIMO codeword, and GF(64) symbols b and c are mapped onto two MIMO codewords. However, for pattern **P2**, each GF(64) symbol is spread out over all of the $m_3 = 3$ MIMO codewords. In terms of complexity of the soft demapper, patterns **P1** and **P3** will enable reduced complexity, whereas the complexity with pattern **P2** will be drastically higher, as shown later in Section 4.4. Now let us observe the first GF(64) symbol $\mathbf{a} = [a_0 a_1 a_2 a_3 a_4 a_5]$ in Pattern **P1** (Table 4.3). This GF(64) symbol is transmitted over two QAM symbols, within only one MIMO codeword: the first QAM symbol is transmitted over the first antenna port,so that it is received through 2 independent paths. The second QAM symbol, containing the remaining part of this GF(64) symbol, is transmitted over the second antenna port and again received through 2 independent paths. So its total DGFS is equal to 4. Following this definition, pattern **P1** achieves a DGFS=4 for any transmitted GF symbol, whereas pattern **P3** achieves a DGFS=4 for GF(64) symbol **a** and **d**, and a DGFS=6 for GF(64) symbol **b** and **c**, with a resulting average DGFS equal to 5. This difference in DGFS between pattern **P1** and **P3** is due to the fact that **P3** respects the third rule, whilst **P1** does not. Pattern **P2** however achieves the maximum DGFS equal to 6 for all four GF(64) symbols but as highlighted earlier it breaks the second rule (i.e. requires a much higher complexity at the receiver). In summary, by obeying all the three rules introduced above, we aim to obtain mapping patterns which ensure the best trade-off between performance and complexity. This will be further detailed and proven in the following sections.

4.4 Low complexity soft demapping algorithms

As highlighted in the third Chapter, the soft demapper at the receiver requires two major operations for the computation of the LLR values of the GF(q) coded symbols: i) **Euclidean distances computation**, and ii) **Marginalization across all possible combinations**. The Euclidean distances computation is typically required for ML hard detector. In our case, since soft values are required, the MIMO ML detection and non-binary soft demapping are combined together into one single function, referred to as Soft ML demapping.

a. **Computation of the Euclidean distances**

In the decoding of the STC, each received MIMO codeword is processed individually in order to obtain its distance to all possible transmitted MIMO codewords. In our non-binary case ($q > 2$), one GF(q) coded symbol may span more than one MIMO codeword. Thus, for the computation of the LLRs of one GF(q) symbol, there is a need to store the Euclidean distances of all the MIMO codewords which carry the binary image of the given GF(q) symbol. Thanks to our second rule in the design of the mapper at the transmitter (which limits the number of MIMO codewords carrying the binary image of one GF(q) symbol to the minimum possible), only the Euclidean distances of $n_3 \leq m_3$ MIMO codewords are needed. This clearly reduces the memory requirements at the receiver.

b. **Marginalization across all possible combinations**

The marginalization takes the form of a summation in the general case (i.e. Log-MAP) reflected in eq. (6). Whether the Max-Log approximation is used, it takes instead the form of a comparison. The marginalization (or summation) involves the Euclidean distances of $n_3 \leq m_3$ MIMO codewords and the binary sub-parts of the $n_1 - 1$ ($n_1 \leq m_1$) GF(q) symbols multiplexing with the binary image of the desired GF(q) symbol in their mapping to the $n_2 \leq m_2$ QAM symbols and $n_3 \leq m_3$ MIMO codewords.

For the sake of simplicity, let us consider first the case where $n_3 = 1$, i.e. the desired GF(q) symbol is mapped onto a single MIMO codeword. This is the case of SISO transmission but also applies for instance to MIMO transmission for the edge GF(q) symbols **a** and **d** in patterns **P1** and **P3** in Table 4.3. Let us focus first on the simple case of SISO transmission with 16QAM as in Table 4.2 with the straightforward mapping **P1** for $m_1 = 2$ and $m_2 = 3$. In order to compute the APP values for the first GF(64) symbol **a**, the Euclidean distances involving the first $n_2 = 2 \leq 3$ QAM symbols are required. For the second GF(64) symbol **b**, those involving the second and the third QAM symbols are required. For the computation of the APP values of **a**, a marginalization is required across all of the possible combinations of the sub-part $b_0 b_1$ from GF(64) symbol **b** due to its mix with the sub-part $a_4 a_5$ in the second QAM symbol (i.e. $a_4 a_5 b_0 b_1$]). The number of all possible combinations is clearly equal to

$2^2 = 4$. The number of operations per received GF(64) symbol is $(q-1) \times 2^2 \times 3$, a factor $2^2/q^{m_1-1} = 4/64 = 1/16$. This is thanks to the specific mapping where the two edge 16QAM symbols carry information from only one single GF(64) symbol. Consider now the more general case of $n_3 > 1$, for example in the case of MIMO transmission for the middle GF(64) symbols **b** and **c** in patterns **P1** and **P3** in Table 4.3, the GF(64) symbol **b** is mapped onto the first $(a_0a_1a_2a_3a_4a_5b_0b_1)$ and second $(b_2b_3b_4b_5c_0c_1c_2c_3)$ MIMO codewords. The marginalization here is required across all the possible combinations of $a_0a_1a_2a_3a_4a_5$ due to the mix with the sub-part b_0b_1 in the first MIMO codeword, and also across all of the possible combinations of $c_0c_1c_2c_3$ due to the mix with the sub-part $b_2b_3b_4b_5$ in the second MIMO codeword. This adds up to the total of $2^6 \times 2^4 = 1024$ combinations per APP value. Demapping complexity clearly depends on the mapping pattern used. In fact Table 4.4 gives an example of the number of distances required for marginalization of each APP value for the two mapping patterns **P2** and **P3** from Table 4.3.

Table 4.4: *Example of number of combinations to be considered for APP marginalization.*

Num. of combinations	**P2**	**P3**
GF**(64) symbol a**	$q^{m_1-1} = 262144$	$2^2 = 4$
GF**(64) symbol b**	$q^{m_1-1} = 262144$	$2^4 \times 2^6 = 1024$
GF**(64) symbol c**	$q^{m_1-1} = 262144$	$2^4 \times 2^6 = 1024$
GF**(64) symbol d**	$q^{m_1-1} = 262144$	$2^2 = 4$

Table 4.4 reflects the huge complexity incurred with mapping pattern **P2** (although as said earlier, this pattern achieves the maximum transmit diversity order 3 for all the GF(64) symbols). This confirms the tremendous complexity advantage of the mapping patterns respecting the second rule devised previously. Yet, whilst only 4 combinations are required for the edge symbols **a** and **d**, 1024 combinations are required for the symbols in the middle **b** and **c**, which is still relatively a high number.

Still, 1024 is a relatively large number causing excessive complexity. To further reduce the number of combinations to a relatively low level, we propose the following algorithm which exploits the correlation existing between GF(64) symbols produced by the code. The algorithm introduces a threshold parameter called N_m. The

algorithm proceeds with the following steps:

- **Step 1:** Set the value of N_m. For example, N_m is set to the value equal to 8.
- **Step 2:** For any GF(q) symbol entailing a number N_e of combinations required for marginalization lower than the threshold N_m, obtain the corresponding APP values using an exhaustive search over all N_e required combinations.

  Example: This applies to the edge GF(64) symbols **a** and **d** in **P1** and **P3** in Table 4.3, where the number of combinations required is $N_e = 4 < N_m = 8$.
- **Step 3:** For GF(q) symbols that multiplex **only** with symbols falling under Step 2, compute the APPs by limiting the combinations associated with the GF(q) symbol from step 2 only to the ones yielding the Nm largest APPs for this symbol.

  Example: Assume we are transmitting 3 consecutive GF(256) symbols ε,υ, and φ mapped onto 2 consecutive MIMO codewords with 64QAM symbols. Then GF(256) symbols ε and φ fall under Step 2, while the APPs for υ have to be computed as above. Assuming $N_m = 16$, then the marginalization over ε and υ will be carried out by considering only $N_m \cdot N_m = 256$ terms instead of the $256 \cdot 256 = 65536$ terms of in the exhaustive search.

  NB: Switching to GF(256) in this example is simply because no such case occurs with our default GF(64).
- **Step 4:** For each remaining GF(q) symbol, not falling under step 2 and 3, proceed with the following sub-steps:
  - **Step 4.1:** Limit the combinations associated with the multiplexing GF(q) symbol from step 2 to the ones yielding the N_m maximum APP values for this multiplexing symbol.
  - **Step 4.2:** Complete the marginalization of the APPs with respect to the adjacent GF(q) symbol whose APPs are still unavailable with an iterative procedure for a number r of iterations and depending on a parameter N_q. At i-th iteration, the marginalization runs across the N_q combinations of the interleaved symbol with the highest N_q APP values. Such combinations are those computed in the previous i-1 iteration of the algorithm. At the initialization stage, the N_q combinations are chosen randomly.

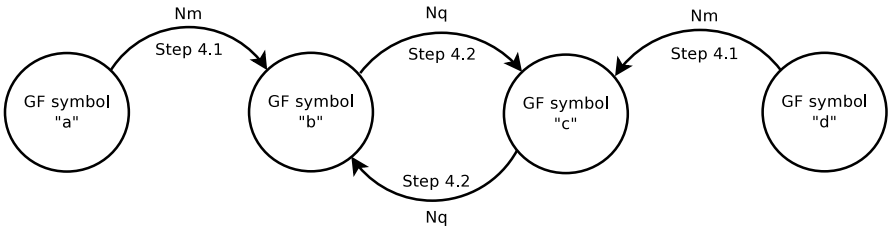

Figure 4.8: *Low complexity algorithm for soft demapping with* $m_1 = 4$

Example: Step 4.1 applies to the middle GF(64) symbol **b** in **P1** and **P3** in Table 4.3, where marginalization is required across the interleaved edge GF(64) symbol **a**. The APP values of the edge GF(64) symbol **a** are obtained from Step 2. Thus, instead of searching over all the $2^6 = 64$ possible values of GF(64) symbol **a**, we only limit the search to the $N_m = 8$ values of symbol **a** yielding the highest APP values (thus 8 highest likelihood values). Step 4.2 applies to the middle GF(64) symbol **b** in **P1** and **P3** in Table 4.3, where marginalization is required across the interleaved other middle GF(64) symbol **c**, whose APP values are not available from Step 2. We start considering $N_q = 8$ randomly selected APP values for symbol **c** (out of the $2^4 = 16$ values theoretically needed) to obtain the (marginalized) APP values of symbol **b**. Then, we compute the APP values for symbols **b** and **c**, with the marginalization limited to the N_q random values of each. We refine then the choice of the N_q combinations used for marginalization to the ones yielding the highest N_q APP values for symbols **b** and **c**. This is repeated for r iterations.

The above algorithm may be better illustrated with the graph depicted in Figure 4.8, where the nodes represent the computation of the APP values for each GF(64) symbol, and the arrows indicate the propagation of the most likely combinations of one GF(64) symbol at a given node to the GF(64) symbol at an adjacent node.

This for the purpose of reduced marginalization according the different steps described in the above algorithm. The edge symbols **a** and **d** fall under step 2 and will therefore get their APP values available simply from step 2. The middle symbols **b** and **c** make use of N_m most likely combinations yielding the highest APP values for the

eddge GF(64) symbol **a** and **d**, respectively. The propagation of these combinations is illustrated in Figure 4.8 by the arrows coming into nodes **b** (from node **a**) and **c** (from node **d**). Since symbols **b** and **c** multiplex together, then an iterative process as described in step 4.2 is followed by reusing the N_q most likely combinations of one symbol for marginalization to obtain the APP values of the adjacent symbol. This exchange of N_q combinations between GF(64) symbols **b** and **c** is illustrasted in the graph by the arrows connecting node **b** to node **c**. Although in the example the same value (equal to 8) is set for both numbers N_m and N_q, this does not reflect the general case where these two variables can be set with different values.

Table 4.5 reports the number of combinations to be explored for extracting the q-ary APP values of each GF(64) symbol first without the low complexity algorithm and then for two settings of the low complexity algorithm. When the low complexity algorithm is selected, GF(64) symbols **b** and **c** require first a number of operations for sorting the APP values of GF(64) symbols **a** and **d**, respectively. The implemented algorithm, which is based on Merge and Sort approach, has a complexity of $nlog(n)$ (with n being the length of the vector to sort). The proposed algorithm reduces the number of combinations used for marginalization to obtain the APP values of the middle symbols **b** and **c** by a factor of ~ 7.5 without iterations, and a factor of ~ 10 with 3 iterations. The impact of the proposed algorithm on the error performance is assessed in Section 4.5.

4.5 Performance Analysis

In this section we analyze the FER performance of the Soft ML using the proposed low complexity algorithm as well as different mapping patterns. The idea of this section is to demonstrate that the mapping strategy stated in Section 4.3 and the low complexity demapping algortihm can be perfectly combined in order to maximize the trade-off between information diversity and demapping complexity. For this reason we will perform a complete analysis, aiming at validating the effectiveness of each mapping rule as well as the low complexity demapping algorithm. Now let us define the simulation set up that have been use to derive performance results and validate the effectiveness of the proposed mapping strategy and the low complexity algorithm. Both a SISO and a MIMO scenario are considered as representative of next generation cellular communication systems.

Table 4.5: *Reduction of the number combinations for **P1** and **P3** from Table 4.4*

Num. of combinations	**Without Algorithm**	**With Algor. $r = 0$,$N_m = 8$**	**With $r = 3$, $N_m = 8$,$N_q = 8$**
GF**(64) symbol a**	$64 \times 2^2 = 256$	$64 \times 2^2 = 256$	$64 \times 2^2 = 256$
GF**(64) symbol b**	$64 \times 2^6 \times 2^4 = = 65536$	$64 \times 6 + 64 \times N_m \times \times 2^4 = 8576$	$64 \times 3 \times N_m \times N_q + +2 \times 64 \times 6 = = 13056$
GF**(64) symbol c**	$64 \times 2^6 \times 2^4 = = 65536$	$64 \times 6 + 64 \times N_m \times \times 2^4 = 8576$	
GF**(64) symbol d**	$64 \times 2^2 = 256$	$64 \times 2^2 = 256$	$64 \times 2^2 = 256$
block of m_1 symbols	$64 \times 2 \times (2^{10} + 2^2) = = 131584$	$2 \times 64 \times (2^2 + 6 + N_m \times 2^4) = 17664$	$2 \times 64 \times (2^2 + 6) + +64 \times 3 \times N_m \times \times N_q = 13568$

The simulation parameters are:

a. **FEC encoder**

- DAVINCI NB LDPC codes
- GF order $q = 64$
- Codeword length $N = 96$ GF(64) symbols = 576 bits

b. **FEC decoder**

- Extended Min-Sum algorithm
- Number of soft values per symbol fed to the decoder = $q_m = 16$ (highest values)
- Maximum number of decoding iterations = 30

c. **Modulation**

- QPSK (only for SISO case), 16QAM, 64QAM

d. **MIMO configuration**

- 2×2 system
- Spatial multiplexing, i.e. $Q = 2$

e. **Soft demapping parameters**

- Soft ML, without and with the proposed low complexity algorithm (with different combinations of r, N_m, N_q)

First of all we have evaluated the performance of different mapping patterns for the SISO case, in order to validate the first rule of the proposed set. Figure 4.9 depicts the Frame Error Rate (FER) results obtained in the SISO scenario using two different patterns to map the GF(64) symbols onto QAM constellation symbols. The first mapping is an arbitrary mapping which does not respect the first rule devised in our solution, whereas the second mapping referred to as optimum mapping does. As illustrated in Figure 4.9, for QPSK and 64QAM, where $m_1 = 1$, there is no significant difference between the arbitrary and the proposed mapping patterns, since inherently here only one GF(64) symbol maps onto 3 QPSK symbols or one 64QAM symbol. However, for 16QAM, where $m_1 = 2$ and $m_2 = 3$, two GF(64) symbols are mapped onto the same mapping onto one 16QAM symbol, and here the results show clear SNR gain of 0.5 dB for the mapping respecting the first design rule as compared to a pattern not respecting this rule, hence validating the merits of this rule. It is noteworthy here that at this stage, there is no issue of trade-off between performance and complexity (this will come later when considering the second and third design rules proposed). We then move to the MIMO context in order to validate the second and third rules introduced in our mapping strategy, which aim to achieve a trade-off between performance and complexity. First we analyze the complexity in terms of number of operations of the APP extraction. Specifically, with the term **operation** we refer to a summation or a comparison of real-valued numbers, so either the summation or comparison operation has the same computational weight. We consider first the case of 16QAM with the three patterns given in Table 4.3, where patterns **P1** and **P3** respect the second rule, but not pattern **P2**. Figure 4.10 depicts the number of operations required for marginalization in the computation of the APP values of the $m_1 = 4$ GF(64) symbols which map together onto $m_2 = 6$ QAM symbols and $m_3 = 3$ MIMO codewords. Four curves show the number of operations (in logarithm scale) as a function of the threshold N_m introduced in the proposed algorithm. The curves

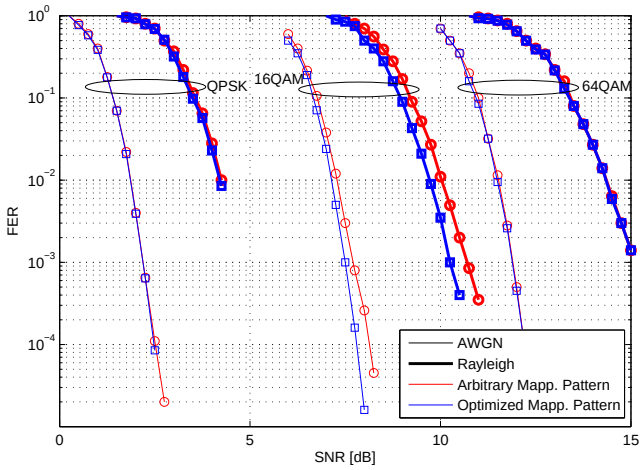

Figure 4.9: *FER for SISO system, using different mapping pattern* $N = 96$*, code rate* $= \frac{1}{2}$.

are as follows:

- The first curve in black circular marker gives the number of operations when an exhaustive search with pattern **P2** is performed.
- The second curve in red circular marker gives the number of operations when an exhaustive search with pattern **P1** or **P3** is performed.
- The third curve in blue downwards triangular marker shows the number of operations using the proposed algorithm ($N_m = 8$) for pattern **P1** or **P3** without the iterative step 4 (i.e. simply replace sub-step 4.2 by an exhaustive search).
- The fourth curve in green with diamond markers considers the iterative step 4 of the proposed algorithm with $r = 3$ iterations, $N_m = 8$ and $N_q = 10$ (still for pattern **P1** or **P3**).

From Figure 4.10, we can clearly appreciate the huge reduction in complexity (cf. gap between first curve using **P2**, and the other curves using **P1** and **P3**). This clearly validates the merit of our second rule from the complexity perspective, since patterns **P1** and **P3** respect this second rule, but not pattern **P2**. Moreover, from

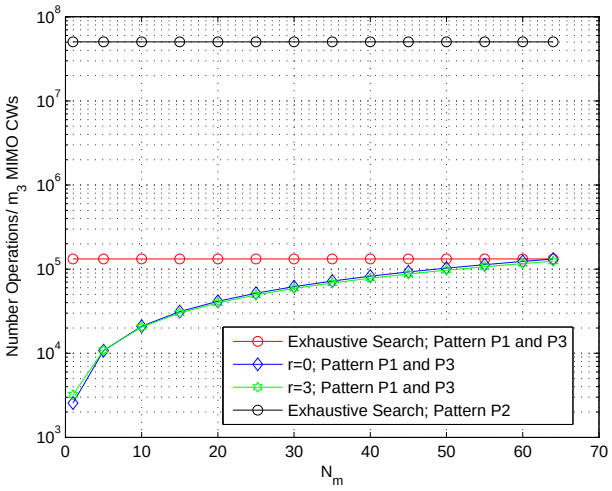

Figure 4.10: *Number of operations required for marginalization with and without the proposed low complexity algorithm.*

Figure 4.10, we can also clearly appreciate the significant reduction in complexity (cf. gap between second curve, and third and fourth curves) brought by the use of the proposed algorithm (with and without iterations) as compared to the exhaustive search. The reduction in complexity clearly decreases when increasing the threshold N_m. For a typical value of $N_m = 8$, we can appreciate nearly one decay (i.e. a factor of 10) complexity reduction thanks to the proposed algorithm.

The second aspect to be assessed here is the impact of the proposed mapping strategy and demapping algorithm on the error protection performance. This is illustrated in Figure 4.11, for patterns **P1** and **P3** with different configurations. It is worth noting here that the pattern **P2** could not be evaluated since its breach of the second rule makes it non practical for computer simulations. Our reference curves are the ones in red solid line which perform an exhaustive search (i.e. do not implement the proposed algorithm). In this figure, square marker is used for mapping pattern **P1**, and circular marker for mapping pattern **P3**.

From Figure 4.11, we first compare the performance gap between patterns **P1** and **P3** with the exhaustive search used in both. This is in order to appreciate the trade-

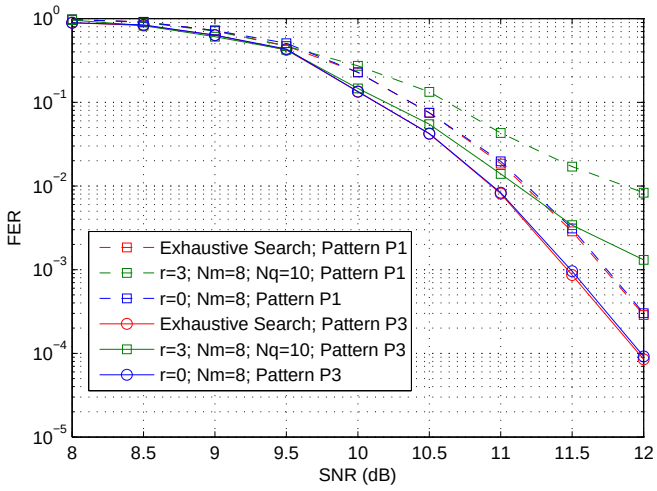

Figure 4.11: *FER for 16QAM with patterns **P1** and **P3** from Table 4.3.*

off in performance due to the second rule and the merits of the third rule. The performance gap between **P1** and **P3** is almost 0.25 dB, when **P1** has a constant DGFS equal to 4 and **P3** has an average DGFS equal to 5 (it is equal to 4 at the edge GF(64) symbols and 6 at the middle GF(64) symbols). As mentioned previously, both patterns **P1** and **P3** respect the second rule, but only **P3** respects the third rule. Hence, from this comparison, the merit of the third rule is clearly appreciated ($\sim$ 0.25 dB SNR gain) at the same level of complexity. The same performance gap is expected between patterns **P2** and **P3** (although as said before simulations with pattern **P2** are not feasible since it breaches the second rule). This expectation is motivated by the fact that the gap in DGFS between **P2** and **P3** is equal to 1, which is the same gap between **P3** and **P1** (PS: the average DGFS is equal to 6, 5, and 4, respectively for patterns **P2**, **P3**, and **P1**). Hence, the penalty in performance of the second design rule is expected to be around 0.25 dB, compared to a pattern **P3** respecting the second and third design rules, and 0.5 dB compared to a pattern **P1** respecting the second rule but not the third rule. Now let us compare the performance of both patterns **P1** and **P3** when using the proposed soft demapping algorithm. From Figure 4.11, for both patterns **P1** and **P3**, we do not notice any appreciable degradation when

using the proposed algorithm with threshold $N_m = 8$, and without using the iterative process, compared to when using the exhaustive search. This is an important result as it shows the potential of the proposed algorithm to reduce the complexity by ten-fold without practical degradation in the FER performance. Further reduction of the complexity by means of the iterative process for example, does degrade the FER performance. The degradation of the iterative process in the waterfall region at target FER of 10^{-2} appears tolerable (up to 0.5 dB), whilst the degradation in the error floor region appears significant. This reflects the trade-off someone can obtain between FER performance and further reduction of the complexity with the iterative process.

Further analysis was carried out for the case of MIMO 64QAM. In such a case, we consider two different mapping patterns as illustrated in Table 4.6.

Table 4.6: *Different mapping patterns for MIMO case with 64QAM*

Pattern	**Antenna**	$\boldsymbol{I_0}$	$\boldsymbol{C_0}$
P1	**A1**	$a_0a_1a_2$	$a_3a_4a_5$
	A2	$b_0b_1b_2$	$b_3b_4b_5$
P2	**A1**	$a_0a_1a_2$	$b_0b_1b_2$
	A2	$a_3a_4a_5$	$b_3b_4b_5$

Both **P1** and **P2** respect the first and second rule, but only **P2** respects the third rule. With 64QAM, the proposed algorithm must necessarily use the iterative process, since there are no edge symbols falling under step 2 of the proposed algorithm. Similarly to the 16QAM case, the sorting of the APP values should be taken into account in the computation of the complexity. Table 4.7 below shows a complexity reduction of 35% with respect to the exhaustive search when N_q is equal to 24 and 44% when N_q is equal to 20.

Figure 4.12 also shows the FER performance results for both patterns with and without the proposed algorithm in the configurations given in Table 4.7. A circle marker is used for the curves with pattern **P1** and square marker for the curves with pattern **P2**. From Figure 4.12, we can first appreciate a gain of nearly 0.8 dB for pattern **P2** as compared to **P1**. This confirms further the potential of the third rule in

Table 4.7: *Reduction of the number combinations for MIMO with 64QAM*

Num. of combinations	**Without Algorithm**	**With Algor. $r = 3, N_q = 20$**	**With Algor. $r = 3, N_q = 24$**
GF**(64) symbol a**	$64 \cdot 2^6 = 4096$	$64{\cdot}3{\cdot}N_q{+}2{\cdot}64{\cdot}6 = = 4608$	$64{\cdot}3{\cdot}N_q{+}2{\cdot}64{\cdot}6 = = 5376$
GF**(64) symbol b**	$64 \cdot 2^6 = 4096$		
block of m_1 symbols	$2 \cdot 64 \cdot 2^6 = 8192$	$64{\cdot}3{\cdot}N_q{+}2{\cdot}64{\cdot}6 = = 4608$	$64{\cdot}3{\cdot}N_q{+}2{\cdot}64{\cdot}6 = = 5376$

achieving much higher diversity. Second, with pattern **P2**, we can clearly appreciate a slight degradation in performance nearly 0.2 dB when using the proposed low complexity iterative demapping algorithm with $N_q = 24$ (35% complexity reduction). The degradation becomes higher 0.5 dB for $N_q = 20$ (44% complexity reduction). So clearly, there is a trade-off between the tolerable FER performance degradation and the target complexity reduction, and the proposed mapping strategy and low complexity demapping algorithm provide the tools to achieve the trade-off desired.

4.6 Conclusions

In the first part of this chapter we have investigated the combination of NB LDPC codes with different STCs from the FER performance and complexity perspectives. Specifically, we have derived the performance of the MIMO link in different scenarios with spectral efficiencies ≤ 3.33 Bits-per-channel-use. For low channel code rates $\leq \frac{2}{3}$ SM outperforms any other STCs by up to 0.5 dB in the waterfall region; for scenarios with higher channel code rate, GC and RS LDC are shown to have better performance than SM by about 0.3 dB. Unfortunately complexity analysis of demapping in terms of the required number of real operations per coded bit shows that Soft ML becomes unaffordable in the case of GC or RS LDC with high order modulations (16QAM and 64QAM). Hence the only concrete possibility for very high spectral efficiencies (up to 10 Bits-per-channel-use), detected with SoftML, is represented by SM, which is not particularly affected by complexity issues. Alamouti coding is admittedly the least complex solution, but it is outperformed by the other STCs.

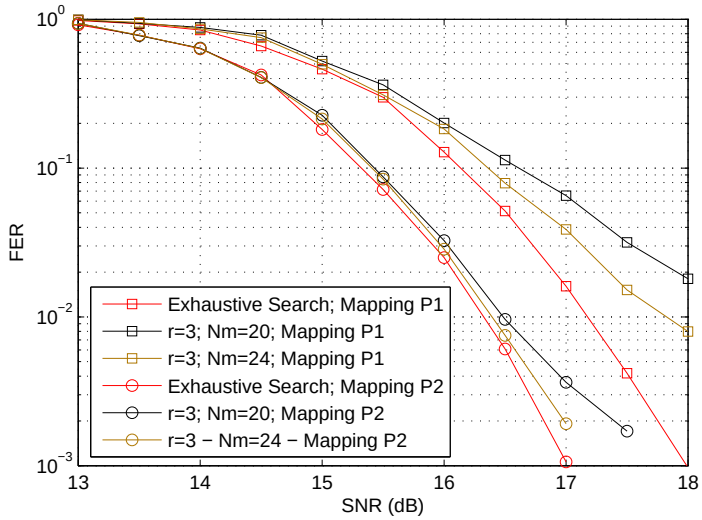

Figure 4.12: *FER for 64QAM with patterns **P1** and **P2** from Table 4.6.*

Later we have addressed the particular complexity challenge of the soft ML demapping faced with non-binary LDPC codes when one GF(q) symbol spreads across multiple QAM symbols and MIMO codewords. A solution is proposed combining a mapping strategy based on three design rules at the transmitter, and a low complexity soft ML demapping algorithm at the receiver. At the transmitter side, the mapping strategy has introduced three design rules to achieve the best trade-off between performance and complexity. In the first rule, the I or C component of an QAM symbol should carry (in part or in full) the binary image of only one GF(q) symbol. This rule was shown to bring an SNR performance gain of ~ 0.5 dB compared to mapping patterns not respecting this rule. In the second rule, the I/C components issued from one GF(q) symbol are carried into the minimum possible number of MIMO codewords. This second rule clearly restricts the freedom to let the GF(q) symbol enjoy higher channel selectivity, but fortunately has the advantage of reducing drastically the complexity of the soft ML demapper. In the third rule, the I/C components issued from one GF(q) symbol are mapped onto the transmission units which ideally can experience independent channel fading within the MIMO codeword carrying this GF(q) symbol.

This third rule aims at exploiting the last degree of freedom left by the binding second rule to achieve high channel selectivity within the GF(q) symbol. With mapping patterns respecting the second rule, it was shown that a ten fold complexity reduction can be achieved compared to patterns not respecting this second rule. The trade-off in performance was shown to be small, 0.25 dB and 0.5 dB performance degradation for the patterns respecting the second rule with and without the third rule, respectively. At the receiver side, an algorithm was proposed to reduce the complexity of the soft ML demapper. The algorithm exploits the correlation existing between GF(q) symbols but also any knowledge available on the APP values of the GF(q) symbols in the vector of m_1 GF(q) symbols, which map together onto the vector of m_2 QAM symbols and further on onto the vector of m_3 MIMO codewords. The algorithm also considers only a limited number of potential combinations for each GF(q) symbol, those associated with this same limited number of highest APP values for this symbol. This latter consideration has been inspired from the original work done by [5], [35] to reduce the complexity of the non-binary LDPC decoder. Our proposed algorithm was shown to further reduce the complexity of the soft ML demapper by up to 85%. The proposed solution mitigates the complexity challenge at the receiver faced with non-binary LDPC codes when one GF(q) symbol spreads across multiple QAM constellation symbols and STBC codewords, at the expense of a slight performance degradation but not sacrificing the performance merits of non-binary LDPC codes. This removess any restriction on the size of the Galois field order, QAM constellation order, and MIMO scheme, whilst preserving the merits of non-binary LDPC codes at very reasonable receiver complexity.

Chapter 5

Conclusions and perspectives

In the first chapter, we have presented the NB LDPC channel coding scheme, highlighting the codec features, before deriving the demapping operations for the SISO scenario. We have also compared the non binary demapping with the one necessary for a binary channel coding scheme, such as DBTCs. Later we have also carried out a FER performance analysis by which we can conclude that for single antenna transmission, NB LDPC codes outperform advanced binary FEC scheme (DBTC) for any analyzed scenario. The gain is found to increase with the constellation order, from 0.1 dB in QPSK to 0.8 dB in 64QAM. The average gain between NB LDPC and DBTC is found around 0.25 dB, in line with the results obtained in the DAVINCI project [14]. However, the correspondent receiver is more complex than the binary one and this complexity increase might be quantified around one order of magnitude.

In the second chapter we have introduced the MIMO concepts in uncoded systems, i.e. without channel coding. Specifically, we have first detailed the MIMO channel model, which will be used all along this work. Later we have analyzed the multiple-antennas system model and presented the STCs under analysis. We have also introduced the universal framework of the LDC, and characterized the selected STCs through the linear dispersion matrices. From the simulation results we have ended up that Alamouti has been shown to always outperform SM and Golden Code in terms of error protection at the constant spectral efficiency of 4 Bpcu. Linear receivers have been proved to achieve the optimal performance only for orthogonal codes.

In the third chapter we have investigated the combination between NB LDPC codes and MIMO techniques. More specifically, we have presented two different demapping approaches for non-binary systems, i.e. the linear equalizer-based one and a second technique, which implements a soft version of the Maximum Likelihood demapper

(Soft ML). First we have detailed these approaches with analythical descriptions. Then we have compared these methods with their binary counterparts, before focusing om the FER performance analysis, which aims to better understand which demapping technique is most suitable for non binary transmission. Specifically, different scenarios have been investigated in order to better understand the general behaviour of the presented methods for different STCs. In some of the analyzed MIMO scenarios we have included the SISO performance at the same spectral efficiency in order to perform a more complete analysis. Through the observation of the simulations results we have drawn the following conclusions:

a. The configuration SM with Soft ML has been shown to produce the best results in terms of FER performance. Specifically, the benefits of this configuration are more evident whether combined with a low channel code rate ($\frac{1}{2}$). If the channel code rate increases this configuration keeps on having a coding gain with respect to any other configuration, but the slope in the FER curve is not the steeper one. In fact Alamouti (independently of the demapping technique, thanks to the orthogonality) in combination with high channel code rate has been shown to achieve the highest slope.

b. Focusing on SM, the coding gain between Soft ML and linear equalizer-based demapper increases if the channel code rate increases.

c. NB LDPC codes have been shown to outperform DBTCs for any configurations in any simulated scenarios.

d. The gain between NB LDPC codes and DBTCs increases when moving from SISO to MIMO whether the configuration SM with Soft ML is adopted.

Later we have also carry out a complexity analysis for both methods, when different combinations of modulations and STCs are selected. From the complexity analysis we can end up that:

a. The Alamouti code can be used with any modulation, without complexity issue, thanks to the use of linear equalizers, despite not leading to the best FER performance.

b. The same conclusion can be drawn for SM detected with MMSE, but this configuration has been proved not to be particularly interesting from FER perspective.

c. SM with Soft ML can be employed with QPSK without complexity issues. The employment of SM with Soft ML in combination with 16QAM and 64QAM might turn out to be too complex for some target hardware and/or application.

For all these reasons we have decided to deeper analyze the Soft ML algorithm, trying to derive sub-optimal versions, which allow to reduce the demapping complexity. This study has been presented in the chapter four.

In the fourth chapter we have first investigated the combination of NB LDPC codes with different STCs from the FER performance and complexity perspectives. Specifically, we have derived the performance of the MIMO link in different scenarios with spectral efficiencies $\leq$ 3.33 Bits-per-channel-use. For low channel code rates $\leq \frac{2}{3}$ SM outperforms any other STCs by up to 0.5 dB in the waterfall region; for scenarios with higher channel code rate, GC and RS LDC have shown to have better performance than SM by about 0.3 dB. Unfortunately complexity analysis of the demapping operation have shown that Soft ML becomes unaffordable in the case of GC or RS LDC with high order modulations (16QAM and 64QAM). Hence the only concrete possibility for very high spectral efficiencies (up to 10 Bits-per-channel-use), detected with SoftML, is represented by SM, which is not particularly affected by complexity issues.

Later we have addressed the particular complexity challenge of the soft ML demapping faced with non-binary LDPC codes when one GF(q) symbol spreads across multiple QAM symbols and MIMO codewords. A solution is proposed combining a mapping strategy based on three design rules at the transmitter, and a low complexity soft ML demapping algorithm at the receiver. This strategy jointly with the low complexity demapping algorithm have been investigated with SM, but it might be applied to different STCs. At the transmitter side, the mapping strategy has introduced three design rules in order to achieve the best trade-off between performance and complexity. In the first rule, the I or C component of a QAM symbol should carry (in part or in full) the binary image of only one GF(q) symbol. This rule was shown to bring an SNR performance gain of $\sim$ 0.5 dB compared to mapping patterns not respecting this rule. In the second rule, the I/C components issued from one GF(q) symbol are

carried into the minimum possible number of MIMO codewords. This second rule clearly restricts the freedom to let the GF(q) symbol enjoy higher channel selectivity, but fortunately has the advantage of reducing drastically the complexity of the soft ML demapper. In the third rule, the I/C components issued from one GF(q) symbol are mapped onto the transmission units which ideally can expperience independent channel fading within the MIMO codeword carrying this GF(q) symbol. This third rule aims at exploiting the last degree of freedom left by the binding second rule to achieve high channel selectivity within the GF(q) symbol. With mapping patterns respecting the second rule, it was shown that a ten fold complexity reduction can be achieved compared to patterns not respecting this second rule. The trade-off in performance was shown to be small, 0.25 dB and 0.5 dB performance degradation for the patterns respecting the second rule with and without the third rule, respectively. At the receiver side, an algorithm was proposed to reduce the complexity of the soft ML demapper. The algorithm exploits the correlation existing between GF(q) symbols but also any knowledge available on the APP values of the GF(q) symbols in the vector of m_1 GF(q) symbols, which map together onto the vector of m_2 QAM symbols and further on onto the vector of m_3 MIMO codewords. The algorithm also considers only a limited number of potential combinations for each GF(q) symbol, those associated with this same limited number of highest APP values for this symbol. The proposed solution mitigates the complexity challenge at the receiver faced with non-binary LDPC codes when one GF(q) symbol spreads across multiple QAM constellation symbols and STBC codewords, at the expense of a slight performance degradation but not sacrificing the performance merits of non-binary LDPC codes. This removess any restriction on the size of the Galois field order, QAM constellation order, and MIMO scheme, whilst preserving the merits of non-binary LDPC codes at very reasonable receiver complexity.

Finally let us conclude with possible future perspetives opened by this work. The demapping complexity using the Soft ML approach, when GC with high order modulations (or a similar STC, encapsulating 4 QAM symbols in a MIMO codeword) might be only partially mitigated through the proposed low complexity algorithm. In fact the intrinsic complexity of the exhaustive search demapping is huge ($o(M^Q) = o(16^4) \sim$ 65536 for 16QAM, or $o(64^4) \sim 16777216$). For this reason the interested researcher might focus on the combination of the low complexity demapping algorithm, proposed in this work, with the well-known sphere demapping. Further analysis on the mapping

strategy might be performed using the EXIT Charts, according to [36].

Bibliography

[1] M. Davey and D. MacKay, "Low density parity check equation over GF(q)," *IEEE Commununications Letters*, vol. 2, no. 6, 1998.

[2] J. Huang and J. Zhu, "Linear time encoding of cycle GF(2^p) codes through graph analysis," *IEEE Commununications Letters*, vol. 10, no. 5, May 2006.

[3] D. Declercq and M. Fossorier, "Decoding algorithms for non-binary LDPC codes over GF(2^q)," *IEEE Trans. Commun.*, vol. 55, no. 4, 2007.

[4] "INFSCO-ICT-216203 FP7 DAVINCI website," 2008, http://www.ict-davinci-codes.eu.

[5] E. Boutillon and L. Conde-Canencia, "Buble check: a simplified algorithm for elementary check node processing in extended min-sum non-binary LDPC decoders," *IET Electronics Letters*, vol. 46, no. 9, pp. 633–634, Apr. 2010.

[6] S. Pfletschinger and D. Declercq, "Getting closer to MIMO capacity with non-binary codes and spatial multiplexing," in *Proc. IEEE Global Telecommunications Conference (GLOBECOM)*, Miami, FL, Dec. 2010.

[7] ——, "Non-binary coding for vector channels," in *Proc. IEEE International Conference on Communications (ICC)*, Kyoto, Japan, 2011.

[8] D. MacKay and M. Davey, "Evaluation of Gallager codes of short block length and high rate applications," in *Proc. IMA Intern. Conf. on Mathem. and its Appl.: Codes, Systems and Graphical Models*, New York, USA, Dec. 2000.

[9] L. Barnault and D. Declercq, "Fast decoding algorithm for LDPC over GF(2^q)," in *Proc. IEEE Information Theory Workshop*, Paris, France, Mar. 2003.

[10] C. Poulliat, M. Fossorier, and D. Declercq, "Design of regular (2,dc)-LDPC codes over GF(q) using their binary images," *IEEE Trans. Commun.*, vol. 56, no. 10, pp. 1626–1635, Oct. 2008.

[11] F. M. Williams and N. J. A. Sloane, *The theory of Error-Correcting Codes*. Amsterdam, The Netherlands: North-Holland Mathematical Library, 1977.

[12] J. Bas, G. Bacci, A. Mourad, and et al., "Link Level Evaluation, issue 1," *INFSCO-ICT-216203 DAVINCI D2.2.1*, dec 2008.

[13] "Iterative solutions - homepage," 2007, http://www.iterativesolutions.com/.

[14] I. Gutierrez, G. Bacci, A. Mourad, and et al., "Final proposal for IMT advanced systems," *INFSCO-ICT-216203 DAVINCI D2.1.4*, nov 2009.

[15] L. Zheng and D. N. C. Tse, "Diversity and multiplexing: A fundamental tradeoff in multiple-antenna channels," *IEEE Trans. Information Theory*, vol. 49, no. 5, pp. 1073–1096, May 2003.

[16] B. Hassibi and B. Hochwald, "High-rate codes that are linear in space and time," *IEEE Trans. Information Theory*, vol. 48, no. 7, pp. 1804–1824, July 2002.

[17] A. Paulraj, R. Nabar, and D. Gore, *Introduction to Space-Time Wireless Communications*. Cambridge, UK: Cambridge University Press, 2003.

[18] IEEE 802.16 Broadband Wireless Access Working Group, "IEEE 802.16m System Description Document (SDD)," *Tech. Rep. IEEE 802.16m-09/0034r2*, sept 2009.

[19] S. Alamouti, "A simple transmit diversity technique for wireless communications," *IEEE J. Select. Areas Commun.*, vol. 16, no. 8, pp. 1451–1458, Aug. 1998.

[20] J. Belfiore, G. Rekaya, and E. Viterbo, "The golden code: A 2x2 full-rate space-time code with non-vanishing determinants," in *Proc. Intern. Symp. in Information Theory ISIT*, Chicago, IL, 2004.

[21] L. Hanzo, O. Alamri, M. El-Hajjar, and N. Wu, *Near-capacity multifunctional MIMO systems: Sphere-packing, iterative detection and cooperation*. New York, NY: J. Wiley and IEEE Press, 2009.

[22] T. Duman and A. Ghrayeb, *Coding for MIMO communication systems.* Wiltshire, UK: Wiley, 2007.

[23] R. Heath and D. Love, "Multimode antenna selection for spatial multiplexing systems with linear receivers," *IEEE Trans. on Signal Processing*, vol. 53, no. 8, pp. 3042–3056, Aug. 2005.

[24] O. M. Picchi, A. Mourad, I. Gutierrez, and M. Luise, "On the performance of non-binary LDPC with MIMO in practical systems," in *Proc. IEEE Intern. Symp. in Wireless Communications Systems (ISWCS)*, Aachen, Germany, Nov. 2011.

[25] D. N. C. Tse and P. Viswanath, *Fundamentals of Wireless Communications.* Cambridge, UK: Cambridge Univ. Press, 2005.

[26] Y. Li and W. E. Ryan, "Mutual-information-based adaptive bit-loading algorithms for LDPC-coded OFDM," *IEEE Trans. Wireless Commun.*, vol. 6, no. 5, pp. 1670–1680, May 2007.

[27] M. Franceschini, G. Ferrari, and R. Raheli, "Does the performance of LDPC codes depend on the channel?" *IEEE Trans. Commun.*, vol. 54, no. 12, pp. 2129–2132, Dec. 2006.

[28] G. Foschini, "Layered space-time architecture for wireless communication in a fading environment when using multi-element antennas," *Bell Labs Tech. Journ.*, pp. 41–59, 1996.

[29] I. Telatar, "Capacity of multi-antenna gaussian channels," *European Trans. Tel.*, pp. 585–595, 1999.

[30] J. Kliewer, S. X. Ng, and L. Hanzo, "Efficient computation of exit functions for non-binary iterative decoding," *IEEE Trans. Commun.*, vol. 54, no. 12, pp. 2133–2136, Dec. 2006.

[31] R. W. J. Heath and A. Paulraj, "Linear dispersion codes for mimo systems based on frame theory," *IEEE Transactions on Signal Processing*, vol. 50, no. 10, p. 24292441, Oct. 2002.

[32] V. Tarokh, S. Alamouti, and P. Poon, "New detection schemes for transmit diversity with no channel estimation," in *Proc. IEEE International Conference on Universal Personal Communications*, Oct. 1998, pp. 917–920.

[33] R. A. Horn and C. R. Johnson, *Matrix Analysis*. Cambridge, UK: Cambridge University Press, 1985.

[34] A. Mourad, O. M. Picchi, I. Gutierrez, and M. Luise, "Low complexity soft demapping for non-binary LDPC codes," *EURASIP Journ. on Wireless Commun. and Network.*, Apr. 2012.

[35] A. Singh, A. Al-Ghouwayel, G. Masera, and E. Boutillon, "A new performance evaluation metric for sub-optimal iterative decoders," *IEEE Communications Letters*, vol. 13, no. 7, pp. 513–515, July 2009.

[36] S. ten Brink, "Convergence behavior of iteratively decoded parallel concatenated codes," *IEEE Trans. Commun.*, vol. 49, no. 10, pp. 1727–1737, Oct. 2001.

Index

List of Publications

Patent Applications

- **O. M. Picchi**, A. Mourad, I. Gutierrez, "Method for Mapping and De-mapping of Non-binary Symbols in Data Communication Systems," Patent Applications **No. GB1009729.3**, **No. US 13/157,743**, June 2010.

International Journals

- G. Baldini, **O. M. Picchi** et al., "The EULER project: application of software defined radio in joint security operations," *IEEE Communications Magazine*, vol.49, n.10, pp. 55-62, Oct. 2011.

- A. Mourad, **O. M. Picchi**, I. Gutierrez and M. Luise, "Low complexity soft demapping for non-binary LDPC codes," *EURASIP Journal of Wireless Commun. and Networking*, to appear.

International Conferences

- **O. M. Picchi**, T. Sturman, et al., "EULER The first pan-European SDR-based platform project," in *Proc. SDR10 Technical Conference and Product Exposition*, Washington DC, USA, Nov. 2010.

- **O. M. Picchi**, A. Mourad, I. Gutierrez and M. Luise, "On the performance of non-binary LDPC with MIMO in practical systems," in *Proc. IEEE Intern. Symp. on Wireless Commun. Syst. (ISWCS)*, Aachen, Germany, Nov. 2011.

- T. Sturman, **O. M. Picchi**, et al., "Employing software defined radios for International public safety," in *Proc. Workshop on Software Radios (WSR)*, Karlsruhe, Germany, Mar. 2012.